SOLID ROCKET BOOSTER THERMAL RADIATION MODEL, VOLUME 1

LOCKHEED MISSILES AND SPACE CO.,
HUNTSVILLE, ALA. THERMAL AND FLUID
PHYSICS GROUP

MAR 1976

Lockheed
Missiles & Space Company, Inc.
HUNTSVILLE RESEARCH & ENGINEERING CENTER
Cummings Research Park
4800 Bradford Drive,
Huntsville, Alabama

SOLID ROCKET BOOSTER THERMAL RADIATION MODEL – VOLUME I

FINAL REPORT

March 1976

Contract NAS8-31310

Prepared for National Aeronautics and Space Administration
Marshall Space Flight Center, Alabama 35812

by

G.H. Watson
A.L. Lee

APPROVED: B. H. Shirley

B.H. Shirley, Supervisor
Engineering Sciences Section

J. S. Farrior

J.S. Farrior
Resident Director

FOREWORD

This document is Volume I of the final report for Contract NAS8-31310. Volume II is printed under separate cover and is entitled "Solid Rocket Booster Thermal Radiation Model – Volume II – User's Manual," LMSC-HREC TR D496763-II. This report was prepared by personnel of the Thermal & Fluid Physics Group, Engineering Sciences Section, Lockheed-Huntsville Research & Engineering Center. The contract period of performance was from 20 January 1975 through 20 March 1976. The work was administered under the technical direction of Mr. William C. Claunch of the Structures and Propulsion Laboratory, NASA-Marshall Space Flight Center.

NOMENCLATURE

Symbol	Definition
English	
A	area
A/E	absorption to extinction ratio
$C_{1,\ldots,10}$	quadric coefficients
d	parameter
E_b	black body emissive power
e	energy per bundle
F	view factor
F(x)	probability density function
H_i	elevation of axial region boundaries
h	elevation along plume axis
I	radiation intensity (also axial region boundary index)
J	volumetric emission of radiant energy (also radial region boundary index)
K	particle-wavelength size parameter
K_a	linear absorption coefficient
ℓ	length
N	$A\ell_2O_3$ particle number density
N_e	sample size (number of emissions)
N_h	number of hits on a surface
$n_{1,2,3}$	direction cosines of line of sight

$P_{1, 2, 3}$	points on a surface
P	pressure or property
P_c	chamber pressure
P_i	intersection point
P_∞	ambient pressure
P(x)	probability distribution function
$Q_{a, e, scat}$	absorption, extinction, scattering efficiencies
q	heating rate
R	distance between plume axis and line of sight in plane at right angles to plume's axis passing through cone vertex
R_{ex}	nozzle exit radius
r	radial coordinate (cylindrical coordinate)
r_p	particle radius
S	length along line of sight
S_p	probable path length
$S(\eta, \theta)$	scatter function
T	temperature
U	random number
$u_{1, 2, 3}$	direction cosines of surface unit normal
V	volume
$X_{1, 2, 3}$	principal coordinates (Cartesian coordinates)
Z	distance along plume axis from base plane (cylindrical coordinate)

Greek

β	angle between r_1 and r_2
γ	cone half angle for radial region boundaries

η	polar angle of line of sight (spherical coordinate)
θ	azimuth angle of line of sight (spherical coordinate)
ϕ	azimuth angle of event site (cylindrical coordinate)
ψ	gimbal angle in yaw plane
σ	gimbal angle in pitch plane (also Stefan-Boltzmann constant)
$\sigma_{a, e, scat}$	absorption, extinction, scattering cross section for $A\ell_2O_3$ particles
τ	optical depth
ω	solid angle
λ	wavelength

Subscripts

a	absorbtion
b	blackbody
g	gas
p	particle
scat	scattering
λ	wavelength

CONTENTS

TABLE OF CONTENTS (CONCLUDED)

LIST OF TABLES

LIST OF ILLUSTRATIONS

LIST OF ILLUSTRATIONS (Continued)

1. INTRODUCTION

Thermal radiation from exhaust plumes of solid rocket boosters (SRB) on the Space Shuttle is a major contributor to the heat load incident on the base region of the Space Shuttle vehicle. The magnitude of this heating rate is expected to be comparable to that caused by the Space Shuttle main engines (SSME). Accurate estimates of SRB thermal radiation is necessary to optimally design the thermal protection system (TPS) for the ascent phase of the Space Shuttle trajectory. These estimates often rely on analytical models of the thermal radiation emitted by plumes.

SRB plumes are composed of a dispersion of $A\ell_2O_3$ particles distributed throughout the gaseous products of combustion of the solid propellant. $A\ell_2O_3$ particles are present in SRB plumes because alumina is added to the solid propellant to increase the specific impulse of the booster. The particles may exist in either the solid or liquid phase. In the solid phase, $A\ell_2O_3$ particles are almost pure scatterers of electromagnetic radiation. However, in the liquid phase $A\ell_2O_3$ has a relatively large absorbtion cross section and contributes significantly to the thermal radiation of the SRB plume. Certain gaseous constituents present in SRB plumes are also strong emitters of radiant energy. So, a realistic model for thermal radiation from SRB plumes must consider coupled radiation from $A\ell_2O_3$ particles as well as emission from the principal emitting gases, namely CO, CO_2, H_2O and $HC\ell$.

At the present time, much of the thermal environment calculations in the base region of the Space Shuttle which account for radiant heating due to SRB plumes are based on a view factor calculation to surfaces in the base region from a diffuse conical surface surrounding the plume. These view factor calculations are used in conjunction with an assumed plume emissive power in order to calculate radiant heating rates. Assumptions are also

necessary regarding an appropriate value for the half angle to be used for the diffuse conical surface representing the SRB plume. Unfortunately, view factor methods for calculating thermal environments due to SRB plumes cannot account for influences on plume radiant heating of such parameters as:

- Chamber pressure
- Propellant composition
- Altitude
- Approach Mach number
- Afterburning, and
- Spatial variations in plume properties, including: (1) gas and $A\ell_2O_3$ particle temperature; (2) gas pressure; (3) $A\ell_2O_3$ particle number density; (4) gas mole fractions; and (5) scatter and absorption cross sections.

This report documents the development and description of a SRB plume thermal radiation model which accounts for the influence of the above parameters on the magnitude and distribution of thermal radiation emanating from SRB plumes. The Monte Carlo method is used to solve the radiation transport problem to provide more flexibility in modeling plume structure. Property definition in the plume may be provided by flowfield calculations or, if available, from experimental data. Spatial distributions of plume properties are approximated by arranging homogeneous regions throughout the plume (in which plume properties are defined) in a manner consistent with plume property variations.

The Space Shuttle will have two SRBs astride the vehicle that will contribute to the base heating. These plumes may intersect close to the base region at high altitudes and may also gimbal one independent of the other. Plume intersection and plume gimbal angle can have a considerable effect on local heating rates. In view of this expected character of SRB thermal radiation, the SRB radiation model described herein considers dual SRB plumes. In this manner, the attenuation of radiant energy from one plume

on its neighboring plume (or shadowing effect) is accounted for in the model's calculations of the distribution of thermal energy leaving the plume.

Space Shuttle surface geometries are modeled as combinations of quadric surfaces. Specific surface geometries that can be considered are:

- Planar (parallelegram or annular)
- Cones and frustums
- Cylinders
- Ellipsoids and spheres, and
- Paraboloids.

These quadric surfaces can be defined in a Cartesian coordinate system by means of a single polynomial expression. Models of specific Space Shuttle surface geometries can be easily constructed with combinations of these surfaces. The individual surfaces can be subdivided to provide more discrete definition of local geometries. Each subdivision of every surface has a unique mathematical definition. This surface characteristic is used in conjunction with the Monte Carlo solution to the radiation transport problem so that radiation heating rates can be calculated to each discrete subsurface. The Monte Carlo method also enables easy and accurate predictions of the effects of shading of one surface by another on the magnitude of radiant heat loads.

The SRB thermal radiation computer code also provides the capability to calculate view factors between one selected surface on the Space Shuttle and the SRB plumes as well as all other surfaces of interest on the Space Shuttle. This capability will allow detailed analysis of SRB thermal radiation at extremely localized areas of the Space Shuttle where the effects of surface shading are considerable.

The SRB thermal radiation model extends to the thermal design engineer the capability to define the influences of plume flow field and propellant composition on the magnitude and distribution of thermal energy emitted by

dual SRB plumes. Also, the capability of delineating the influence of surface shading on the magnitude of SRB radiant heating rates is provided. These capabilities are provided with a computer code that is easy to input for purposes of performing a detailed and extended parametric analysis of SRB thermal radiation in the base region of the Space Shuttle.

2. SRB PLUME STRUCTURE

2.1 PARAMETERS INFLUENCING SRB FLOW FIELDS

SRB exhaust plume flow fields are composed of the gaseous products of combustion as well as solid and/or liquid particles of Al_2O_3. Although the flow field of a single plume may be considered to be axisymmetric, calculation of the distribution of particle and gaseous properties in SRB plumes is a difficult task because the properties of the gas and particles are not contiguous at any location. The particles are accelerated in the nozzle plume flow field due to pressure gradients and drag forces exerted on them by the gaseous flow and they retain temperatures that are generally higher than the gas temperature because of their thermal capacitance. Realistic flowfield calculations require accurate modeling of the interchange of momentum and thermal energy between the gaseous flow field and the dispersion of Al_2O_3 particles immersed in the gases in order to establish distributions of particles and gas properties in the plume.

A number of parameters influence SRB plume flowfield structure. One of the more influential parameters is the ratio of pressure in the SRB combustion chamber to the ambient pressure (P_c/P_∞). This ratio determines, to a large degreee, the amount of gaseous expansion that takes place in the plume and subsequently the plume's overall size. Analytical studies of SRB plume flow fields indicate that the initial expansion angle, γ, (measured relative to the plume axis) of the plume at the nozzle exit plane can be as large as 35 degrees. Figure 2-1 shows the effect of P_c/P_∞ on initial plume expansion. These data were obtained from several flowfield calculations using Lockheed's two-phase plume flowfield computer code.[1] At the lower values of P_c/P_∞, the SRB plume contains shock structures and associated localized regions of high temperature gases and, to a lesser extent, Al_2O_3 particles with locally higher temperature. These shocks tend to increase the magnitude

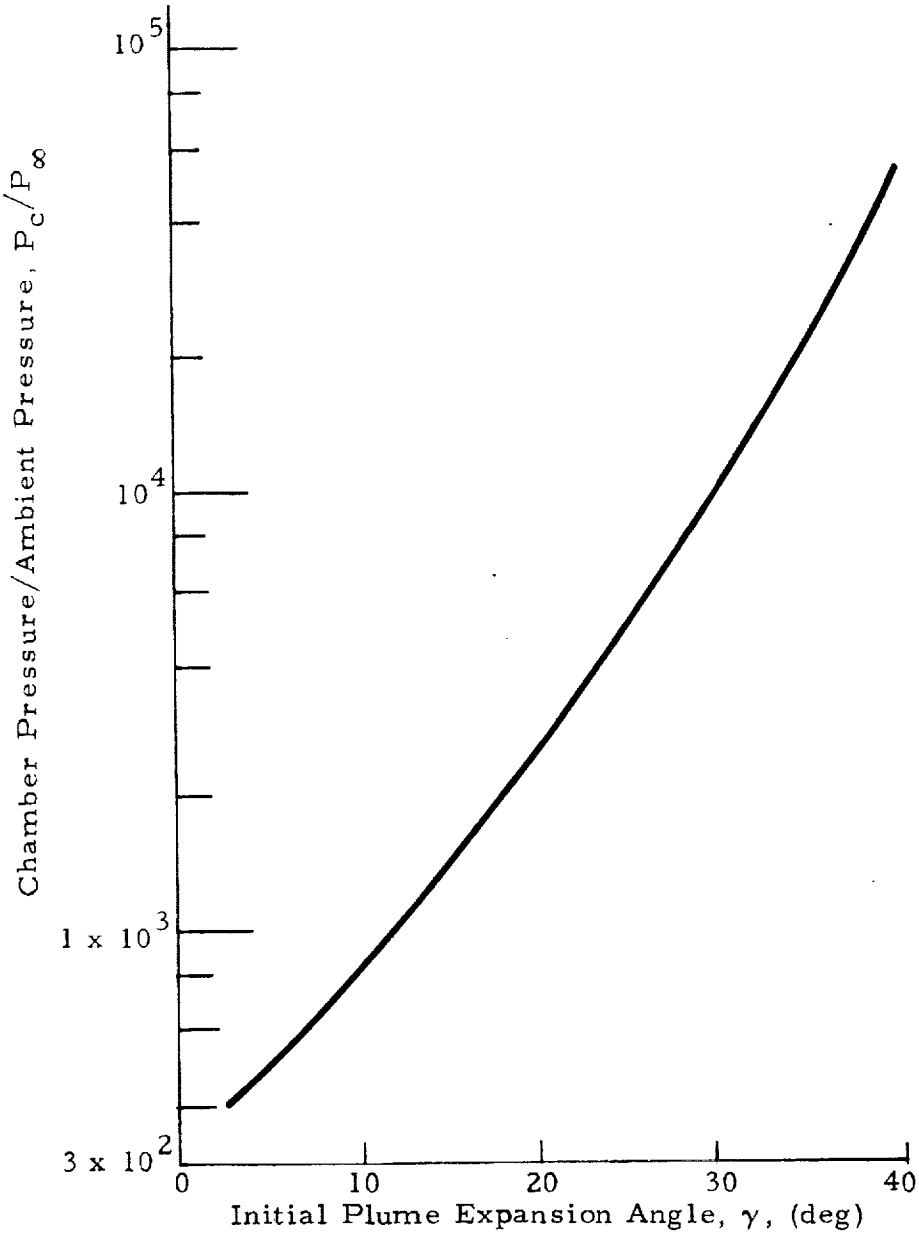

Fig. 2-1 - Initial Plume Expansion Angle for SRB Plumes as a Function of Chamber/Ambient Pressure Ratio

of thermal radiation leaving the plume. At high altitudes and corresponding high values of P_c/P_∞, the plume expands considerably which reduces gas temperatures. Typical variations of chamber pressure during a nominal trajectory are shown in Table 2-1 as a function of time. Also shown are the ambient pressure and the ratio P_c/P_∞.

The influence that P_c/P_∞ exerts on the plume flow field is often referred to as "an altitude effect" since the magnitude of the pressure ratio is largely determined by changes in P_∞. However, there are other characteristics of SRB plumes that are due to variations in altitude as well as vehicle velocity. At low altitudes viscous mixing between the quiescent atmosphere and the plume leads to afterburning at the plume boundary. This occurs because the plume tends to be fuel-rich due to incomplete burning of the propellant in the combustion chamber. Afterburning caused by the mixing of oxygen in the atmosphere with the fuel-rich plume can greatly increase the heat load to the base plane of the Space Shuttle due to the plume boundaries proximity to the base region. Another parameter influencing plume structure that is somewhat dependent on altitude is the approach Mach number. The approaching freestream tends to lessen the amount of plume expansion at high values of freestream dynamic pressure. On typical trajectories freestream dynamic pressure is maximum at 35,000 to 45,000 feet and then diminishes with altitude. To include these altitude effects on the SRB flow field in the thermal radiation calculations, a sophisticated treatment of the flowfield problem is required. To a large extent, this is available in Lockheed's two-phase SRB flowfield code. Some SRB flowfield predictions from this code are shown in Section 2.3.

2.2 GEOMETRY MODEL FOR SRB PLUME STRUCTURE

The properties of the gaseous constituents and the Al_2O_3 particles vary along the axial and radial coordinates of the plume. To make these variations in plume properties easily handled by a math model for the solution of the radiation transport problem, it is necessary to represent the spatial variations by means of relatively simple geometries but still provide a representative description of the plume. This can be provided by considering the plume

Table 2-1

TYPICAL VARIATIONS IN CHAMBER PRESSURE, AMBIENT PRESSURE AND P_c/P_∞ DURING NOMINAL SPACE SHUTTLE TRAJECTORY

Time (sec)	P_∞ (psia)	P_o (psia)	P_c/P_∞
2	14.7	768.8	52
4	14.7	781.5	53
6	14.6	792.1	54
10	14.3	802.7	56
16	13.5	814.1	60
18	13.2	817.6	62
20	12.8	812.2	63
22	12.4	774.5	63
24	11.9	744.9	62
32	9.9	661.1	66
40	7.8	593.0	76
48	5.8	543.7	99
50	5.4	534.3	98
52	4.9	525.0	109
54	4.4	527.9	119
56	4.0	532.0	132
58	3.6	534.5	147
64	2.6	544.7	207
72	1.5	568.5	367
80	0.9	584.3	647
88	0.5	596.3	1190
94	0.3	607.2	2025
96	0.26	611.2	2350
100	0.18	610.8	3390
110	0.07	570.0	8140
114	0.05	488.8	9780

to be constructed of homogeneous regions wherein appropriate values of gaseous and particle properties are defined. These homogeneous regions are stacked along the axis and radius of the axisymmetric flow field. A region is bounded along the radial coordinate by concentric, conical surfaces emanating from a common vertex and is bounded along the axial coordinate by planes at right angles to the conical surface axes (see Fig. 2-2). Properties are defined in a

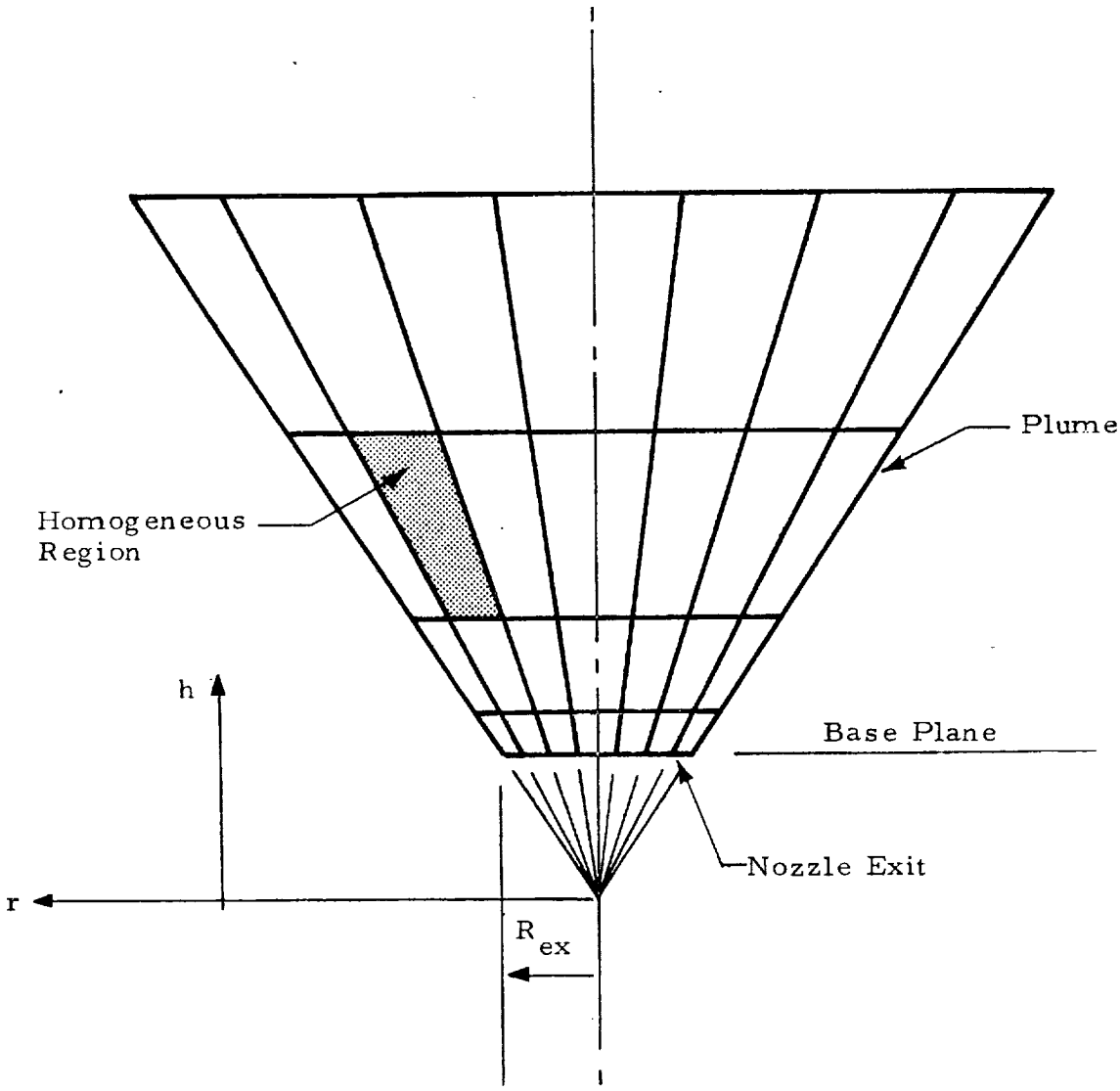

Fig. 2-2 - Geometry Model for SRB Plume Structure

cylindrical coordinate system with its origin at the vertex of the cones. Average properties for each region are calculated based on assigned properties on the four corners of each region. The assigned values for these properties may be determined from a two-phase flow calculation for the gasdynamic definition of the SRB plume using Lockheed-Huntsville's two-phase plume flowfield calculation. However, any valid definition of the spatial distribution of plume properties may be used as input data.

The scheme used for defining properties for each homogeneous region of the plume makes use of volumetric averaging. One plume region is shown in Fig. 2-3. The property P(h, r) is taken to be a linear function of h and r as shown in Eq. (2.1).

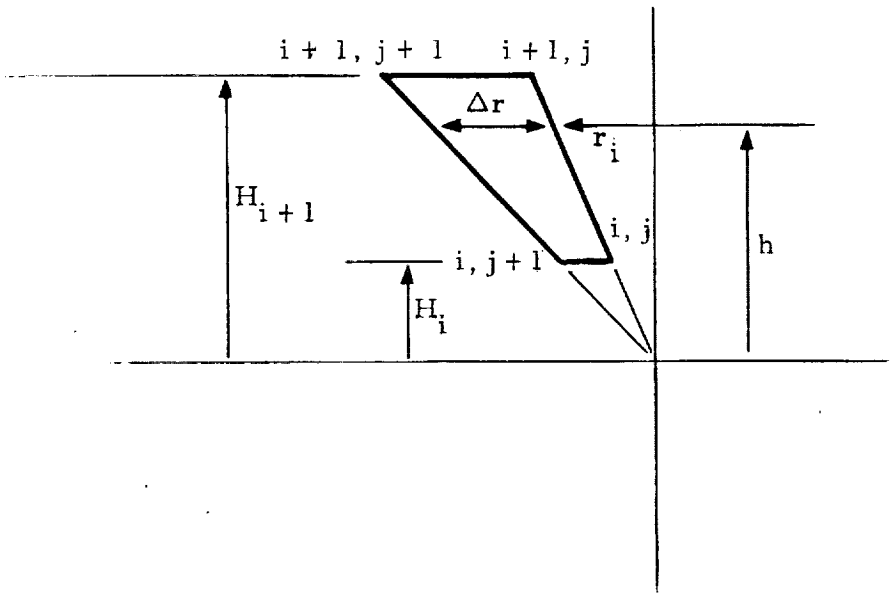

Fig. 2-3 - Property Definition for Plume Region

$$P(h, r) = P_{i,j} + \left.\frac{\Delta P}{\Delta h}\right|_j (h - H_i) + \left.\frac{\Delta P}{\Delta r}\right|_h (r - r_i) \tag{2.1}$$

where

$$\left.\frac{\Delta P}{\Delta h}\right|_j = \frac{P_{i+1,j} - P_{i,j}}{H_{i+1} - H_i} \tag{2.2}$$

and

$$\left.\frac{\Delta P}{\Delta r}\right| = \frac{\left[P_{i,j+1} + \left.\frac{\Delta P}{\Delta h}\right|_{j+1} (h - H_i)\right] - \left[P_{i,j} + \left.\frac{\Delta P}{\Delta h}\right|_j (h - H_i)\right]}{\Delta r} \tag{2.3}$$

The average value for the property P is found by integrating P(h, r) over the volume of the region and dividing by the volume of the region.

$$\bar{P} = \int_V P(h, r)\, dV \Big/ \int_V dV \tag{2.4}$$

Average values for the following plume properties are assigned to each plume region by means of the above averaging technique:

- Particle number density, parts/ft^3 (parts/cm^3)
- Particle temperature, R (K)
- Particle radius, ft (microns)
- Gas temperature, R (K)
- Static pressure, atm
- Mole fraction for CO, (-)
- Mole fraction for CO_2, (-)
- Mole fraction for H_2O, (-), and
- Mole fraction for HCℓ, (-)

The above properties result from a two-phase flowfield calculation for the SRB plume using Lockheed's code. The mole fractions of the principle gaseous emitters (CO, CO_2, H_2O and $HC\ell$) are influenced by the method with which the plume chemistry is modeled. Available options for simulating plume chemistry are provided by using equilibrium chemistry properties or non-equilibrium chemical kinetics. However, representative calculations of SRB plume chemistry is provided by using equilibrium chemistry.

2.3 EXAMPLES OF SRB FLOW FIELDS

Some results of Lockheed's two-phase flowfield calculations for SRB plumes are presented in this section. Data are shown for a sea level plume without an afterburning calculation, for a sea level plume with afterburning, and for a plume at an altitude of 72,000 feet without afterburning. Figures 2-4, 2-5 and 2-6 show the boundaries for the gaseous and particle plumes. The particle plume boundary is defined by the limiting streamline of the particle trajectories at the edge of the plume. The limiting streamline (the streamline beyond which there are no more particles) is usually defined by the smaller particles in the flow field which are accelerated more rapidly in the radial direction by pressure gradients in the expanding plume than are the large particles. Defining the gaseous boundary is a much more difficult task, particularly for low altitude plumes where mixing with the ambient atmosphere occurs along with afterburning. The plume boundary for the sea level plume (Fig. 2-4) can be taken as the inviscid boundary when a mixing and afterburning calculation is not considered. The gaseous plume boundary for the afterburning simulation (Fig. 2-5) is taken to be the region where the gases in the afterburning shear layer drop below 3000 R (1667 K). The gaseous plume boundary for the plume at 72,000 feet (Fig. 2-6) is defined by the inviscid plume.

Also shown in Figs. 2-4, 2-5 and 2-6 are the grids for approximating the property variations with homogeneous regions stacked along the axis and radius of the plume. Flowfield properties are supplied at the intersections of the conical rays and the horizontal lines. For grid points that lie outside the plume boundaries, the property values are simply set equal to zero.

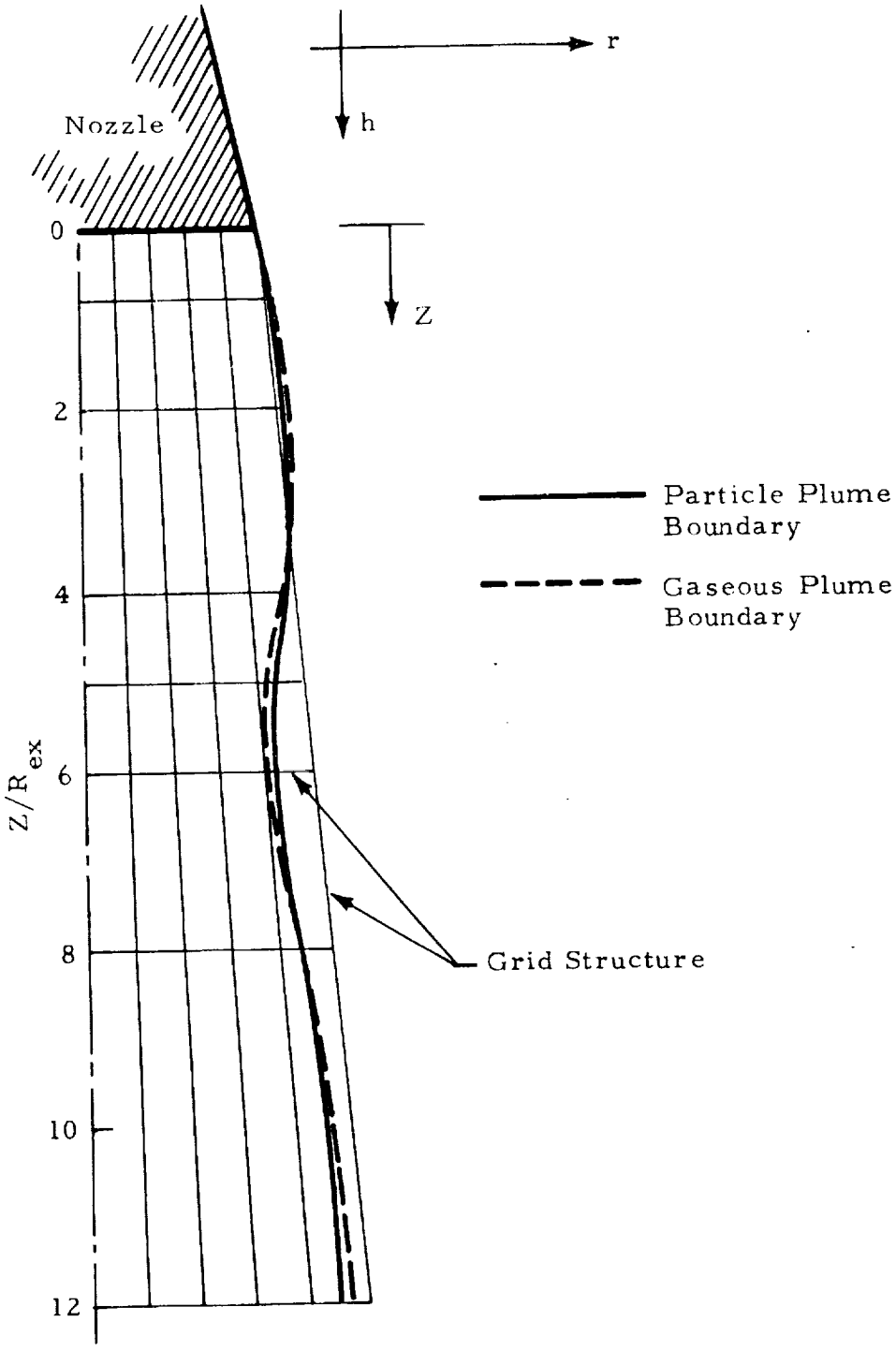

Fig. 2-4 - Gaseous and Particle Plume Boundaries for SRB Sea Level Plume Without Afterburning

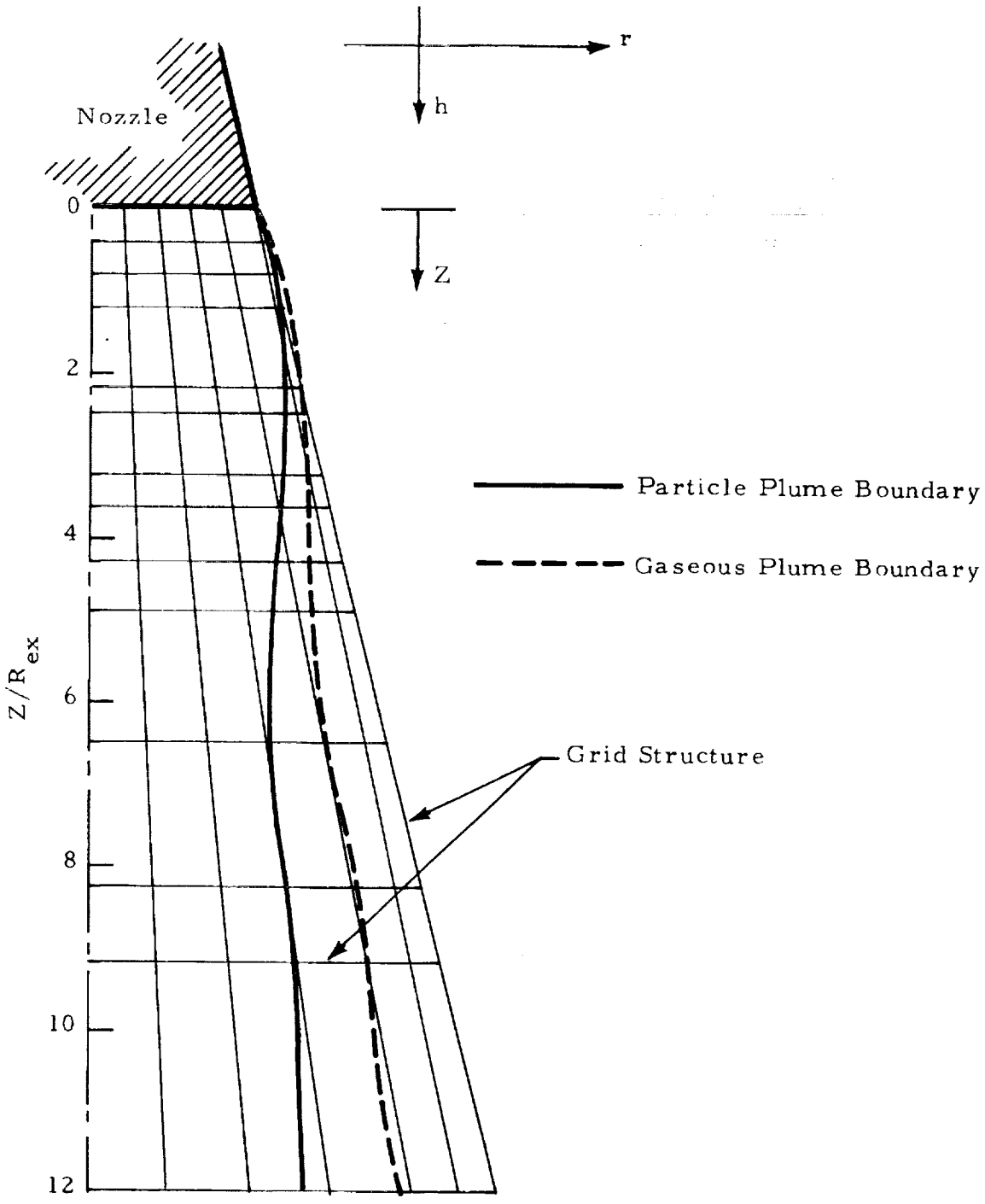

Fig. 2-5 - Gaseous and Particle Plume Boundaries for SRB Sea Level Plume with Afterburning

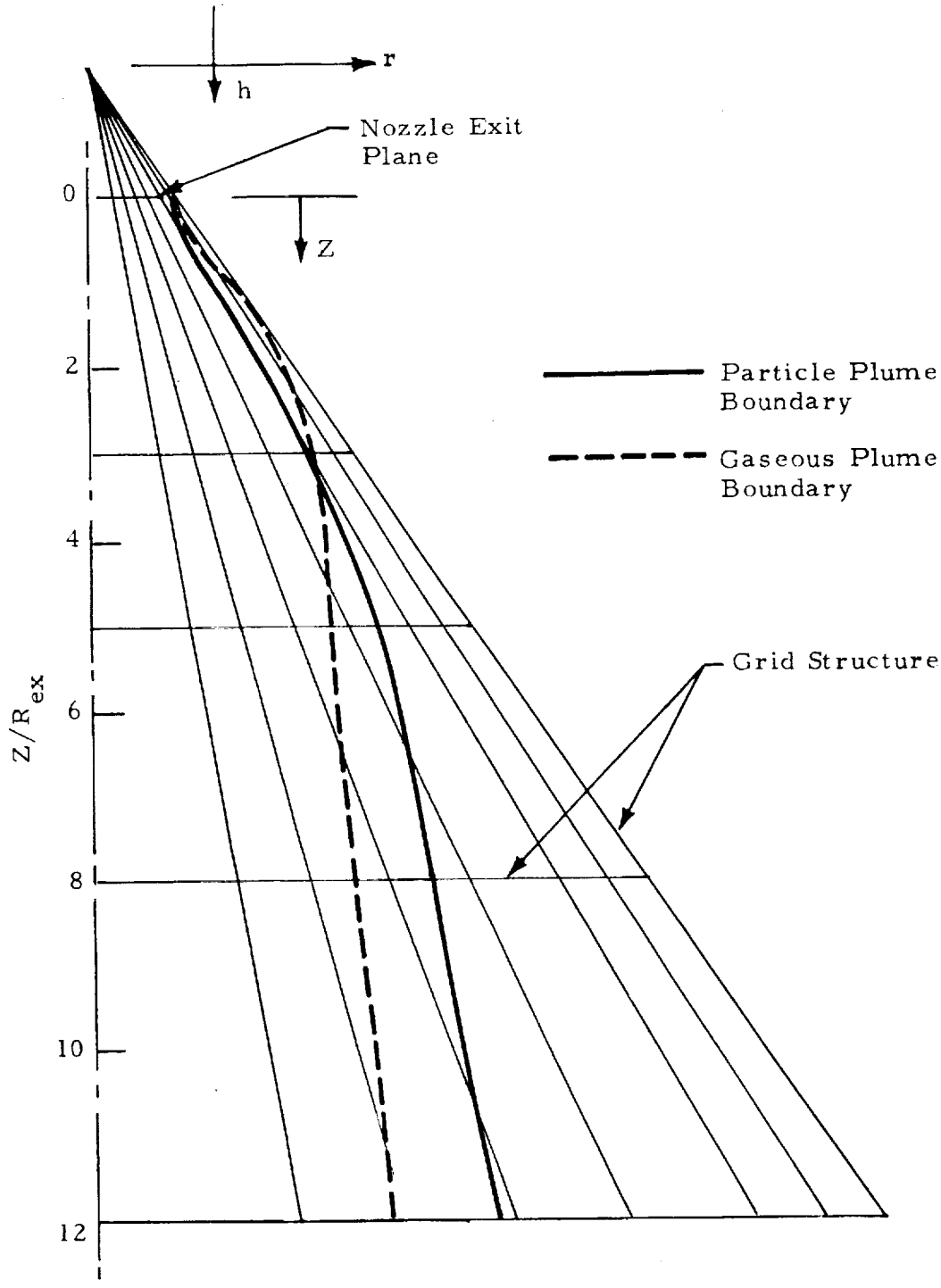

Fig. 2-6 - Gaseous and Particle Plume Boundary for 72,000 ft SRB Plume

This is particularly evident for the 72,000 foot plume where the large initial expansion angle at the nozzle exit plane requires a large cone angle for the outer grid rays. However, the plume flow field expansion is retarded downstream (at $Z/R_{ex} = 6$) by the approaching freestream which has a Mach number of 2.5 at the 72,000 foot trajectory point.

Figure 2-7 shows the radial distributions of the properties of the $A\ell_2O_3$ particles that enter into thermal radiation calculations, namely particle number density (N), particle radius (r_p) and particle temperature (T_p). These data are shown at three axial stations in the plume $Z/R_{ex} = 0.8$, 4.0 and 11.0. The particle radius tends to drop at the edge of the plume because smaller properties "migrate" to the edge more rapidly than do larger particles as the plume expands down its axis. The particle temperature drops at the edge due to the presence of smaller particles which more quickly adopt the cooler gas temperature. The particle number density diminishes as the flow proceeds down the plume axis because of the expanding volume of the plume. The particle distributions shown in Fig. 2-7 are used for both sea level plumes calculated for afterburning and without afterburning.

The gas temperature and pressure and the mole fractions for the four principle gaseous emitters (CO, CO_2, H_2O and $HC\ell$) are shown in Figs. 2-8 and 2-9 for the sea level plume without an afterburning calculation and with an afterburning calculation. The gas temperature and the mole fractions are strongly influenced by the afterburning calculation as is evident by comparing Figs. 2-8 and 2-9. If mixing in the shear layer between the ambient atmosphere and the plume flow is not considered, the combustibles in the plume are maintained in a chemically frozen state as is indicated by the lack of change (with respect to r/R_{ex}) in the mole fractions shown in Fig. 2-8. However, if afterburning is simulated, a strong combustion process occurs at the plume boundary as is evident from the large changes in the mole fractions at the edge of the plume that results as CO and $HC\ell$ burn to CO_2 and H_2O (see Fig. 2-9). The gas temperature is raised at the edge of the plume. Also, the volume of hot gases that will radiate back to the base plane is increased

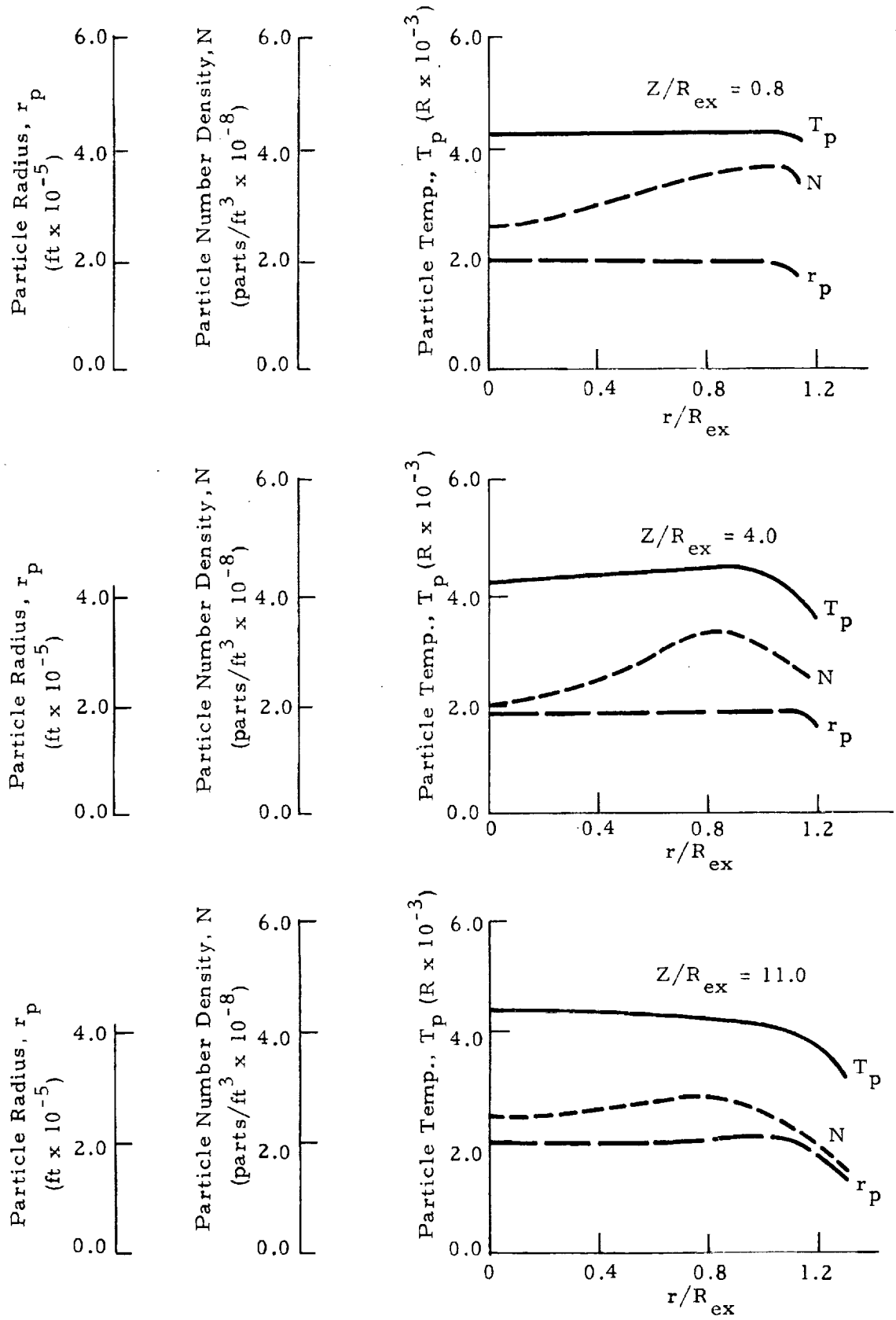

Fig. 2-7 - Radial Particle Property Distributions for Sea Level Plume Without Afterburning

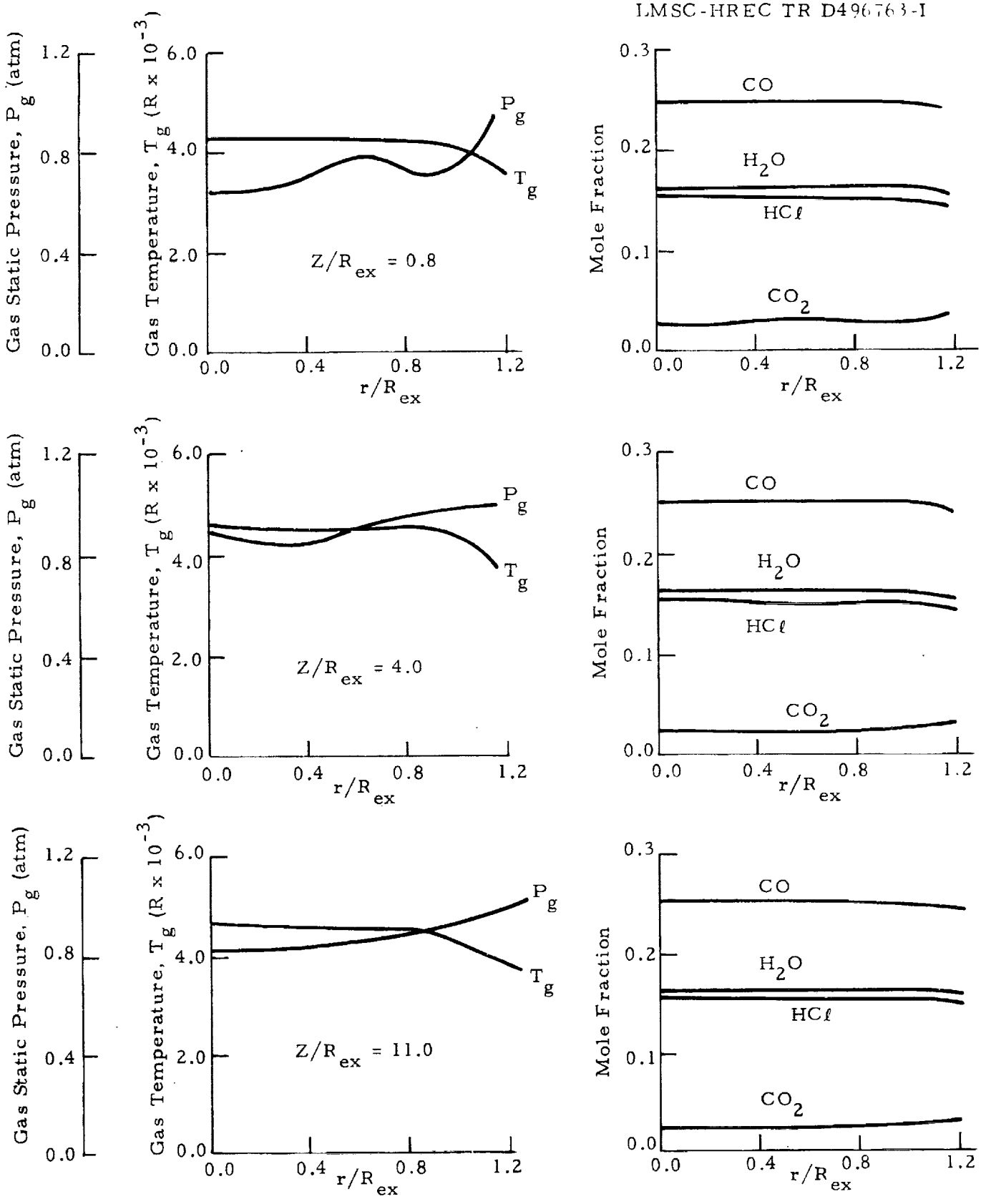

Fig. 2-8 - Radial Gas Property Distributions for Sea Level Plume Without Afterburning

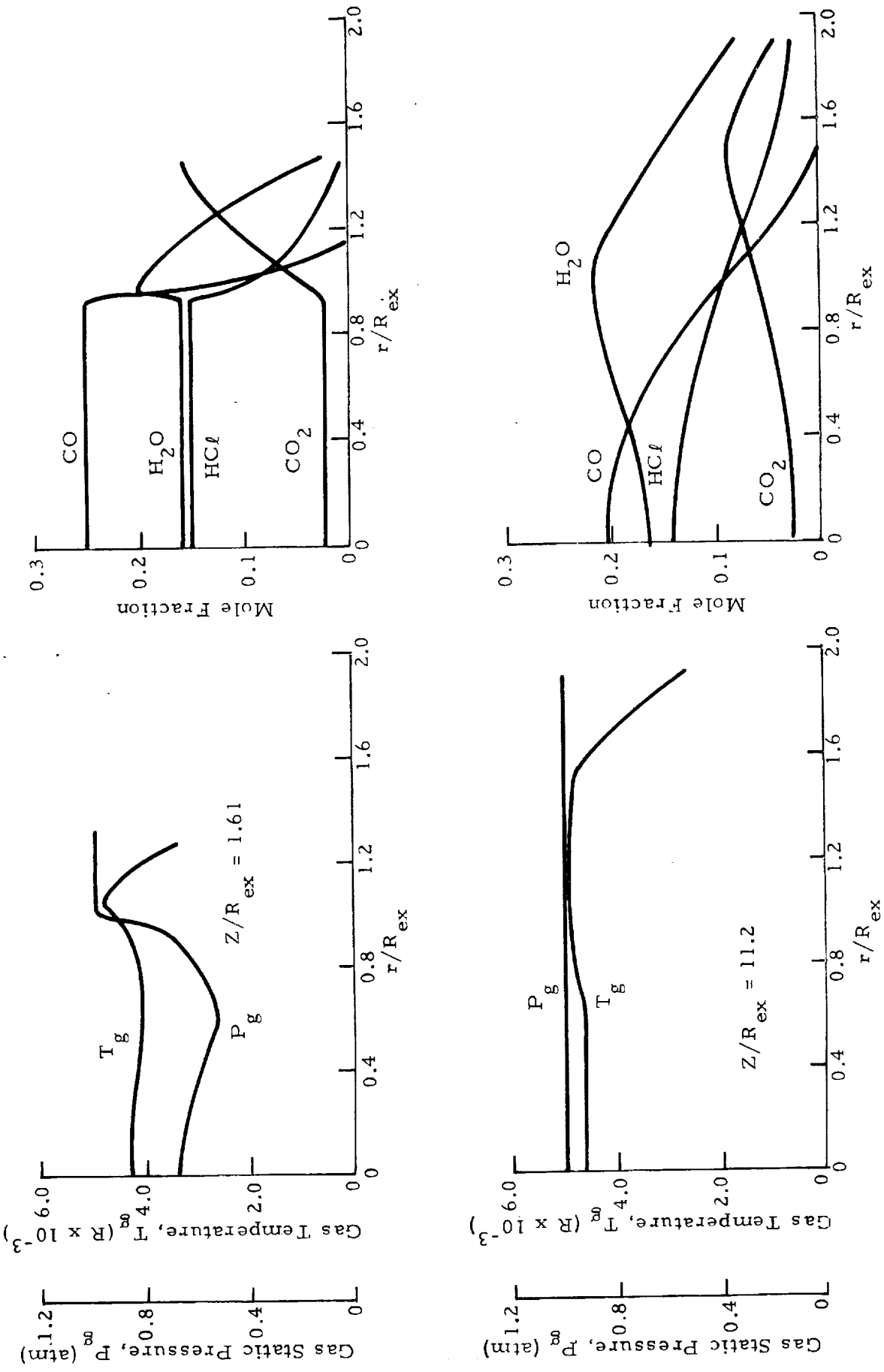

Fig. 2-9 - Radial Gas Property Distributions for Sea Level Plume with Afterburning

because the atmosphere at the edge of the plume enters into the combustion process. Comparison of Figs. 2-8 and 2-9 shows that the afterburning calculation causes the effective plume to spread considerably at axial stations removed from the nozzle exit plane (Z/R_{ex} = 11.2). The gaseous plume boundary is taken to be at the region where the gas temperature drops below 1667 K.

Property data for a SRB plume at 72,000 feet are shown in Fig. 2-10 (for particles) and Fig. 2-11 (for gases). The 72,000 feet plume has no afterburning simulation as the ambient atmosphere is rarefied to the point where the amount of afterburning is expected to be low.

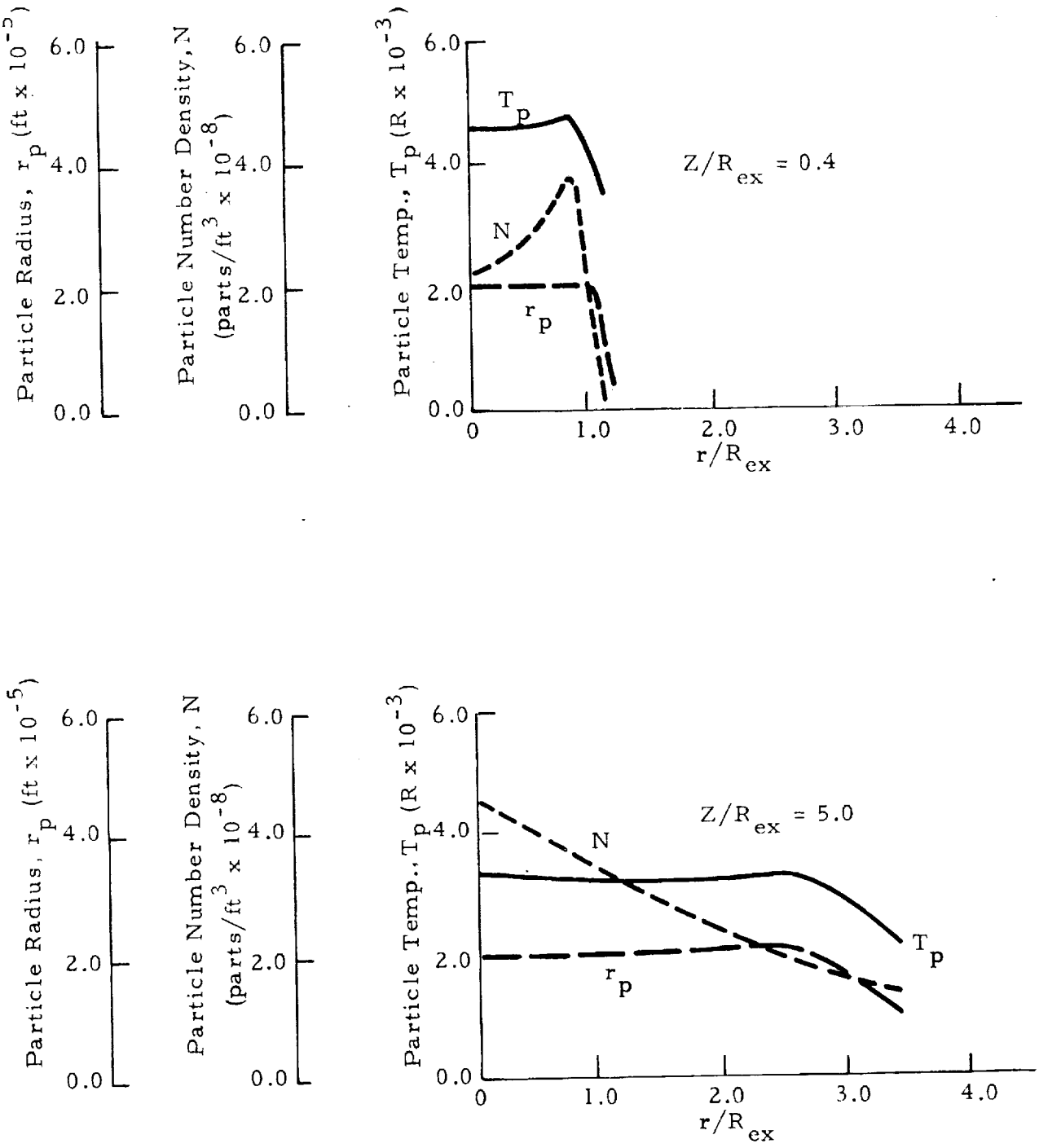

Fig. 2-10 - Radial Particle Property Distributions for SRB Plume at 72,000 ft Altitude

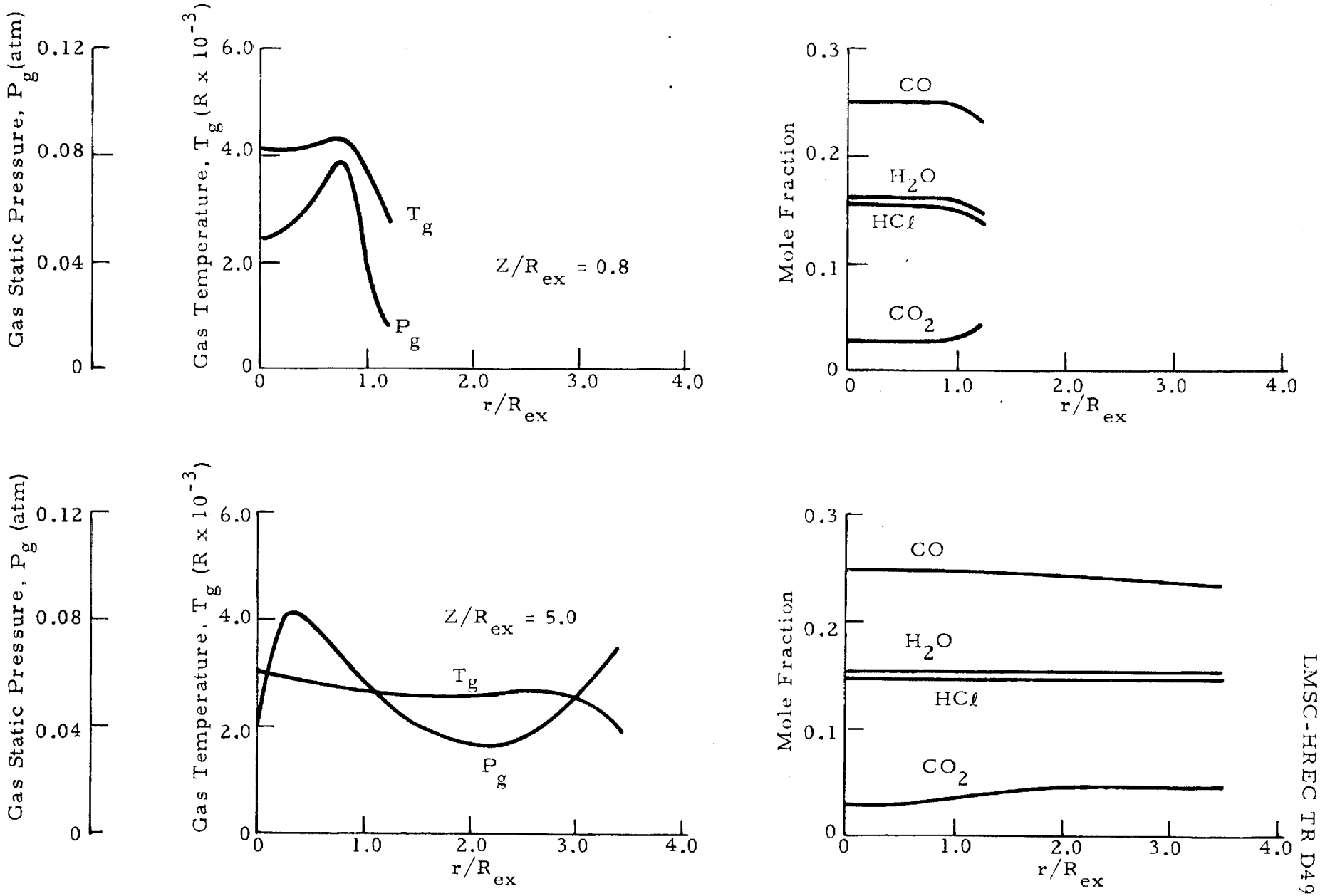

Fig. 2-11 - Radial Gas Property Distributions for SRB Plumes at 72,000 ft Altitude

3. SPACE SHUTTLE BASE HEATING FROM DUAL SRB PLUMES

The two SRBs astride the external tank (ET) on the Space Shuttle contribute significantly to the heat loads incident on spacecraft surfaces in the base region. In order to calculate radiant heat rates to these surfaces with realistic representation of the SRB plume radiation field, it is necessary as a first priority to establish the magnitudes and distribution of flowfield properties which contribute to the radiant energy leaving the plume. This information can be provided by Lockheed's two-phase flowfield code as described in Section 2.

3.1 DUAL SRB PLUME GEOMETRY MODEL FOR THERMAL RADIATION

Two SRB plumes are considered in the SRB thermal radiation model. The plume locations are defined in a central Cartesian coordinate system (X_1, X_2, X_3) centered between the dual SRB nozzles. The X_1 coordinate is parallel to the plume Z-axis at zero gimbal. The X_2 coordinate passes through the center of the exit plane of the two SRB nozzles and the X_3 coordinate is at right angles to X_1 and X_2. Both plumes are considered to be axisymmetric and the distributions of plume properties along the axial and radial coordinates are approximated by defining homogeneous regions along the axis and radius of the plume as outlined in Section 2. The geometry model allows the SRB plumes to be gimbaled parallel to one another in the yaw and pitch planes or they may be gimbaled independently with different yaw and pitch gimbal angles. Figure 3-1 shows the dual plume geometry model for zero gimbal, parallel gimbal and independent gimbal in the yaw plane. The same type of gimbal angle options are available for gimbal in the pitch plane. Simultaneous gimbal in both yaw and pitch planes may also be modeled.

The SRB plume may be considered to extend several hundred feet downstream of the nozzle exit plane. However, for purposes of calculating radiant

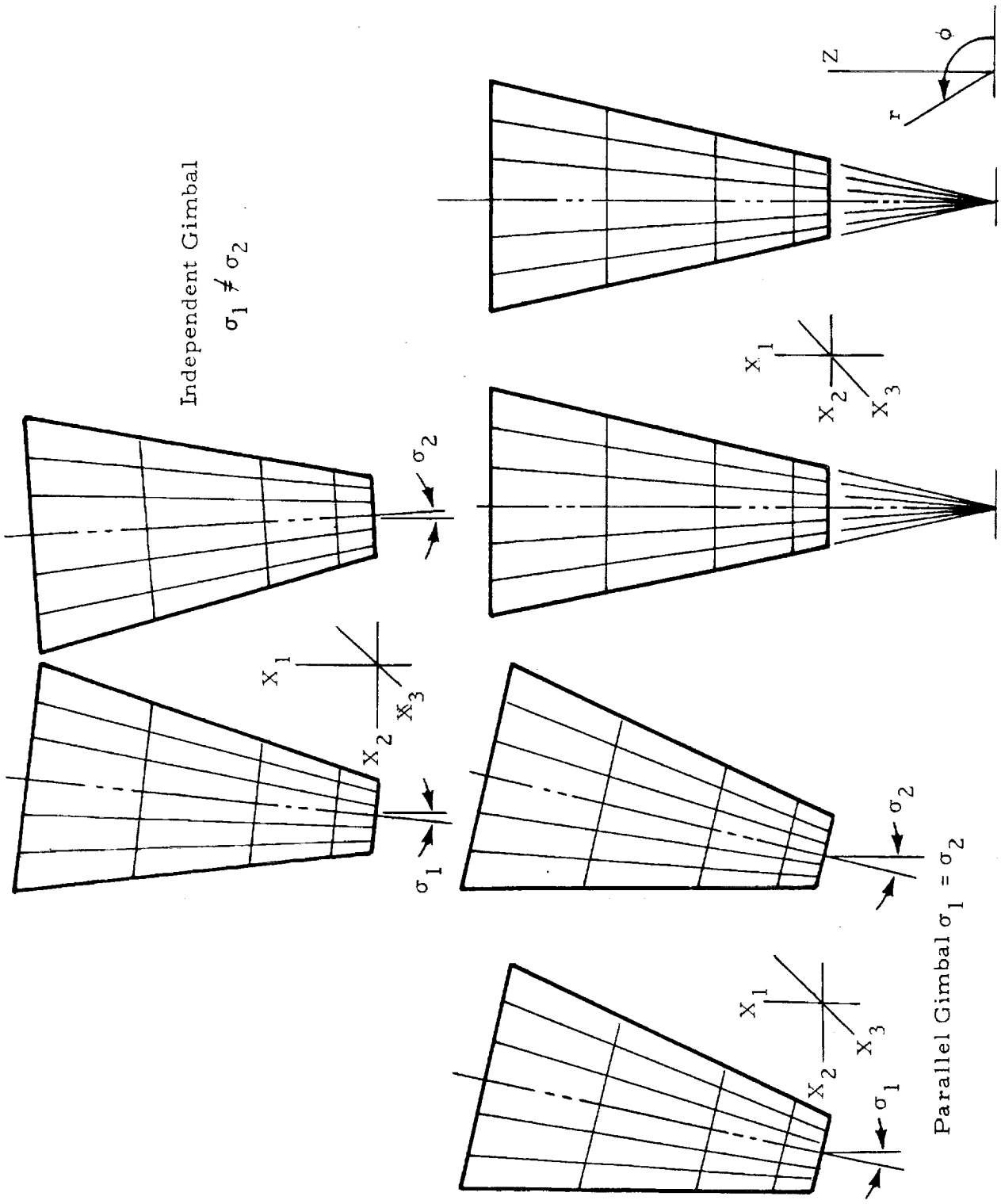

Fig. 3-1 - SRB Plumes Gimbaled in Yaw Plane

heat loads to the base region of the Space Shuttle, only a finite portion of the plume need be considered. Often the nature of the SRB flow field can be used to determine how much of the plume should be used in calculating radiant heat transfer rates. The variation of plume temperature along the axial coordinate provides a good indication of how significantly portions of the plume will contribute to thermal radiation in the base plane. Usually a plume axial length of 10 to 15 exit radii is sufficiently long to provide good estimates of radiant heating. Longer plume lengths are not necessary because of the diminishing view of the plane to the base region. As the plume length considered for heating rate calculations increases, it is likely that the dual plumes used in the heat rate calculations will intersect. Plume intersection will certainly occur for the finite plume lengths used to simulate plume structures of high altitude plumes because of the high degree of plume expansion at altitude. The dual SRB plume geometry model considers the possibility of plume intersections as will be discussed later in this report.

3.2 THERMAL RADIATION FOR GRAY MEDIA

The spatial distribution of radiant energy leaving the SRB plumes is established by the Monte Carlo method. This method considers the radiant energy to be divided into several discrete bundles of equal energy. These bundles are considered to obey the physical laws that govern the emission, absorption, and scattering of photons. In the Monte Carlo method a large number of these energy bundles (referred to as the sample size) are traced as they undergo simulated emission, scattering, or absorption and subsequent re-emission until they eventually escape from the boundaries of the plume. Upon escaping the plume, the energy bundle travels along a straight line (referred to as a line of sight) as would a photon leaving the plume. This line of sight is easily defined by a linear algebraic expression. In the computer simulation of tracing the energy bundles as they leave the plume, the algebraic definition of the line of sight may be checked to determine if the energy bundle intersects one of the simulated surface geometries that represent spacecraft components. If the bundle strikes one of the Space Shuttle surfaces, the energy contained in the bundle is considered to contribute to the radiant heat

load on that surface. The problem of spacecraft surface heating will be discussed later. This section addresses the formulations required to model magnitude and distribution of thermal radiation leaving SRB plumes.

3.2.1 Thermal Radiation from a Participating Medium

An expression for the magnitude of radiant energy emitted locally in SRB plumes may be obtained by considering the attenuation of radiation intensity in the plume. Consider a volume element of the SRB plume. Contained within the volume element are a homogeneous dispersion of Al_2O_3 particles immersed in the gaseous products of combustion. Although there are several gaseous constituents present, only CO, CO_2, H_2O and HCl contribute significantly to thermal radiation. Radiation intensity at a given wavelength in the volume element will be attenuated in a manner represented by the following expression

$$\frac{dI_\lambda}{dx} = - (N \sigma_{a,\lambda} + K_{a,\lambda}) I_\lambda \qquad (3.1)$$

where

N = particle number density

$\sigma_{a,\lambda}$ = spectral absorption cross section of the particles, and

$K_{a,\lambda}$ = volumetric absorption coefficient of the gas

Imposing the constraints of local thermodynamic equilibrium (LTE) requires that the net change of radiation intensity be zero along a given line of sight. This condition is satisfied when there is an amount of energy emitted by the volume element equal to that absorbed. Let J_λ represent local emission in the volume element into the solid angle about the line of sight. Then imposing LTE requires

$$\frac{dI_\lambda}{dx} = - (N \sigma_{a,\lambda} + K_{a,\lambda}) I_\lambda + J_\lambda = 0 \qquad (3.2)$$

or

$$J_\lambda = (N \sigma_{a,\lambda} + K_{a,\lambda}) I_\lambda \qquad (3.3)$$

Equation (3.3) is applicable for an incremental solid angle, $d\omega$, about the line of sight under consideration. Integrating Eq. (3.3) over 4π steradians and over a finite volume gives

$$J_\lambda = 4 \left(N \sigma_{a,\lambda} E^p_{b,\lambda} + K_{a,\lambda} E^g_{b,\lambda}\right) V \qquad (3.4)$$

where

$E^p_{b,\lambda}$ and $E^g_{b,\lambda}$ = spectral black body functions for the particles and gases, and

V = volume under consideration.

Equation (3.4) represents the spectral radiant energy emitted by a homogeneous volume of particles and gases under conditions of LTE. Rigorous calculations of thermal radiation leaving a volume of emitting, absorbing, and scattering medium would account for the influence of wavelength dependent properties. However, for purposes of calculating the total thermal radiation heat load, the gray approximation to the radiation transport phenomenon is often sufficient. Simulating the coupled radiation from the particles and the gaseous emitters in SRB plumes as a gray medium requires that appropriate wavelength averaged values be obtained for the absorbing and scattering properties of the medium. The gaseous constituents of the plume are almost pure absorbers of radiant energy. Conversely, the $A\ell_2O_3$ particles are almost pure scatterers of radiant energy when they are in the solid phase. Liquid $A\ell_2O_3$ particles, however, can have significantly large absorption cross sections.

3.2.2 Gray Absorption Coefficients for SRB Plume Gases

Gases tend to absorb and emit radiant energy in discrete wavelength bands. The absorbing properties of the gases can change by several orders of magnitude over a small wavelength interval. An appropriate averaging of absorbing properties over the wavelength spectrum must be performed in order to calculate meaningful radiant heating rates. Abu-Romia and Tien[2] have made a study of appropriate mean absorption coefficients to be used in thermal radiation calculations for gases. It is recommended in Ref. 2 that the

Planck mean absorption coefficient be used for gases that approach the optically thin limit. Considering the gaseous phases alone, the thin limit is approximated in SRB plumes and the Planck mean absorption coefficient becomes a valid means of removing spectral dependence from plume properties in the thermal radiation calculations.

The Planck mean absorption coefficient is defined as

$$\bar{K}_a(T, P) = \frac{\int_0^\infty K_{a,\lambda}(\lambda, T, P)\, E_{b,\lambda}(\lambda, T)\, d\lambda}{\int_0^\infty E_{b,\lambda}(\lambda, T)\, d\lambda} \qquad (3.5)$$

wherein the spectral variations of the volumetric absorption coefficient is weighted by the blackbody function. The Planck mean absorption coefficient will be independent of wavelength but will still be a function of the partial pressure and temperature of the gas under consideration. Figure 3-2, taken from Ref. 2, presents the Planck mean absorption coefficients for CO, CO_2 and H_2O as functions of gas temperature for a partial pressure of one atmosphere. The Planck mean absorption coefficients shown in Fig. 3-2 are used to represent CO, CO_2 and H_2O as gray gases in the thermal radiation model. Similar data for HCℓ are needed but are not available. In order to include HCℓ in the thermal radiation calculations, the Planck mean absorption coefficient for HCℓ is taken to be that of CO. This approximation should provide a preliminary estimate of the absorption coefficient for CO in that the spectral absorption coefficient for HCℓ is lower than that for CO but, on the other hand, the band for HCℓ subtends a greater fraction of the blackbody function than does CO. These two effects should mitigate against each other and make the approximation more valid.

The Planck mean absorption coefficients shown in Fig. 3-2 were calculated for a partial pressure of 1 atm. In order to use these coefficients directly in calculations of thermal radiation, it is necessary to ratio the coefficient in Fig. 3-2 from 1 atm to the partial pressure of the gas being modeled.

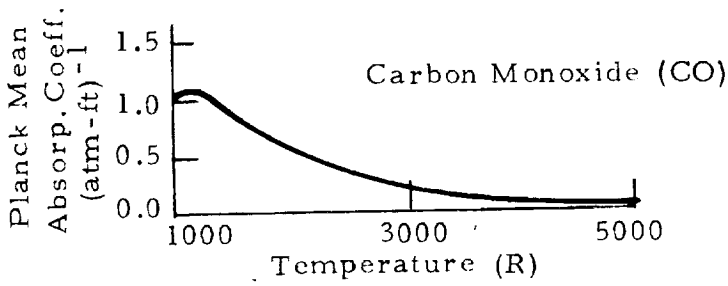

Planck Mean Absorption Coefficient of Carbon Monoxide

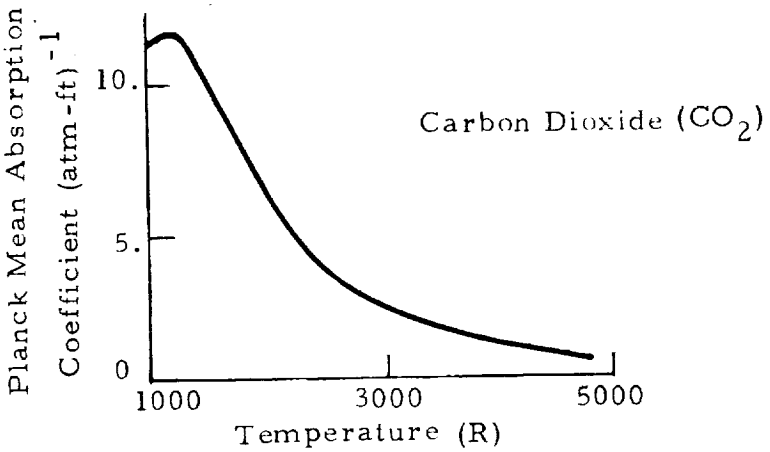

Planck Mean Absorption Coefficient of Carbon Dioxide

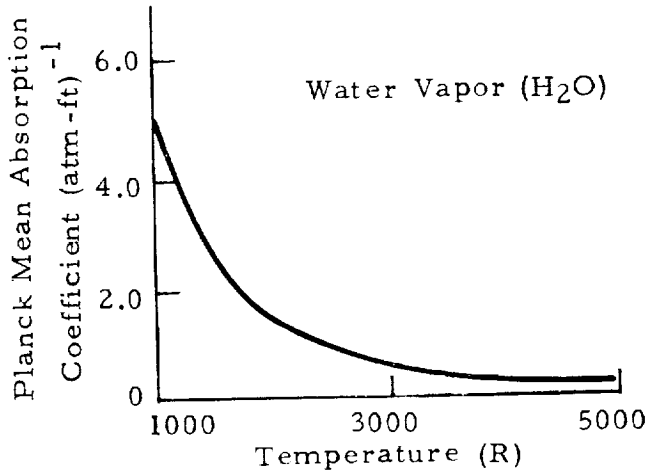

Planck Mean Absorption Coefficient of Water Vapor

Fig. 3-2 - Planck Mean Absorption Coefficients for CO, CO_2 and H_2O at a Partial Pressure of One Atmosphere (from Ref. 2)

Taking this into consideration, the absorption coefficients for CO, CO_2, H_2O and $HC\ell$ are added linearly in order to obtain the absorption coefficient for the entire mixture as in Eq. (3.6).

$$\bar{K}_{a_{mixture}} = \frac{P}{1\ atm} \sum_{\lambda=1}^{4} \bar{K}_{a_i} M.F._i \qquad (3.6)$$

where

P = static pressure of the gas mixture

K_{a_i} = linear absorption coefficient of constituent gases CO_2, CO, H_2O and $HC\ell$, and

$M.F._i$ = mole fraction of constituent gases.

3.2.3 Scattering and Absorbing Properties of $A\ell_2O_3$ Particles

$A\ell_2O_3$ particles can possess substantial absorption characteristics as well, depending on the magnitude of the imaginary portion of the index of refraction. For liquid particles of $A\ell_2O_3$ the index of refraction can be large which leads to relatively large absorption cross sections. On the other hand, solid $A\ell_2O_3$ particles are almost pure scatterers of radiant energy. The calculation of the magnitude of the absorption and scattering of electromagnetic radiation by particulate matter, such as the distribution of $A\ell_2O_3$ particles in the SRB plume, can be done by using the Mie theory; its application to calculating the absorbing and scattering properties of $A\ell_2O_3$ clouds is contained in the following paragraphs.

The problem in scattering of electromagnetic radiation by particulate matter, such as spherical particles immersed in a vacuum, is to relate the properties of the particles (i.e., size, shape, index of refraction) to the spatial distribution of the scattered radiation and to the absorption of radiation by the particulate matter. Basically, there are three regimes for the solution of this problem. The limits of each regime are dependent on a size parameter, namely, the ratio of the circumference of the scattering particle to the wave length of the incident radiation

$$K_a = \frac{2\pi\ r_p}{\lambda} \qquad (3.7)$$

For wave lengths of incident radiation orders of magnitude larger than the dimensions of the particle, the Rayleigh approximation to scattering of the radiation is applicable. For wave lengths orders of magnitude less than the dimensions of the particle, classical optics may be applied to the scattering of the incident electromagnetic radiation. When the wave length of the incident radiation and dimensions of the scattering particle are on the same order of magnitude, recourse to sophisticated treatment of the scattering and absorption phenomenon at the particle is required.

The Mie theory treats the case where the wave length of incident radiation and the size of the particle are comparable. Mie theory is concerned with a very idealized situation, that is, a sphere composed of homogeneous, isotropic material embedded in a homogeneous, isotropic, dielectric, infinite medium irradiated by a plane wave propagating in a specified direction. The dielectric properties of the matrix medium imply that this medium is non-absorbing. The gaseous constituents in the SRB plume are physically representative of such a medium. For a sphere composed of a conducting material, that is, a non-dielectric material, any incident radiation on the sphere is partly absorbed, scattered and transmitted by the sphere. The Mie solution predicts the scattering and absorption cross sections (or efficiencies) as well as the spatial distribution of the scattered intensity. The efficiencies are the extinction, absorption, and scattering cross sections normalized by the geometric cross section

$$Q_{e,a,scat} = \frac{\sigma_{e,a,scat}}{\pi r_p^2} \tag{3.8}$$

The Mie solution is effected in the form of complicated series that involve the Riccati-Bessel functions and Riccati-Hankel functions of increasing order. A computer program for the Mie solution is discussed and listed in Ref. 3.

The extinction and absorption efficiencies and the absorption to extinction ratio for Al_2O_3 particles are shown in Fig. 3-3 as a function of wavelength. Particle radii of 5, 6 and 7 microns are considered and the index of refraction for Al_2O_3 is taken to be 1.8 + .008i. The magnitude of Q_e and Q_a as predicted by Mie theory are actually a function of one variable, namely $K_a = 2\pi r_p/\lambda$, but

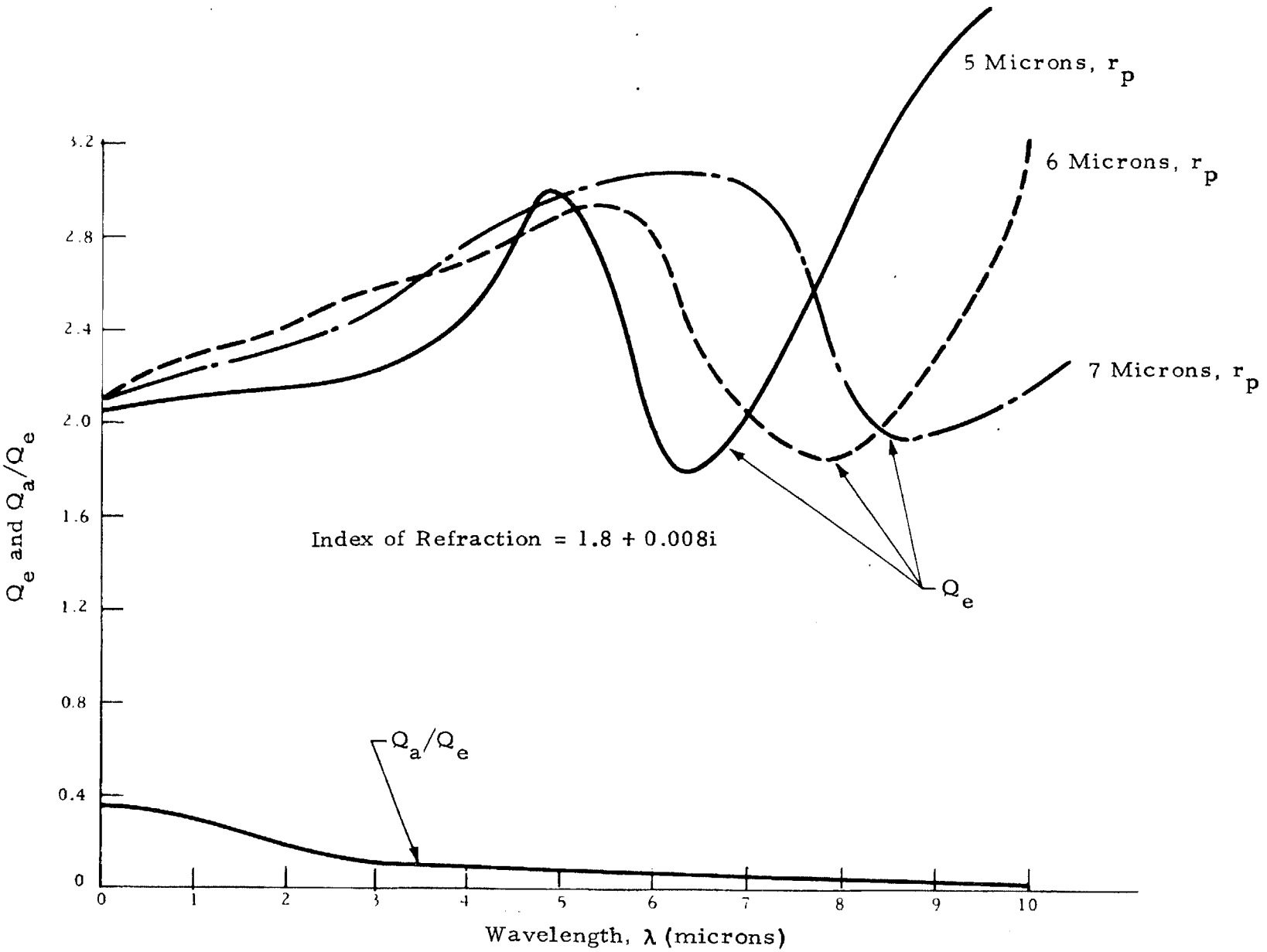

Fig. 3-3 - Spectral Variation of Extinction Efficiency and the Absorption/Extinction Ratio

the physical influence of r_p and λ are perhaps best pointed out in parametric form as in Fig. 3-3. It is clear from Fig. 3-3 that the Q_a (and therefore σ_a) is influenced substantially by wavelength of the radiation field. Although the wavelength dependence of σ_a and σ_e for $A\ell_2O_3$ is less critical than the dependence of linear absorption coefficients for gases, a mean value for σ_e and σ_a for the particle dispersion should be used. The Planck mean is again used for this purpose as shown in Eq. (3.9):

$$\overline{\sigma}_a, \overline{\sigma}_e = \frac{\int_0^\infty \sigma_a(\lambda), \sigma_e(\lambda)\, E_b(\lambda, T)\, d\lambda}{\int_0^\infty E_b(\lambda, T)\, d\lambda} \tag{3.9}$$

3.2.4 Total Thermal Radiation Emitted by the SRB Plume

Using the Planck mean values for the absorbing properties of the constituent gases of the SRB plume and the $A\ell_2O_3$ particles, an estimate may be made of the spontaneous emission of radiant energy of the participating medium that comprises the SRB plume. Using Eqs. (3.6) and (3.9) an expression may be obtained for the gray approximation for radiant energy leaving one region of the plume as shown in Eq. (3.10):

$$\overline{J} = 4\,(N\,\overline{\sigma}_a\,E_b^p + \overline{K}_a\,E_b^g)\,V \tag{3.10}$$

The total radiation emitted by the entire volume of the plume is taken to be the sum of the radiant energy emitted by all regions of the plume.

$$\overline{J}_{total} = 4 \sum_{i=1}^{\text{all regions}} \left(N\,\overline{\sigma}_a\,E_b^p\Big|_i + \overline{K}_a\,E_b^g\Big|_i\right) V_i \tag{3.11}$$

3.3 APPLICATION OF THE MONTE CARLO METHOD TO SRB PLUME THERMAL RADIATION

The Monte Carlo method is generally used for solving problems in which the physics of the phenomenon of interest is understood but in which

the equations that describe the physics are difficult to solve due to complicated boundary conditions. Application of the Monte Carlo method to thermal radiative transfer problems involves establishing a math model of the physics that govern the thermal radiation processes. The physics modeled are those that characterize the emission, scattering and absorption of photons. Basically, the solution consists of a group of a large number of photons throughout the system. For an emitting, scattering, and absorbing medium such as a solid rocket plume, the groups of photons, herein referred to as energy bundles, are considered to be emitted at appropriate points throughout the plume. The bundles are then traced along probable paths that may lead to several scattering and/or absorption events with the $A\ell_2O_3$ particles and the gaseous constituents of the plume. An absorbing collision will, in effect, terminate interest in the subject bundle in that the bundle cannot escape the plume and there is no possibility that the energy in the bundle will be imparted to a target of interest. When an energy bundle is absorbed, a second bundle is considered to be emitted at the absorption site in order to satisfy LTE. If an energy bundle escapes the plume either directly upon emission or after several scatterings and re-emissions, its path upon escaping the plume is analyzed to determine if it hits or misses some predetermined target. If the bundle strikes some target which models a Space Shuttle surface of interest, a portion or all of the energy in the bundle may be considered to be absorbed by the target surface depending on the manner in which the absorbing properties of the surface are simulated.

In order to perform a Monte Carlo simulation of the thermal radiation leaving SRB plumes it is necessary to properly select emission sites and directions as well as to set up geometry models to track energy bundles within the plumes. This section addresses these topics and presents expressions for calculating heat flux to target surfaces.

3.3.1 Distribution Functions

The emission, scattering and absorption (and re-emission) of energy bundles must be simulated in accordance with the physical laws known to

govern photons. Howell[4] demonstrated that appropriate selection of random events may be achieved by setting the cumulative distribution function for the variable equal to a set of random numbers that is uniform between 0 and 1 and then solving for the variable. Sets of random numbers are easily generated by a digital computer. Random number generators are usually supplied in subroutine form as part of the digital computer software. The nature of the random number generator available on the MSFC Univac 1108 is reviewed here. A more detailed discussion is available in Ref. 5. The random number is generated by squaring a six-digit integer and then taking the middle six digits from the squared value which is then divided by 10^6 resulting in a number between 0 and 1. The six digit number which initializes the random number array is supplied as an input value (NSTART) for the Univac random number generator. The same sequence of random numbers is generated if the same value for NSTART is used as an initializing value. Such a sequence is referred to as pseudo-random and the process of the multiplicative congruential method. The method supplies a distribution of random numbers which is uniform over the interval from 0 to 1.

So, a uniform set of random numbers is conveniently supplied as part of the MSFC Univac 1108 software. Now, if the cumulative distributions for the variables of interest in solving the radiation transport problem can be defined, the radiation transport problem can be solved with the Monte Carlo technique. References 4 and 6 outline the method for obtaining cumulative distribution functions which amounts to integrating the probability density function as

$$F(x) = \int_{-\infty}^{x} P(x)\, dx \qquad (3.12)$$

where

$P(x)$ = probability density function
$F(x)$ = cumulative distribution function, and
x = variable of integration.

$P(x)$ defines the probability that an event will lie between x and $x + dx$. As such, the integral of $P(x)$ over all x is unity. Thus, the cumulative distribution function has a value between 0 and 1 for any value of x.

Cumulative distribution functions must be derived which simulate the following phenomena in order to calculate the distribution thermal radiation leaving SRB plumes:

- Uniform distribution of emission sites over each homogeneous region of the plume
- Isotropic emission from a volume element
- Isotropic scattering
- Anisotropic scattering, and
- Attenuation of radiant intensity in a homogeneous medium.

- Selection of Emission Sites

Each region of the plume emits an amount of energy as thermal radiation as defined by Eq. (3.10). The number of spontaneous emissions that are allowed to take place in each region is determined by the fraction of the total energy leaving the plume that is emitted by the given region as shown in Eq. (3.13):

$$N_{e,i} \Big/ \sum_{i=1}^{\text{all regions}} N_{e,i} = \frac{J_i}{J_t} = \frac{\left(N \bar{\sigma}_a E_b^p\Big|_i + \bar{K}_a E_b^g\Big|_i\right) V_i}{\sum_{i=1}^{\text{all regions}} \left(N \bar{\sigma}_a E_b^p\Big|_i + \bar{K}_a E_b^g\Big|_i\right) V_i} \qquad (3.13)$$

where $N_{e,i}$ is the number of energy bundles emitted by region i. In this manner the number of energy bundles emitted by each region is made proportional to the amount of radiant energy leaving the region.

It is also necessary that a uniform distribution of emission sites is achieved within a given region. The SRB plumes are assumed to be axisymmetric and their structure is defined in a cylindrical coordinate system centered at the vertex of the conical surface boundaries. So, proper values must be assigned to the cylindrical coordinates r, ϕ and h. A uniform distribution within the homogeneous region implies that

$$\frac{d N_e}{N_e} = \frac{dV}{V} = \frac{r\, dr\, d\phi\, dh}{V} \tag{3.14}$$

The volume of a region of the plume may be expressed as

$$V = \int_0^{2\pi} \int_{H_i}^{H_{i+1}} \int_{h \tan\gamma_j}^{h \tan\gamma_{j+1}} r\, dr\, d\phi\, dh = \pi \left(\tan^2\gamma_{j+1} - \tan^2\gamma_j\right) \frac{\left(H_{i+1}^3 - H_i^3\right)}{3} \tag{3.15}$$

Reference to Fig. 3-4 will aid in defining the variables. Now

$$\frac{dV}{V} = \frac{2r\, dr}{h^2\left(\tan^2\gamma_{j+1} - \tan^2\gamma_j\right)} \frac{d\phi}{\pi} \frac{3h^2\, dh}{H_{i+1}^3 - H_i^3} \tag{3.16}$$

The fact that the coordinates r, ϕ and h are independent and that Eq. (3.16) integrates to unity, implies that Eq. (3.16) is the joint probability density function for the selection of emission sites within the prescribed volume. The probability functions for each coordinate may be taken as (since coordinates are independent)

$$F(\phi) = \int_0^{\phi} \frac{d\phi}{2\pi} = U_\phi \Longrightarrow \phi = 2\pi\, U_\phi \tag{3.17}$$

$$F(h) = \int_{H_i}^{h} \frac{3h^2\, dh}{H_{i+1}^3 - H_i^3} = U_h \Longrightarrow h = \left[\left(H_{i+1}^3 - H_i^3\right) U_h + H_i^3\right]^{1/2} \tag{3.18}$$

$$F(r) = \int_{h \tan\gamma_j}^{r} \frac{2r\, dr}{h^2\left(\tan^2\gamma_{j+1} - \tan^2\gamma_j\right)} = U_r \tag{3.19}$$

$$\Longrightarrow r = h \sqrt{U_r\left(\tan^2\gamma_{j+1} - \tan^2\gamma_j\right) + \tan^2\gamma_j}$$

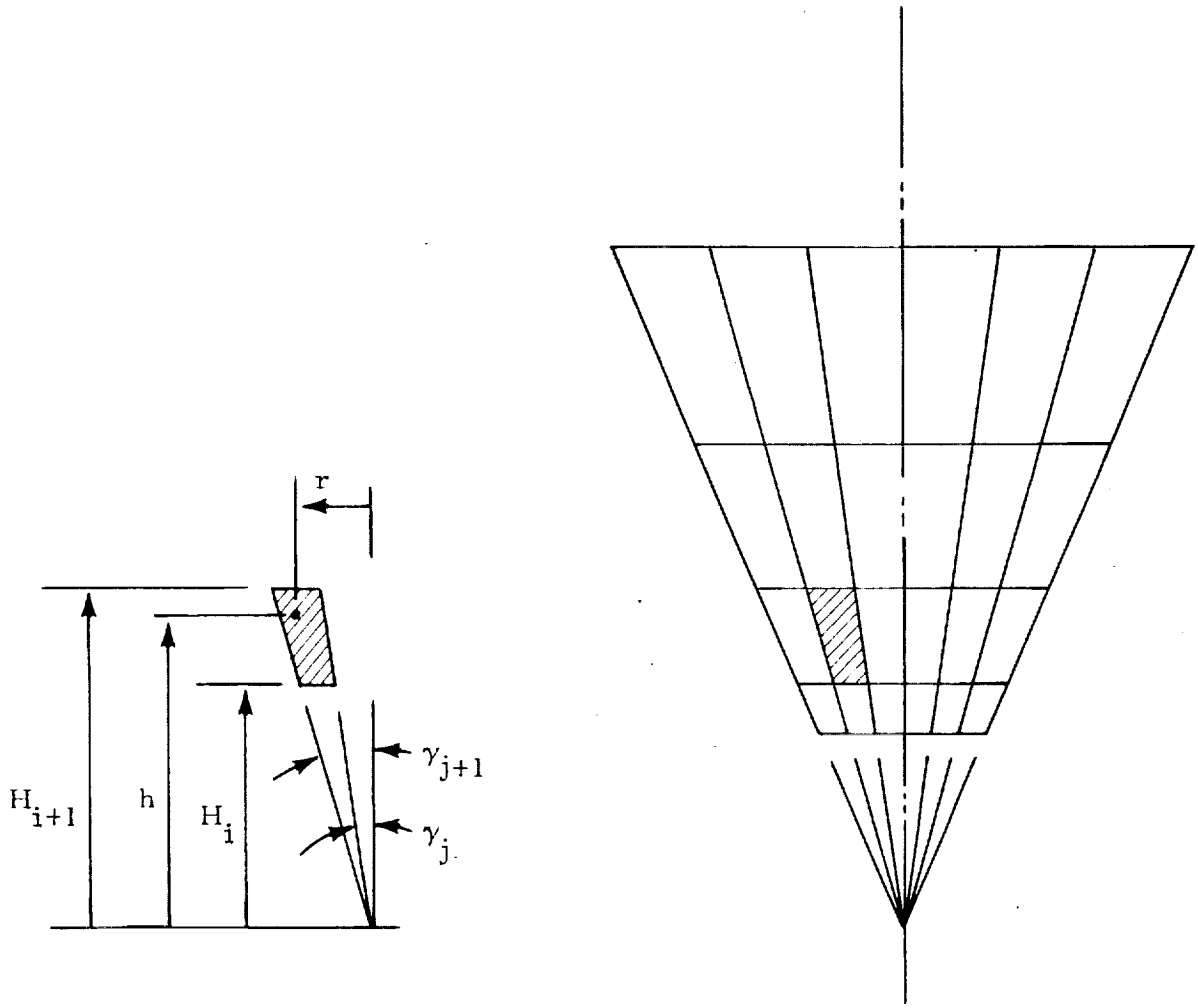

Fig. 3-4 - Definition of Symbols for Emission Site Distribution

Equations (3.17), (3.18) and (3.19) have been attained by integrating (with respect to the coordinate) the probability density function for each coordinate in order to obtain the cumulative distribution function. The cumulative distribution function is then set equal to a random number (U_ϕ, U_h, U_r). Using these equations, the random selection of emission sites may be put into effect with assurance that the emission sites so selected will be uniformly distributed over the given volume.

- Isotropic Emission and Scattering

Once an emission site has been selected it is necessary to select the direction of travel of the subject energy bundle defined in a spherical coordinate system centered at the event site. Isotropic implies that the direction selected will have no bias for any given direction. This requires that the probability of emission into any incremental solid angle, $d\omega$, be identical. Thus,

$$\frac{d\omega}{4\pi} = \frac{\sin\eta \, d\phi \, dh}{4\pi} = \frac{\sin\eta \, dh}{2} \frac{d\theta}{2\pi} \tag{3.20}$$

is the joint probability density function for the selection of coordinates of isotropic emission. Further,

$$F(n) = \int_0^\eta \frac{\sin\eta \, d\eta}{2} = U_\eta \Longrightarrow \cos\eta = 1 - 2\,U_n \tag{3.21}$$

$$F(\theta) = \int_0^\theta \frac{d\theta}{2\pi} = U_\theta \Longrightarrow \theta = 2\pi\,\theta \tag{3.22}$$

Equations (3.21) and (3.22) govern the selection of direction coordinates for isotropic emission as well as isotropic scattering since the selection of coordinates for isotropic scattering is governed by the lack of direction bias.

- Anisotropic Scattering

A Mie theory prediction of the scatter function $S(\eta, \theta)$ for anisotropic scattering from $A\ell_2O_3$ particles is shown in Fig. 3-5. A scatter function for

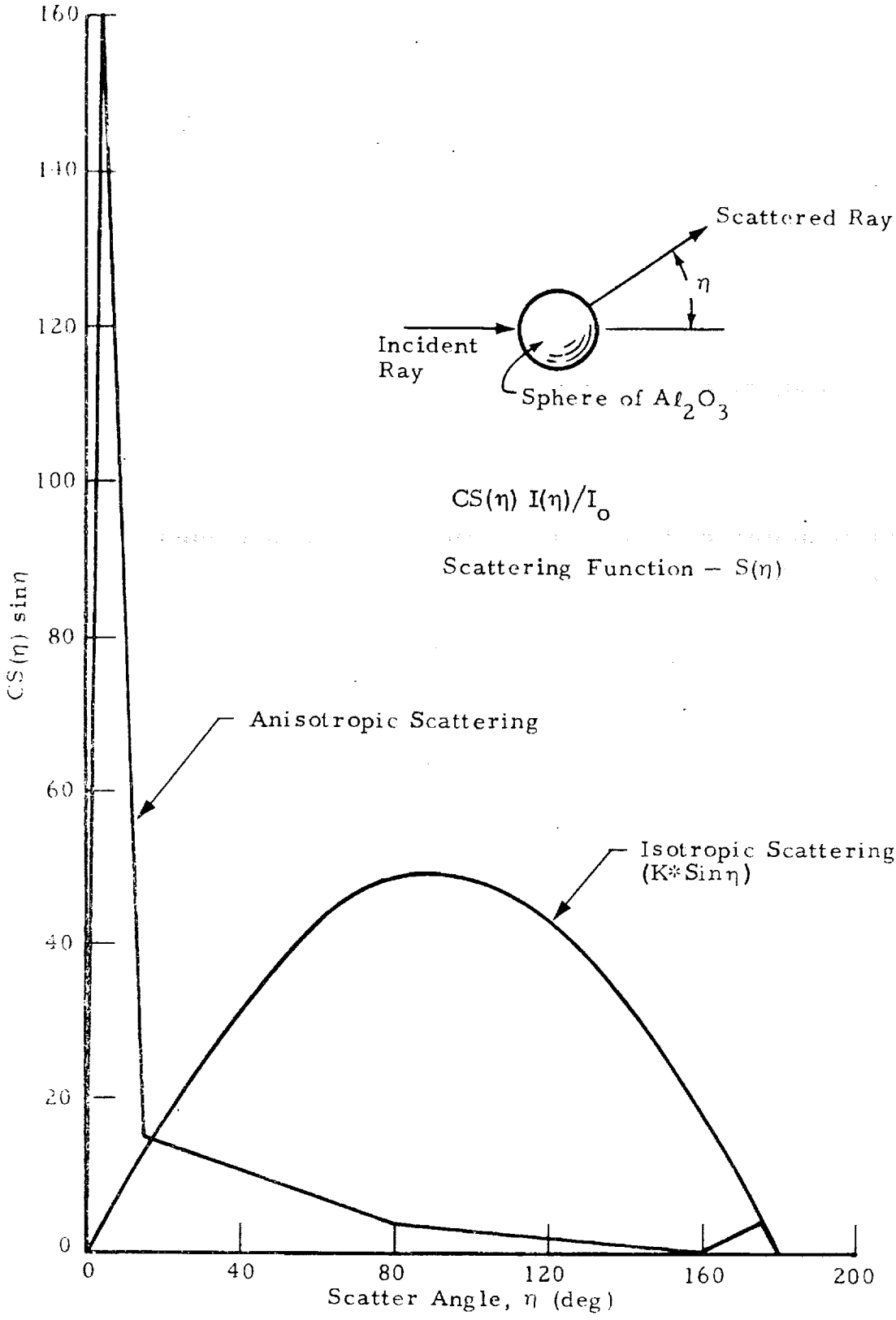

Fig. 3-5 - Averaged Product of Scattering Distribution Function and Sine of Scattering Angle as Predicted by Mie Theory for Wavelengths Between 0.5 to 3.0 μ

isotropic scattering is also shown for comparison. The scatter function is defined as the probability that the scatter direction relative to the direction of the incident radiation will fall into the solid angle, $d\omega'$. Thus,

$$S(\eta, \theta) \frac{d\omega'}{4\pi} = \frac{1}{4\pi} S(\eta,\theta) \sin\eta' \, d\eta' \, d\theta'$$

If unpolarized radiation is considered, an even distribution of scattered radiation about the incident direction results. Then,

$$F(\eta') = \frac{1}{2} \int_0^{\eta'} S(\eta') \sin\eta' \, d\eta' = U_{\eta'} \tag{3.23}$$

and

$$F(\theta') = \frac{1}{2\pi} \int_0^{\theta'} d\theta' = U_{\theta'} \Longrightarrow \theta' = 2\pi \, U_\theta \tag{3.24}$$

The anisotropic nature of scattering by $A\ell_2O_3$ is manifested principally by a strong bias for scattering into the solid angle in the forward direction. In order to simulate this phenomenon some means of solving the integral expression in Eq. (3.23) must be performed. Stockham[7] has discussed a convenient method for doing this. The area under the curve of $S(\eta') \sin\eta'$ versus η' shown in Fig. 3-5 is normalized to unity. This area may be represented by the sum of the areas of triangles and rectangles which constitute the total area under the curve. Then, the polar angle for anisotropic scattering may be obtained from the expression

$$A(\eta') = U_{\eta'}$$

where

$A(\eta')$ is the functional relationship for the summation of triangular and rectangular areas under the curve of $S(\eta') \sin\eta'$ versus η'.

- Attenuation of Radiation Intensity

The intensity of a beam of radiation traversing an absorbing and scattering medium is attenuated in proportion to the intensity of the beam and the optical properties of the medium. This is expressed by Eq. (3.1) wherein

spectral values are considered. Rewriting Eq. (3.1) for a grey medium composed of $A\ell_2O_3$ particles and portions of CO, CO_2, H_2O and $HC\ell$ gives

$$\frac{dI}{dS} = - (N \bar{\sigma}_a + \bar{K}_a) I \tag{3.25}$$

or

$$\frac{dI}{I} = - (N \bar{\sigma}_a + \bar{K}_a) dS \tag{3.26}$$

In a homogeneous region, N, $\bar{\sigma}_a$, and $\bar{K}_a$ are constant and

$$\int_{I_o}^{I} \frac{dI}{I} = - (N \bar{\sigma}_a + \bar{K}_a) \int_{o}^{S} dS \tag{3.27}$$

which integrates to

$$\frac{I}{I_o} = e^{-(N \bar{\sigma}_a + \bar{K}_a) S} \tag{3.28}$$

Equation (3.28) represents the fraction of the original beam intensity at Station S relative to the beam intensity at Station 0. The fraction of intensity removed prior to S is

$$1 - \frac{I}{I_o} = 1 - e^{-(N \bar{\sigma}_a + \bar{K}_a) S} \tag{3.29}$$

and Eq. (3.29) can be thought of as the probability that the path length will be less than or equal to S and thus constitutes the cumulative distribution function for defining S.

$$F(S) = 1 - e^{-(N \bar{\sigma}_a + \bar{K}_a) S} = U_S \Longrightarrow S'_p = \frac{-1}{N \bar{\sigma}_a + \bar{K}_a} \ln U_S \tag{3.30}$$

Since U_S is equivalent to $(U_S - 1)$ in the random sense, S'_p represents the probable length of travel in the medium.

It is convenient to normalize the length dimensions with the exit radius of the SRB nozzle in order to more conveniently represent the optical properties of the plume in terms of optical depths (really optical radius) which are dimensionless. Dividing Eq. (3.30) by R_{ex}

$$S_p = \frac{S'_p}{R_{ex}} = \frac{-1}{(N \bar{\sigma}_a + \bar{K}_a) R_{ex}} \ell n \, U_S \tag{3.31}$$

The optical properties of the $A\ell_2O_3$ particles and gaseous constituents can now be expressed in terms of optical depths based on the nozzle exit radius, R_{ex}.

$$\tau_p = N \bar{\sigma}_a R_{ex} \tag{3.32}$$

$$\tau_g = \bar{K}_a R_{ex} \tag{3.33}$$

$$\tau = \tau_p + \tau_g = (N \bar{\sigma}_a + \bar{K}_a) R_{ex} \tag{3.34}$$

and

$$S_p = -\frac{1}{\tau} \ell n \, U_S \tag{3.35}$$

Equation (3.35) defines, in terms of random numbers, the probable length of travel of an energy bundle prior to either a scatter or absorption event in a single homogeneous region. However, the SRB plume is not homogeneous and is modeled as a composite of homogeneous regions as discussed in Section 2. The probable length of travel for an energy bundle may take it across several different homogeneous regions before it either suffers a scatter or absorption event or escapes the plume. Each region of the plume has its own unique optical properties and attenuates the radiation intensity passing through it at different rates. Consider a beam of radiation passing through a series of homogeneous media as sketched in Fig. 3-6. The line of sight passes through five different regions numbered successively 1 through 5. The length of travel in each region and the optical properties of the region define the rate of attenuation of radiant energy from the beam.

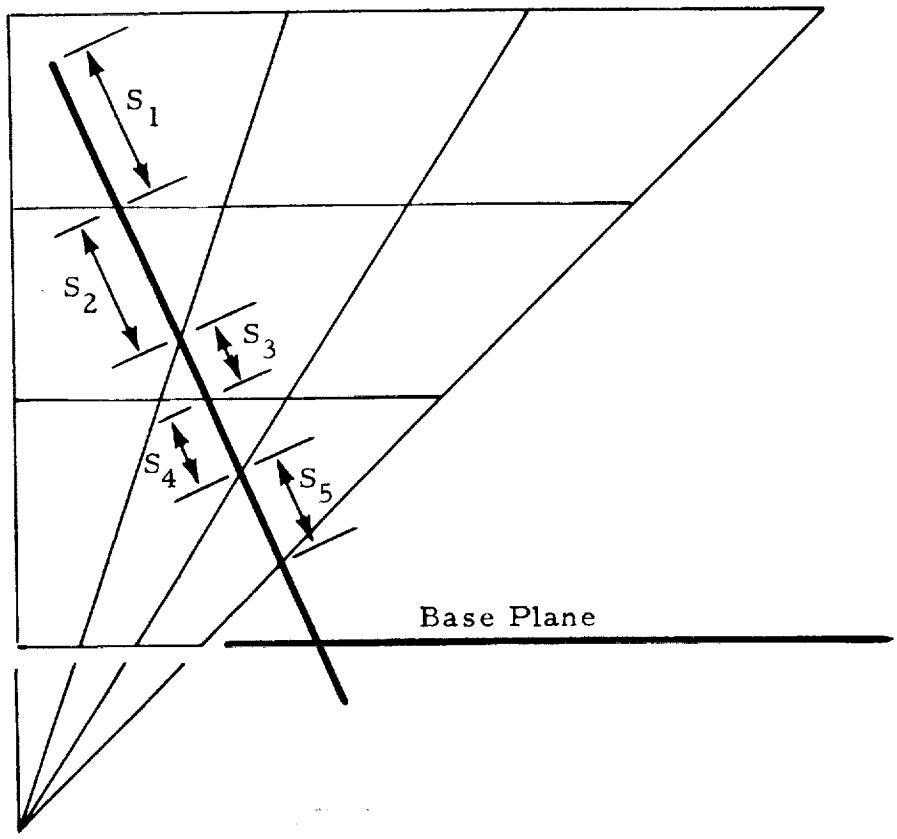

Fig. 3-6 - Line of Sight of Energy Bundle Traversing Several Plume Regions

The attenuation from S = 0 to any station along the line of sight is expressed as

$$\frac{I}{I_o} = e^{-(\tau_1 \ell_1 + \tau_2 \ell_2 + \ldots + \tau_i \ell_i)} \tag{3.36}$$

The probability of collision along the line of sight is

$$1 - \frac{I}{I_o} = 1 - e^{-(\tau_1 S_1 + \tau_2 S_2 + \ldots + \tau_{n-1} S_{n-1} + \left[S_p - (S_1 + S_2 + \ldots + S_{n-1})\right] \tau_n)} \tag{3.37}$$

$$= F(S) = U_S$$

or

$$- \ell n\ (U_S) = \sum_{i=1}^{n-1} \tau_i S_i + \left[S_p - \sum_{i=1}^{n-1} S_i \right] \tau_n \tag{3.38}$$

where the subscript n refers to the region in which the scatter or absorption event occurs. Solving explicitly for the probable length of travel

$$S_p = \sum_{i=1}^{n-1} S_i - \frac{\ell n\ U_S + \sum_{i=1}^{n-1} \tau_i S_i}{\tau_n} \tag{3.39}$$

It is again noted that all lengths are normalized with respect to the exit radius.

- Selection of Scatter or Absorption Event

As the life history of an energy bundle is followed during its residence within the boundaries of the plume, the bundle may be subjected to several scatter and absorption events. Once it is determined that the subject energy bundle will suffer a collision event, it is necessary to specify whether the event is an absorption or a scatter event. This is done by establishing the absorption to extinction ratio for the various regions of the plume. The $A\ell_2O_3$ particles have a significant scattering cross section while the gaseous constituents of the SRB plume are pure absorbers. So an expression for the absorption to extinction ratio for a homogeneous region may be expressed as

$$A/E = \frac{\bar{\sigma}_a / \bar{\sigma}_e\ \tau_p + \tau_g}{\tau} \tag{3.40}$$

A/E is compared with a random number, U. If U is less than A/E, the event is considered to be an absorption event. For U larger than A/E, the event is a scatter event.

3.4 TRACING ENERGY BUNDLES WITHIN THE PLUME

It is necessary to track the location of energy bundles as they are emitted, scattered or absorbed and reemitted during their lifetime within the plume. It is also necessary to identify the region of the plume that the bundle is traversing in order to attenuate the radiation intensity at the appropriate rate. The first step in this procedure is to calculate the elevations of intersections of the line of sight with the conical surfaces which define the boundaries between regions along the radial coordinate of the plume.

3.4.1 Calculation of Line-of-Sight Intersections with Conical Region Boundaries

The method used to calculate the elevations along the Z-axis of intersections of the line of sight with the conical boundaries follows that used by Tien and Abu-Romia.[8] As a first step the distance is calculated between the axis of the conical surfaces and the point where the line of sight pierces a plane at right angles to the axis and passes through the cone vertex. Figure 3-7 shows this intersection point, P_i; h and r_1 locate the point within the plume where an emission, scatter or absorption/reemission event occurs. Using the law of cosines, the distance R between the plume axis and the piercing point is

$$R = \sqrt{r_1^2 + (h \tan\eta)^2 - 2 r_1 h \tan\eta \cos(\pi - (\theta - \phi))} \qquad (3.41)$$

Now referring to Fig. 3-8 the following geometric identities are apparent

$$\tan\gamma = \frac{e}{Z_{i1}} = \frac{d}{Z_{i2}} \qquad (3.42)$$

$$\tan\eta = \frac{i}{Z_{i1}} \qquad (3.43)$$

$$\tan\eta' = \frac{j}{Z_{i1}} = \frac{R+c}{Z_{i2}} \qquad (3.44)$$

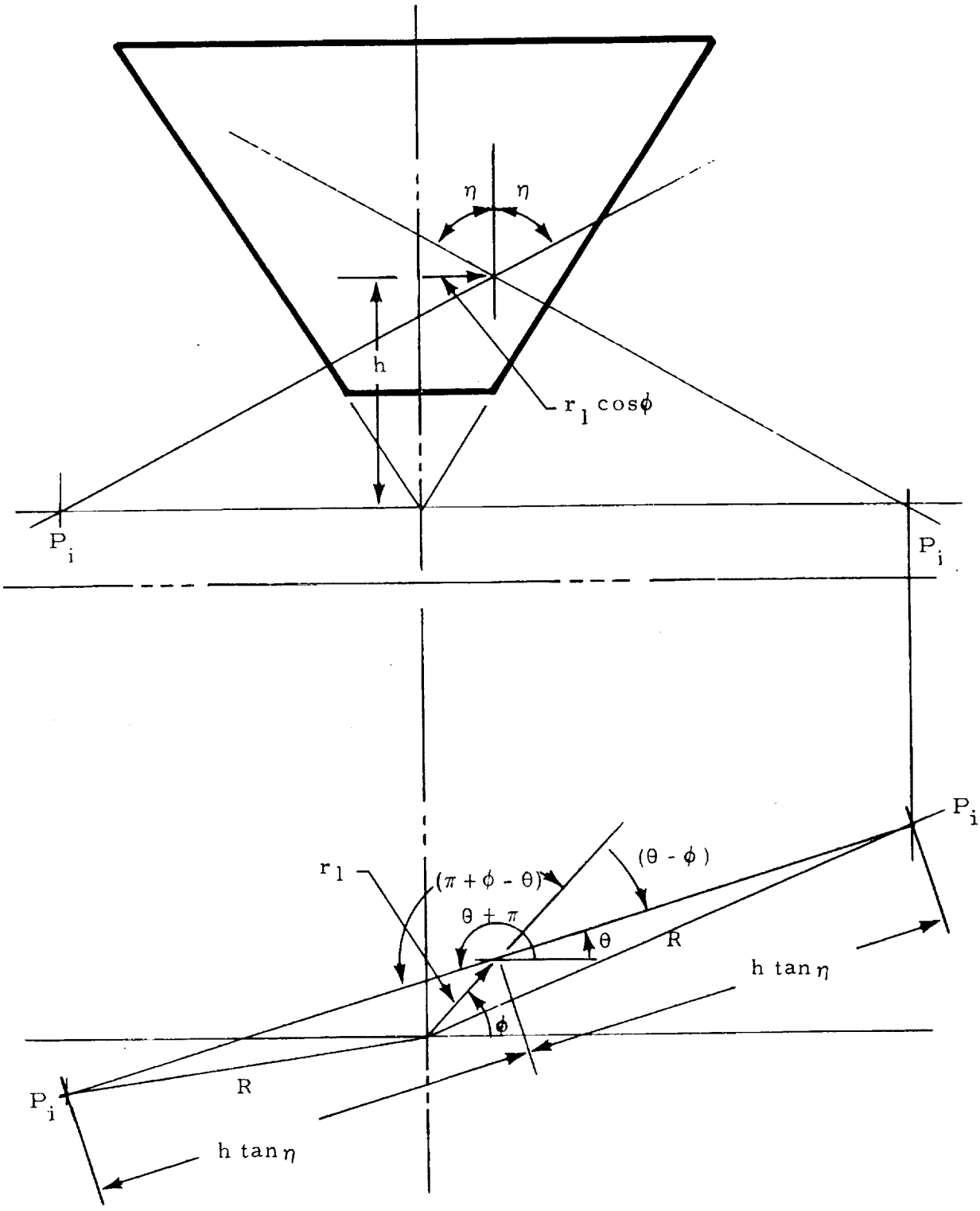

Fig. 3-7 - Orthographic Projections of Line of Sight to Piercing Point in Plane Through Vertex

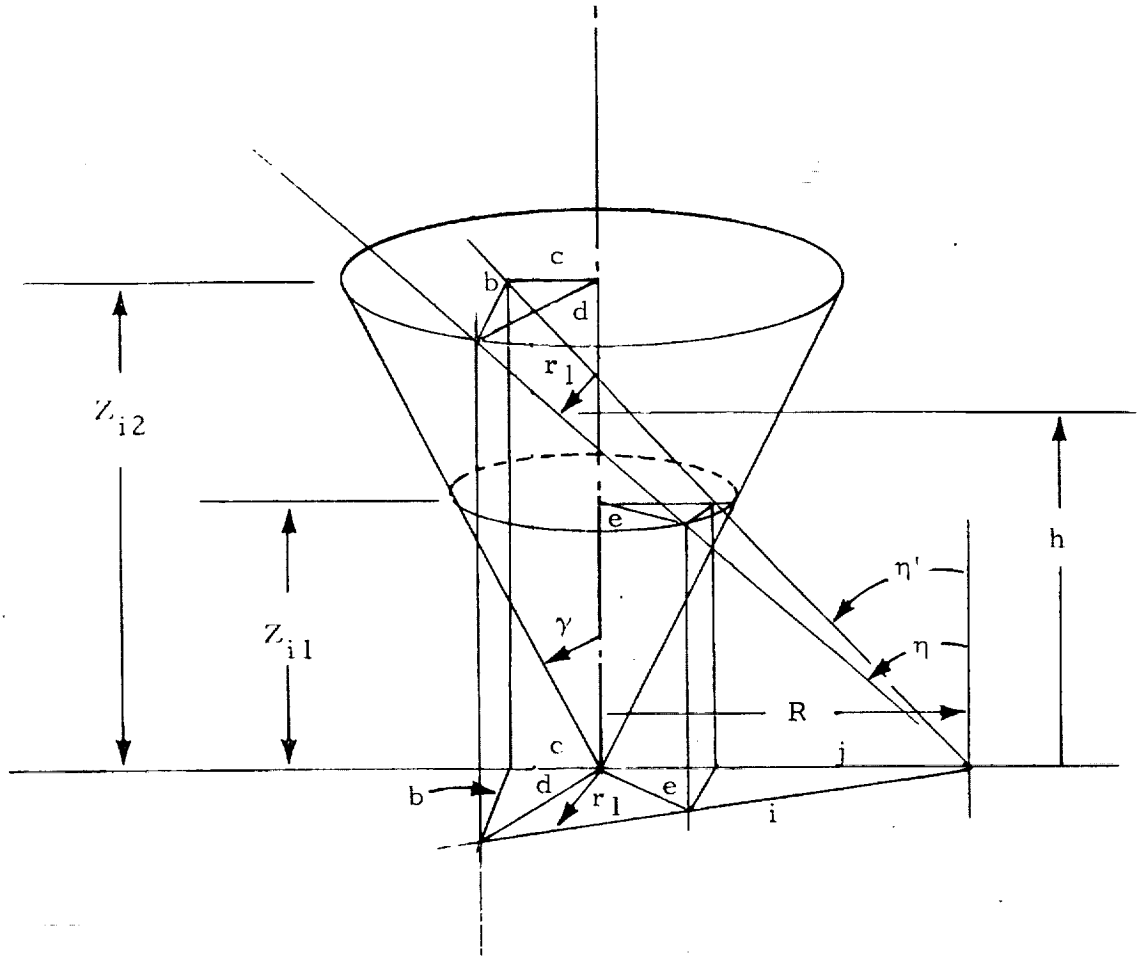

Fig. 3-8 - The Path Length Through a Conical Body

Through use of Pythagoras theorem and the quadratic equation, the following expressions are obtained which give the Z elevations for intersections of the line of sight with the conical boundaries relative to a plane through the vertex in terms of γ, η, η' and R.

$$Z_{i1} = \frac{\sqrt{\tan\gamma + R\tan\eta' - \left[(\tan\gamma + R\tan\eta')^2 + (1 - R^2)(\tan^2\eta - \tan^2\gamma)\right]}}{\tan^2\eta - \tan^2\gamma} \quad (3.45)$$

$$Z_{i2} = \frac{\sqrt{\tan\gamma + R\tan\eta' + \left[(\tan\gamma + R\tan\eta')^2 + (1 - R^2)(\tan^2\eta - \tan^2\gamma)\right]}}{\tan^2\eta - \tan^2\gamma} \quad (3.46)$$

Equations (3.45) and (3.46) apply only when $\eta > \gamma$. If $\eta < \gamma$, the line of sight exists through the base of the plume. For $\eta < \gamma$ the Z elevation of the intersection of the line of sight with the cone region boundary is simply the elevation of the base. If $\eta > 90$ deg, Eq. (3.45) is used to calculate the Z coordinate of the intersection. If $\gamma < \eta < 90$ deg, Eq. (3.46) is used. These equations are used to calculate the intersection of the line of sight with all conical region boundaries used to construct the plume.

3.4.2 Attenuation Along the Line of Sight

Once an energy bundle is emitted, scattered or absorbed/reemitted, the line of sight that the bundle follows may cross several regions before leaving the plume. In order to calculate the probable length of travel as per Eq. (3.39), the length of travel (S_i) in each plume region must be calculated. Figure 3-9 will aid in visualizing the manner in which S_i is calculated. In the following discussion the planes at right angles to the plume axis used to bound plume regions along the axis are referred to as I surfaces. The conical boundaries are called J surfaces. An event site is shown in Region I = 2, J = 2. For ease in visualizing the method, the trajectories of the energy bundle are shown for the case where the line of sight passes through the plume axis (which corresponds to an azimuth angle of θ = 0 or 180 deg). This expedient makes the lines of sight shown in Fig. 3-9 appear in true

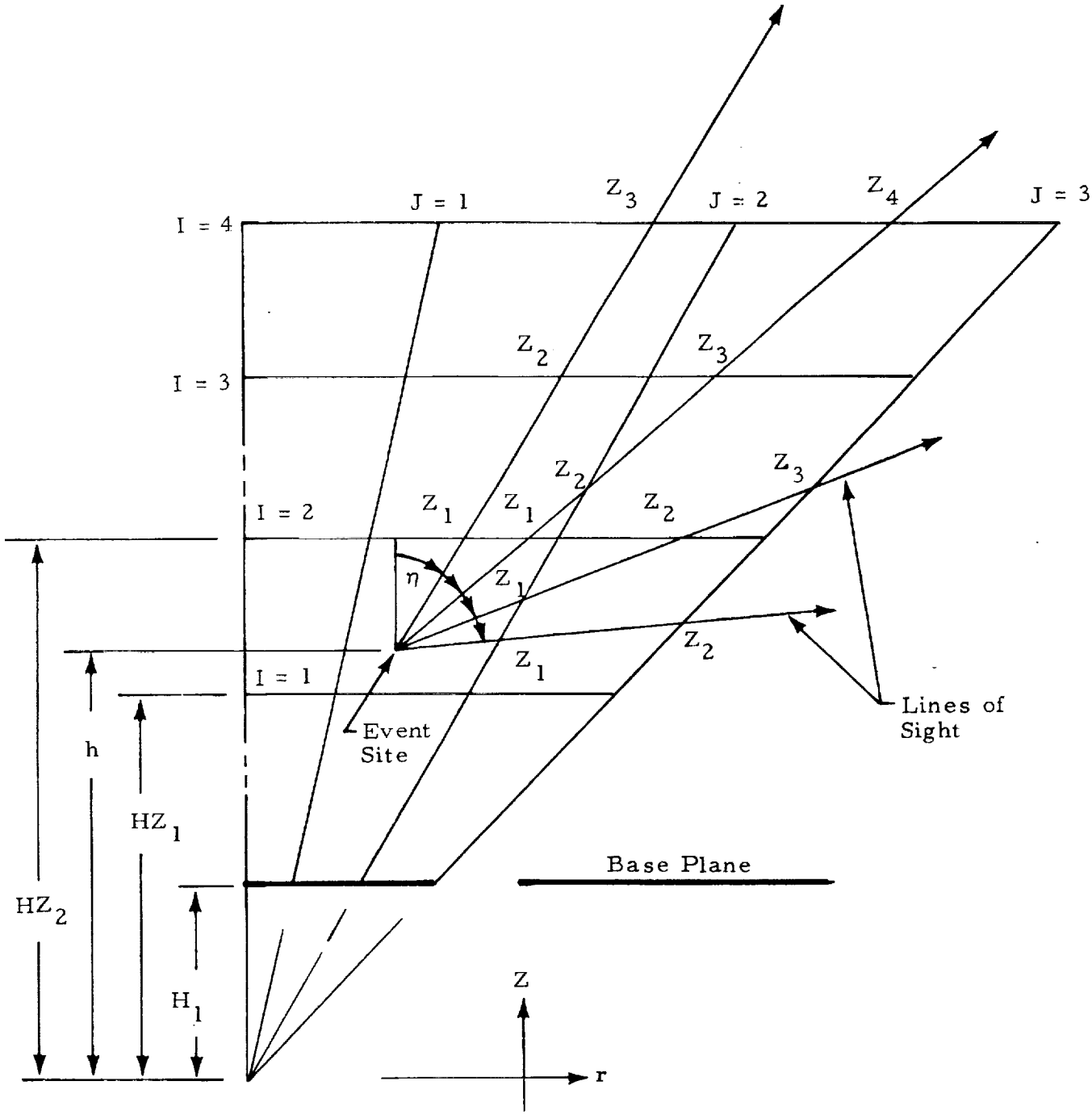

Fig. 3-9 - Line-of-Sight Intersections with Plume Region Boundaries

length. However, the equations to be derived for calculating the length of travel in each region are valid for any θ and ϕ.

The location of event sites in the plume are tracked in a cylindrical coordinate system centered at the common vertex of the conical surfaces used to construct the plume. The true length of travel in any region may be determined by identifying the Z-coordinate of the intersections of the line of sight with the boundaries of the region and dividing the difference in elevation by the cosine of the polar angle, η, of the line of sight. These intersections may occur on any combination of the I and J surfaces. The possible combinations of intersections are with I-I surfaces, I-J surfaces, J-I surfaces or J-J surfaces. These combinations of line-of-sight surface intersections are shown in Fig. 3-9. However, note that there are only two combinations of line-surface intersections from the event site to the region boundary, namely site to I-surface or site to J-surface. The Z coordinate of the intersections with the I surfaces are available from data used to construct the plume structure, namely in the array of HZ_i values. The intersections with the J surfaces are available from either Eq. (3.45) or (3.46). The true length of travel in any plume region may now be conveniently calculated from

$$S_i = \frac{Z_{n+1} - Z_n}{\cos\eta} \tag{3.47}$$

These values of S_i may be used in conjunction with Eq. (3.39) in order to calculate the probable length of travel, S_p, of an energy bundle.

3.4.3 Location of Scatter and Absorption Event Sites

In the simulation of SRB thermal radiation using the Monte Carlo method, the energy bundles are tracked in a cylindrical coordinate system centered at the vertex of the conical boundary surfaces with the positive Z-coordinate aligned with the cone axis. The direction of travel of an energy bundle is assigned in a spherical coordinate system centered at the event site. Emission sites within the plume are selected based on Eqs. (3.13), (3.17), (3.18) and (3.19).

Equation (3.13) is used to select the plume region in which the emission site occurs. Equation (3.17) selects the azimuth angle measured counter-clockwise with respect to a line parallel to the positive X_2 coordinate of the principal coordinate system and at right angles to the plume axis. The evaluation of the emission site, h, relative to the vertex of the conical boundaries along the Z-axis of a single SRB plume is determined by Eq. (3.18). The radial distance from the plume axis, r, is determined by Eq. (3.19). Once an emission site is selected, the energy bundle is followed along a line of sight with polar and azimuth angles defined by Eqs. (3.21) and (3.22). The polar angle, η, is measured with respect to the positive Z-axis of the plume. The azimuth angle, θ, of the line of sight is measured with respect to a line parallel to X_2-coordinate and at right angles to the plume axis. A probable length of travel is then selected based on Eq. (3.39). The energy bundle is tracked along the line of sight until it either escapes the plume or until a collision event occurs. The occurrence of a collision event is determined when the predetermined value for S_p is less than S_i for any region. This circumstance implies that the energy bundle failed to escape the plume along the specified line of sight. Once a collision event occurs it is necessary to calculate the cylindrical coordinates of the new event site. Reference to Fig. 3-10 should be made for the following discussion. Figure 3-10 is a schematic of the geometry involved in tracing energy bundles. The plume shown in Fig. 3-10 is composed of a single region. However, the relations derived for tracking energy bundles from site to site are valid for a plume composed of any number of regions.

The Z-coordinate of the new event site is obtained by adding the projection of S_p onto the Z-axis of the plume

$$h_2 = h_1 + S_p \cos\eta \tag{3.48}$$

The new value for the r-coordinate is obtained from the law of cosines. Consider the r_1, the new value of r_1 (r_2 in Fig. 3-10), and the projection of S_p onto a plane at right angles to the Z-axis. The projection of S_p onto

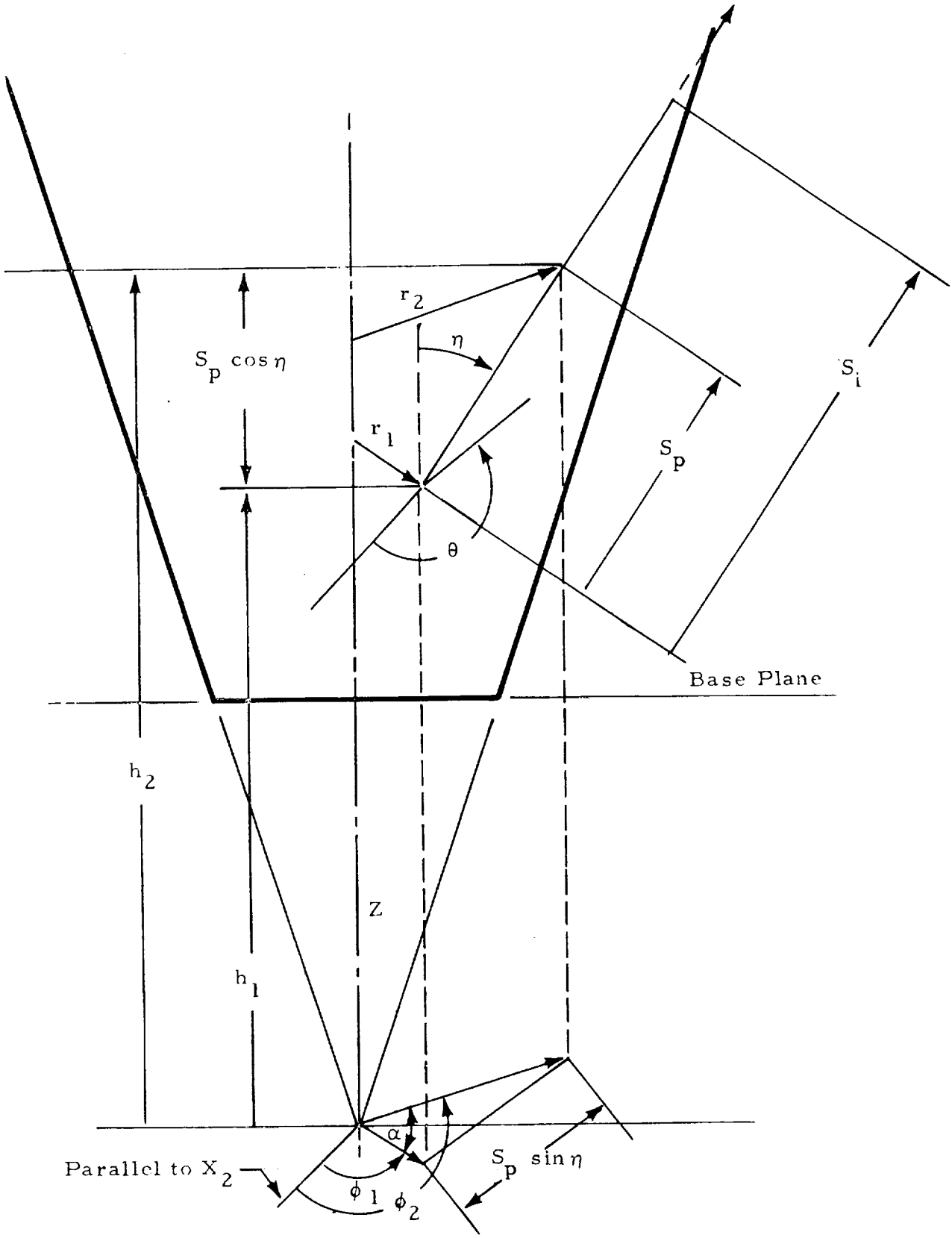

Fig. 3-10 - Geometry for Ray Tracing in the Plume

such a plane is simply $S_p \sin\eta$ and the law of cosines gives

$$r_2 = \sqrt{r_1^2 + (S_p \sin\eta)^2 - 2r_1 S_p \sin\eta \cos(\pi - (\theta - \phi_1))} \qquad (3.49)$$

The new value for ϕ_1 (ϕ_2 in Fig. 3-10) is obtained by calculating the angle α from the law of cosines

$$\left.\begin{aligned} \alpha &= \arccos\left(\frac{\sqrt{r_1^2 + r_2^2 - (S_p \sin\eta)^2}}{2 r_1 r_2}\right) \\ \text{and} \\ \phi_2 &= \phi_1 + \alpha \quad \text{if} \quad \theta - \phi_1 < \pi \\ \text{and} \\ \phi_2 &= \phi_1 - \alpha \quad \text{if} \quad \theta - \phi_1 > \pi \end{aligned}\right\} \qquad (3.50)$$

Equations (3.48), (3.49) and (3.50) are used to update the cylindrical coordinates (r, h and ϕ) of energy bundles as they undergo scatter or absorption/reemission events throughout a single SRB plume. When an energy bundle escapes the boundaries of one plume, it is necessary to check whether the line of sight of the bundle intersects the neighboring plume. This check is provided by representing the neighboring plume as a quadric surface in a central coordinate system (Fig. 3-11). The left plume in Fig. 3-11 contains an event site with the line of sight of the energy bundle passing through the neighbor plume. The right plume is defined by a quadric expression in the central coordinate system. The definition of the line of sight is also translated to the central coordinate system and the algebraic expressions for the line of sight and the quadric expression for the conical surface of the external boundary of the neighbor plume are checked for a possible solution. If a real solution exists, there is an intersection of the line of sight with some portion of the infinite conical surface. The coordinates of this intersection are checked to determine if it lies within the limits of the finite plume. The method for representing the plume as a quadric surface is discussed in Section 3.5.

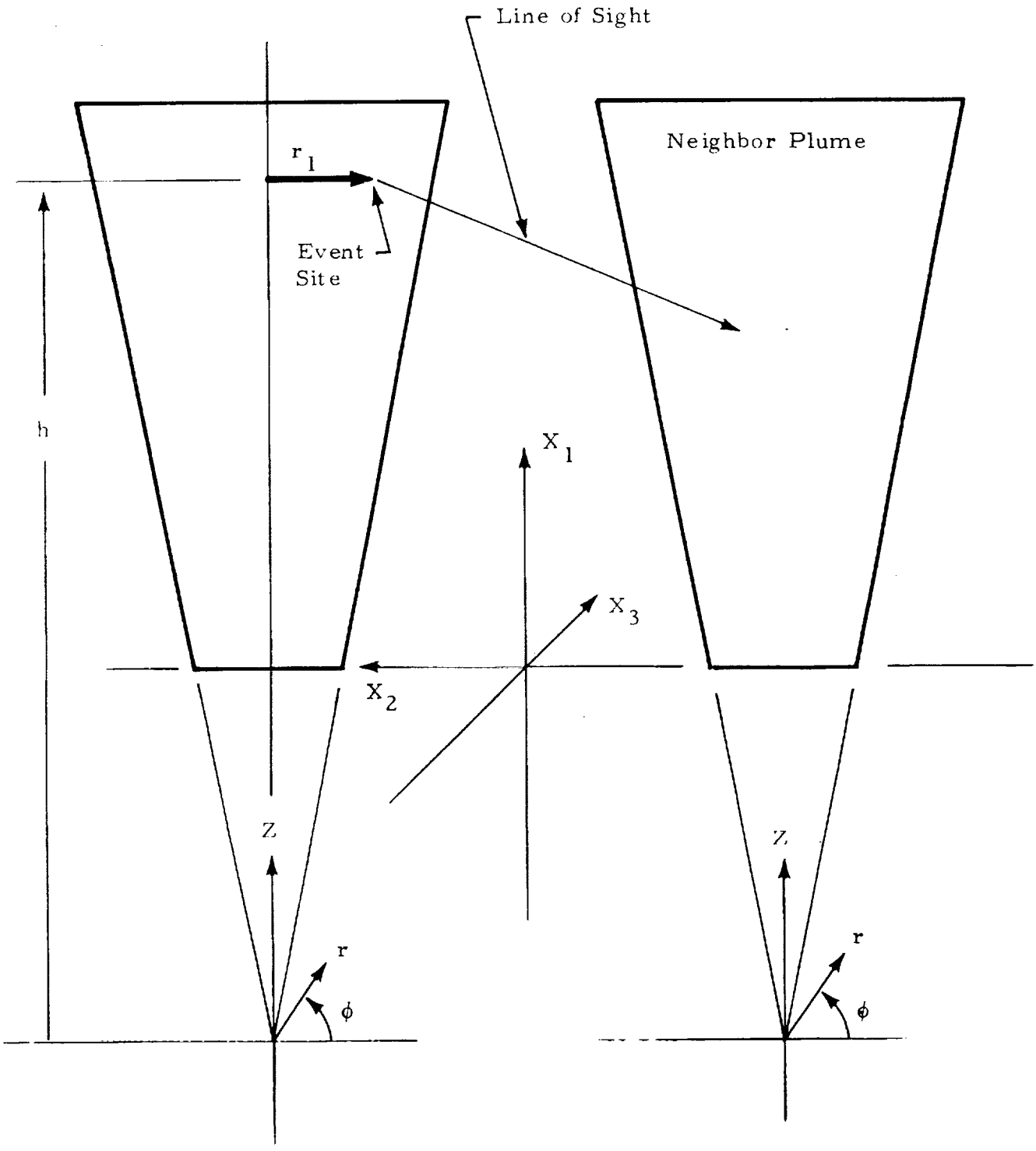

Fig. 3-11 - Dual Plume Geometry Model

3.5 SURFACE GEOMETRY PACKAGE

Heated surface geometries are represented by quadric surfaces. These surfaces may be grouped in various combinations to simulate Space Shuttle geometries. The external boundaries of the dual plumes are also represented as a quadric surface (cone) to facilitate modeling the shading effect of the adjacent plumes on the emitted radiation.

3.5.1 Quadric Surfaces

The heated surfaces can be described as either quadric surfaces or planar surfaces. The surfaces of cylinder, cone, sphere, ellipsoid and paraboloid belong to the former type; the surfaces of parallelogram and disk belong to the latter. These surfaces can be represented by a general quadric equation of the following form

$$C_1 X_1^2 + C_2 X_2^2 + C_3 X_3^2 + C_4 X_1 X_3 + C_5 X_2 X_3 + C_6 X_2 X_3 + C_7 X_1 + C_8 X_2 + C_9 X_3 + C_{10} = 0 \tag{3.51}$$

The X_1, X_2 and X_3 are the coordinates of the system. The $C_1, C_2, \ldots$ are the coefficients that determine the properties of the surface. A detailed discussion on these surfaces is found in Ref. 9.

There are altogether six surfaces, namely: cylinder, frustum, paraboloid, ellipsoid, parallelogram and annular disk. On the first three types of surfaces, there are optional constraint planes to define the extent of these surfaces. The constraint planes are assumed to be perpendicular to the body axis of the surface.

The surfaces are defined by eleven parameters in general. These parameters are two radii and the coordinates for three points, as summarized in Table 3-1. The target surface may be a simple surface as in the cases of ellipsoid, parallelogram and disk or a simple surface plus constraint planes perpendicular to its axis, as in the cases of cylinder, frustum and paraboloid. The

Table 3-1
INPUTS OF TARGET SURFACES

	R_1	R_2	P_1	P_2	P_3
Cylinder	Radius	N/A	Center of Top	Center of Bottom	A Point not on Body Axis
Frustum	Radius of Top	Radius of Bottom			
Paraboloid	Radius of Constraint Plane Passing Through P2	N/A	Vertex	Center of the Base	
Ellipsoid	N/A	N/A	Center	Pole	Zero Meridian
Parallelogram	N/A	N/A	P_1, P_2, P_3 are three consecutive corners, counterclockwise about the outward normal.		
Disk	Outer Radius	Inner Radius	Center	Arbitrary Point on Disk	Normal Vector

N/A: Not applicable.

basic target surfaces are transformed from the central coordinates to body coordinates in which the shape of the quadric surface is readily recognizable.

3.5.2 Subdivision of Surfaces

The main surfaces and their constraint planes are further divided into sub-areas for more precise heating rate prediction. Four integer numbers are used to describe the subdivision. These numbers are NN1, NN2, NRING1 and NRING2 in the program. Their meaning is indicated in Fig. 3-12.

The area of each sub area and the position vector of its center are computed. Each area is further assigned a number. When a photon trajectory intercepts a target surface either on the main surface or on the constraint plane, the position vector of the hit point is calculated. Comparisons of this hit point position vector to all the position vectors of the sub-areas on the given surface are then made in order to identify the proper sub-area which was hit.

3.6 RAY TRACING FROM PLUME TO SURFACE

The ray tracing scheme can be described as follows. Assume a ray originating from point (X1, Y1, Z1) in the direction (U1, U2, U3). Its trajectory which is a straight line in the three-dimensional space can be described in the parametric form:

$$\begin{aligned} X &= X1 + U1 \cdot d \\ Y &= Y1 + U2 \cdot d \\ Z &= Z1 + U3 \cdot d \end{aligned} \tag{3.52}$$

where d is a parameter characterizing the distance between an arbitrary point (X, Y, Z) on the line to a fixed point (X1, Y1, Z1) on the same line.

The target surfaces, six in total, can be classified into two categories, i.e., the planar surface and the quadric surface. A planar surface can be

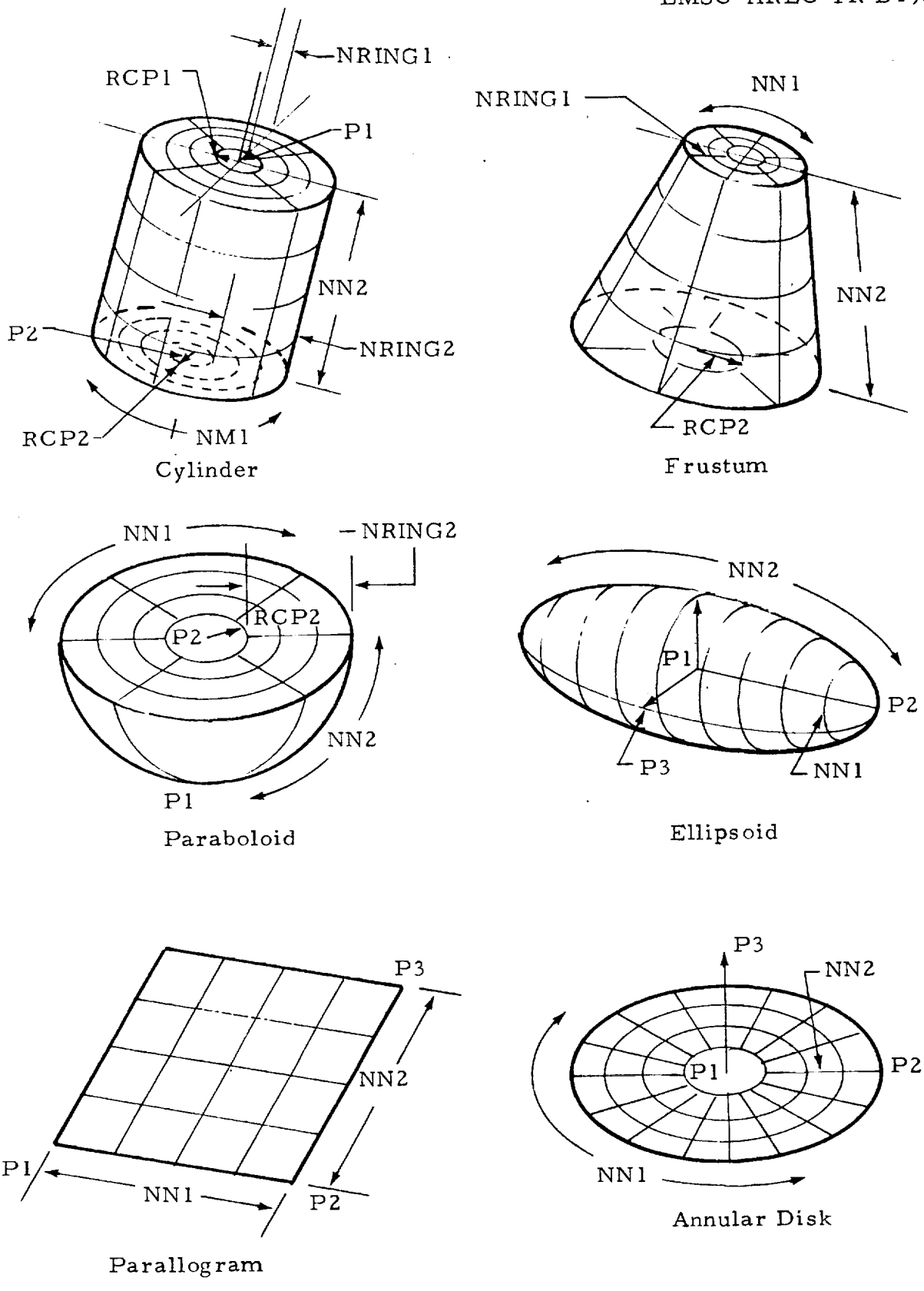

Fig. 3-12 - Sub-Areas of the Target Surfaces

expressed as

$$(X - X0) \cdot n1 + (Y - Y0) \cdot n2 + (Z - Z0) \cdot n3 = 0 \qquad (3.53)$$

where (X0, Y0, Z0) are given points on the plane; (n1, n2, n3) are the direction cosines of its normal and (X, Y, Z) are the general points on the plane. If the straight line, as given in Eq. (3.52), intercepts the plane, there will be common point (X, Y, Z) such that

$$(X1 - U1 \cdot d - X0) \cdot n1 + (Y1 - U2 \cdot d - Y0) \cdot n2 + (Z1 - U3 \cdot d - Z0) \cdot n3 = 0$$

therefore

$$d = \frac{(X1 - X0) \cdot n1 + (Y1 - Y0) \cdot n2 + (Z1 - Z0) \cdot n3}{U1 \cdot n1 + U2 \cdot n2 + U3 \cdot n3} \qquad (3.54)$$

The position vector of the hit point is obtained by substituting d obtained in Eq. (3.54) into Eq. (3.53). A closer look at Eq. (3.54) reveals the following observations:

a. When the denominator vanishes, there is no solution. This is the case in which the trajectory is parallel to the plane.

b. When the numerator vanishes, it means that the given point of the trajectory is already a point on the plane.

c. When the distance, d, is a negative number, it means that the direction of the trajectory is in the sense away from the plane from the given point.

Hit points on the quadric surfaces are calculated in a similar way. To illustrate the procedure, a cylindrical surface of radius R is considered. Let the surface be given in its body coordinates as follows:

$$X^2 + Y^2 = R^2 \qquad (3.55)$$

The common solution of Eq. (3.55) and Eq. (3.52) leads to

$$(X1 + U1 \cdot d)^2 + (Y1 + U2 \cdot d)^2 = R^2$$

Thus
$$d = \frac{-B \pm \sqrt{B^2 - 4 \cdot A \cdot C}}{2A} \tag{3.56}$$

where

$$A = (U1)^2 + (U2)^2 = 1 - (U3)^2$$

$$B = 2\ (U1 \cdot X1 + U2 \cdot Y1)$$

$$C = (X1)^2 + (Y1)^2 - R^2$$

If the discriminant, $B^2 - 4AC$, is less than zero, there is no solution. This means the trajectory does not intercept the target surface. The sign of the square root is chosen in such a way that d is the positive and the smaller of the two real roots. When d is computed, the hit point on the target surface is readily known by substituting d into Eq. (3.52).

When there is more than one target surface in the computation, the shading effect needs to be considered. The photon ray, being a straight line and absorbed by the first intercepting surface, stops at the nearest surface it intercepts. The mathematical expressions of all the possible intercepting points, however, are calculated in the program. A comparison is made to pick the shortest distance and therefore the correct hit point. After the hit point is determined, a further check is made to determine the sub-area on the surface that is hit. The number of hits of that sub-area is then incremented.

The algorithm of the dual plume simulation can be described as follows: the two plumes are assumed to be identical in every respect except their location and orientation. Each plume has a local coordinate system which is centered at the center of its exit plane with X1' axis coinciding with the plume axis. In addition there is a central coordinate which is located midway between the centers of the exit planes of the two plumes at their zero gimbal angles. Each plume can then be located freely with respect to the central coordinate system. The coordinate systems and the gimbal angles are shown in Fig. 3-13 and Fig. 3-14, respectively.

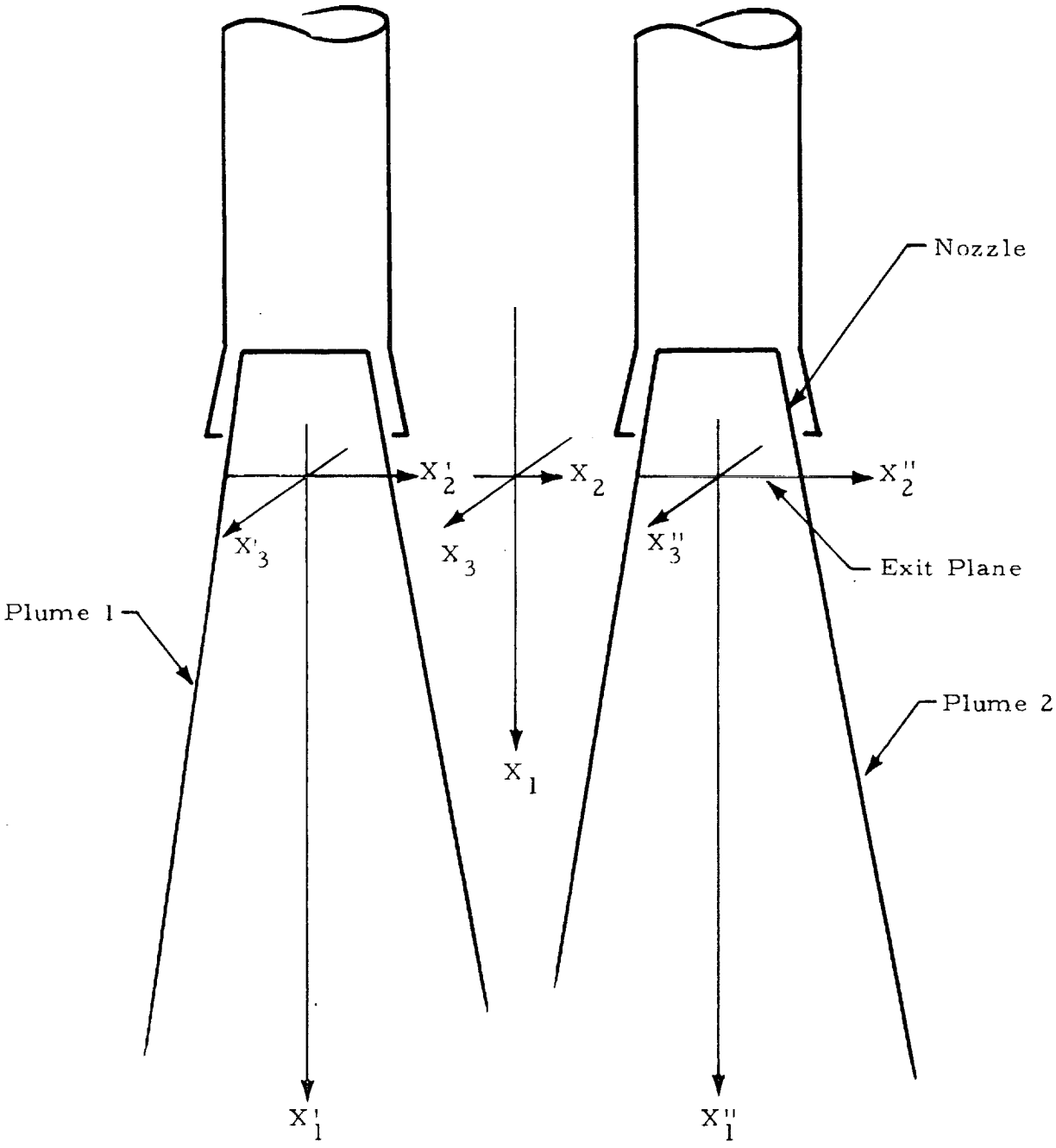

Fig. 3-13 - The Coordinate Systems of Dual Plumes

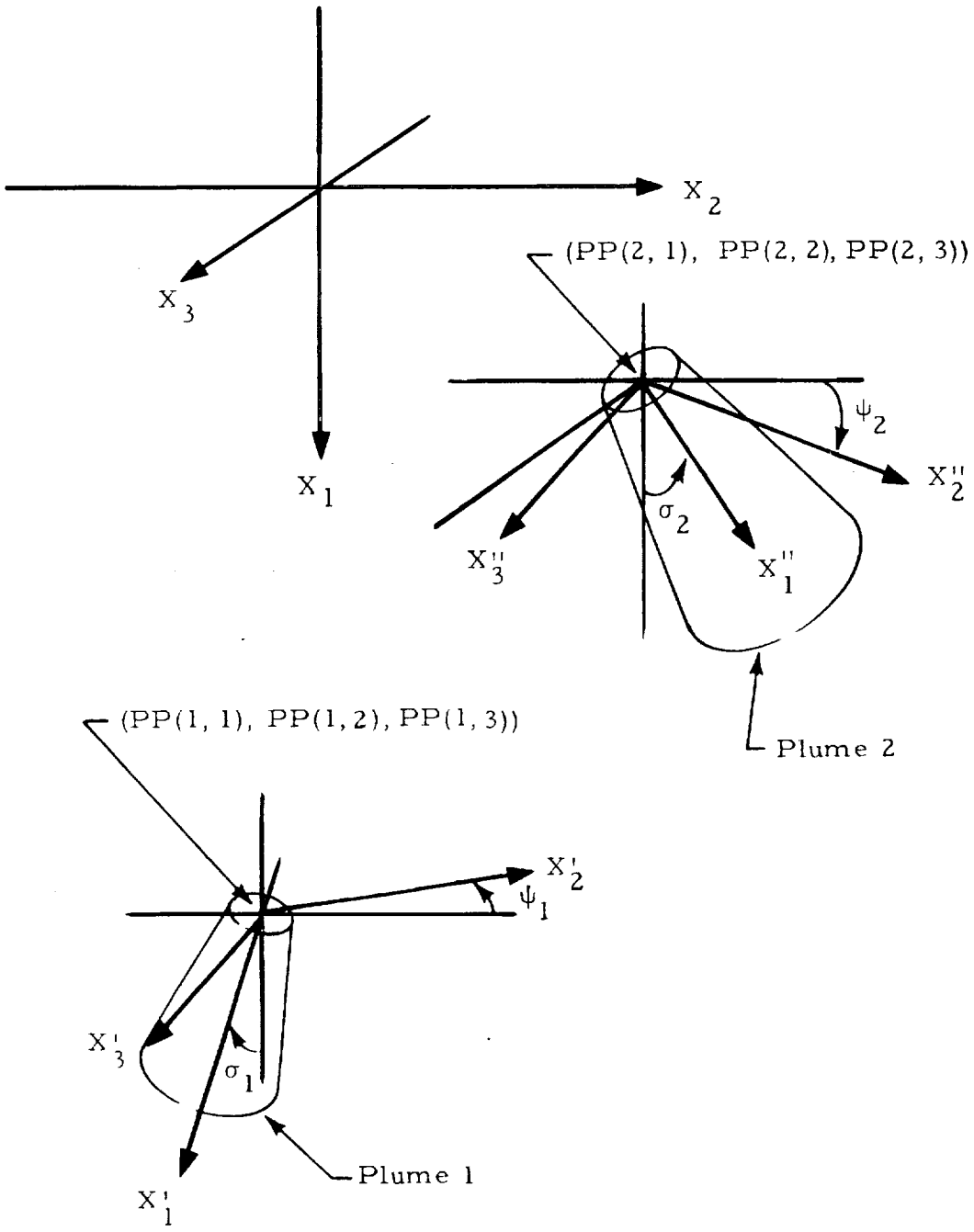

Fig. 3-14 - Gimbal Angles of Dual Plumes

Let (X1, X2, X3) and (U1, U2, U3) be the position vector and the trajectory direction cosines in the central coordinate system. The primed quantities (X1', X2', X3') and (U1', U2', U3') are the corresponding quantities in the plume local coordinates. (PP(1), PP(2), PP(3)), ψ and σ are the location and gimbal angles of either plume. Transformation from the plume coordinates to the central coordinate can be done by following matrix multiplications. Note that ψ is either ψ_1 or ψ_1 plus $\pi/2$ and σ is either σ_1 or σ_2 as the case may be.

$$\begin{pmatrix} X1 \\ X2 \\ X3 \end{pmatrix} = \begin{pmatrix} \cos\sigma & 0 & \sin\sigma \\ \sin\sigma\sin\psi & \cos\psi & -\cos\sigma\sin\psi \\ -\sin\sigma\cos\psi & \sin\sigma & \cos\sigma\cos\psi \end{pmatrix} \begin{pmatrix} X1' \\ X2' \\ X3' \end{pmatrix} + \begin{pmatrix} PP(1) \\ PP(2) \\ PP(3) \end{pmatrix} \quad (3.57)$$

$$\begin{pmatrix} U1 \\ U2 \\ U3 \end{pmatrix} = \begin{pmatrix} \cos\sigma & 0 & \sin\sigma \\ \sin\sigma\sin\psi & \cos\psi & -\cos\sigma\sin\psi \\ -\sin\sigma\cos\psi & \sin\psi & \cos\sigma\cos\psi \end{pmatrix} \begin{pmatrix} U1' \\ U2' \\ U3' \end{pmatrix} \quad (3.58)$$

Transformations from the central coordinate system to either plume coordinate system are the inverse of the above and are given as follows:

$$\begin{pmatrix} X1' \\ X2' \\ X3' \end{pmatrix} = \begin{pmatrix} \cos\sigma & \sin\sigma\sin\psi & -\sin\sigma\cos\psi \\ 0 & \cos\psi & \sin\psi \\ \sin\sigma & -\cos\sigma\sin\psi & \cos\sigma\cos\psi \end{pmatrix} \begin{pmatrix} X1 - PP(1) \\ X2 - PP(2) \\ X3 - PP(3) \end{pmatrix} \quad (3.59)$$

$$\begin{pmatrix} U1' \\ U2' \\ U3' \end{pmatrix} = \begin{pmatrix} \cos\sigma & \sin\sigma\sin\psi & -\sin\sigma\cos\psi \\ 0 & \cos\psi & \sin\psi \\ \sin\sigma & -\cos\sigma\sin\psi & \cos\sigma\cos\psi \end{pmatrix} \begin{pmatrix} U1 \\ U2 \\ U3 \end{pmatrix} \quad (3.60)$$

When an energy bundle escapes the boundary of a plume, the location of the point on the plume boundary and the direction of the bundle can be recorded on a data tape. When a large number of sample energy bundles are collected, typically 100,000 samples, the data will give a good definition of

the plume's radiation field. This process is the IPLUME = 3 option in the computer code. The energy bundle can be traced directly as it leaves a plume. A random number is first called to determine in which plume this energy bundle is originated. The location and direction are then transformed to the central coordinate system. A check must be made at this point to determine if this energy bundle will intercept the other plume. If it does, the interception on the other plume is treated as a reemission point in that plume, and the tracing process described in preceding sections is continued in that plume until the energy bundle again leaves the plume. If the energy bundle leaves a plume and does not intercept the other plume, then the geometry package is called to determine if it hits any part of its surfaces. This procedure is the IPLUME = 1 option in the code.

If the data tape is used as in the case of IPLUME = 4 option, instead of generating the energy bundles within the plumes, the presence of the other plume is treated as a shading surface. When the energy bundle hits the boundary of the other plume, the energy bundle stops there. Otherwise a check is made to determine the hit point. Moreover, due to the assumption that the dual plumes are identical when the location and direction of an energy bundle are read from the data tape, the same set of data applies to both plumes. Therefore when a set of data is read from the tape, two rays which are originated at each of the two plumes in a mirror symmetrical position are calculated. In the case when the plumes are gimbaled, this symmetry still applies, because the location and direction are given in terms of the plume local coordinates which are not affected by the gimbal angles.

3.7 HEAT FLUX EXPRESSIONS

When an energy bundle escapes the boundaries of the dual SRB plumes, it may or may not strike a surface of the geometric model of Space Shuttle surfaces. The methodology for discriminating whether the bundle intersects a spacecraft surface has been discussed in Section 3.5. If the bundle hits a surface, the energy contained in the bundle is absorbed by the surface. The radiant heat flux to a given surface is ultimately determined by tabulating the number of energy bundles that strike the given surface relative to the total

number of bundles used in calculating the distribution of thermal radiation leaving the plumes.

The amount of energy contained in an energy bundle for a specific SRB plume is dependent on the number of samples, N_e, and the number of absorption/reemission events that occur during the simulation. The total number of samples plus reemissions multiplied by the energy per bundle must equal the total energy emitted by all regions of the plume as given by Eq. (3.11), as

$$(N_e + N_{re})\, e = 4 \sum_{i=1}^{\text{all regions}} \left(N\, \bar{\sigma}_a\, E_b^p\Big|_i + \bar{K}_a\, E_b^g\Big|_i \right) V_i \qquad (3.61)$$

Equation (3.61) defines the energy per bundle for a specified sample size, N_e.

The heat flux to a given surface is given by

$$q_n = N_h\, e / A_S \qquad (3.62)$$

where A_S is the area of the sub-surface and N_h is the number of hits in that area.

4. VIEW FACTOR MODEL

4.1 HEAT TRANSFER CALCULATIONS USING VIEW FACTORS

The radiative heat exchange between surfaces can be calculated with the help of the view factor concepts. The view factor, dF_{1-2}, which is also known as configuration factor, shape factor and other names, is defined as the fraction of energy leaving black surface dA_1 that arrives at black surface dA_2 (Fig. 4-1),

$$dF_{1-2} = \frac{\cos\beta_1 \cos\beta_2}{\pi S^2} dA_2 \tag{4.1}$$

Equation (4.1) shows that the view factor depends only on the size of dA_2 and its orientation with respect to dA_1. The differential notation dF indicates that the view factor is for energy transfer to a differential element, dA_2, from a differential element, dA_1. The view factor for two finite areas, A_1 and A_2, is calculated by integrating over both A_1 and A_2

$$F_{1-2} = \frac{1}{A_1} \int_{A_1}\int_{A_2} \frac{\cos\beta_1 \cos\beta_2}{\pi S^2} dA_2 \, dA_1 \tag{4.2}$$

The view factor F_{2-1} which is defined as the fraction of energy leaving black surface A_2 that arrives at black surface A_1, can be given similar to Eq. (4.2)

$$F_{2-1} = \frac{1}{A_2} \int_{A_2}\int_{A_1} \frac{\cos\beta_2 \cos\beta_1}{\pi S^2} dA_1 \, dA_2 \tag{4.3}$$

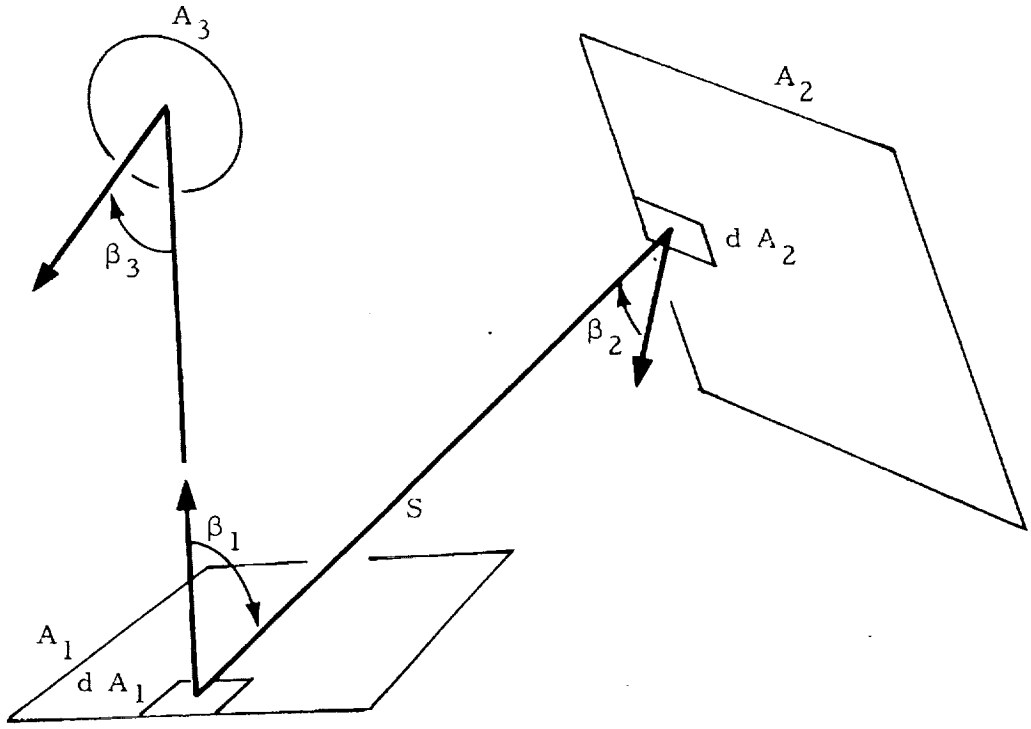

Fig. 4-1 - Schematic of View Factor F_{1-2}

Therefore, the reciprocity relation follows

$$A_1 F_{1-2} = A_2 F_{2-1} \tag{4.4}$$

The radiation exchange from A_1 to A_2, q_2, and that from A_2 to A_1, q_1, can be given immediately.

$$q_2 = \sigma A_1 F_{1-2} T_1^4 \tag{4.5}$$

$$q_1 = \sigma A_2 F_{2-1} T_2^4 \tag{4.6}$$

The view factors, F_{1-2} and F_{2-1}, depend on not only the area and orientation of the surface but also on the shape and local curvature of the surface. The view factors of some standard configurations are found in the literature. For those configurations for which the view factors are not available, the process to compute the view factor by evaluating the integration given in Eq. (4.2) is difficult in general.

4.2 MONTE CARLO METHOD

Since the view factor is defined as the fraction of total energy leaving one surface that arrives at the other, it is possible to divide this total energy into many bundles which are emitted diffusely from the emitting surface. The fraction of the total bundles that is intercepted by the other surface would be the view factor F_{1-2}. In this manner the view factor is obtained without carrying out the lengthy integration as given in Eq. (4.2). This is the underlying idea of the Monte Carlo method.

The Monte Carlo method is especially powerful when the geometry of the exchange surfaces is complex. There are, however, assumptions involved. The assumptions required when using the view factor to compute radiant heat exchange are that the surfaces involved are diffuse-gray emitters and reflectors, that each surface is isothermal and that the total flux arriving at and leaving each surface is evenly distributed across the surface. The

assumption required with the Monte Carlo method is that the reflector surface is of some reasonable finite size so that the number of hits recorded on the surface would be statistically meaningful. This assumption is not as restrictive as it appears. In the case where the reflector is small the view factor can be calculated with reciprocity relation by first computing the reverse view factor from the reflector to the emitter. However, there is no apparent criterion to distinguish a small target surface from a non-small target surface. It is a matter of how large a solid angle that the target surface subtends and how many emitting bundles are used. In the present code, the view factor and its corresponding reciprocal are computed at the same time. These are given in the output side by side for convenient reference.

4.3 DISTRIBUTION FUNCTION

In the Monte Carlo method the energy bundles are emitted from a surface uniformly in a cosine distribution. The process involves picking an emission site on the surface and choosing a direction of the trajectory. When a large number of energy bundles are dispensed, the emission sites will be distributed uniformly over the emitter surface and the trajectory directions will be distributed according to the cosine law. The spatial distribution will be discussed in the next section. The directional distribution is discussed here.

The direction of the trajectory can be determined by the angles η and θ (Fig. 4-2) when the location and the local normal are given on the emitting surface. When a large number of emissions are chosen, the trajectories will be distributed according to the cosine law about the local normal.

Let N_e be the total number emitted from the source point and dn the number emitting through dA. Since the number density is proportional to $\cos\eta$, the number of trajectories lying within $d\omega$ is

$$d\omega = \sin\eta \, d\eta \, d\theta$$

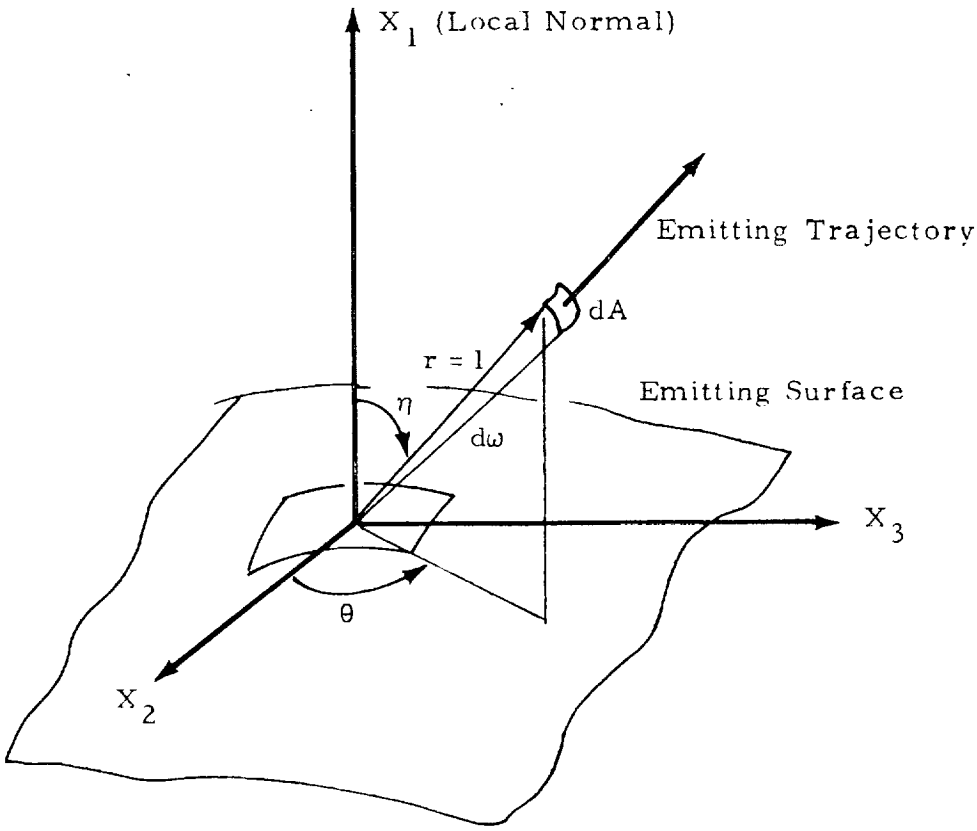

Fig. 4-2 - Direction of Emitting Trajectory

$$dN_e = \frac{d\omega}{4\pi} N_m \cos\eta$$

$$= \frac{N_m}{4\pi} \sin\eta \cos\eta \, d\eta \, d\theta$$

where N_m is the maximum number density. The total number N_e is

$$N_e = \int_0^{\pi/2} \int_0^{2\pi} \frac{N_m}{4\pi} \sin\eta \cos\eta \, d\theta \, d\eta$$

$$= \frac{N_m}{4}$$

The joint probability density function is therefore,

$$\frac{dN}{N} = f \, d\theta \, d\eta = \frac{1}{\pi} \sin\eta \cos\eta \, d\theta \, d\eta$$

The marginal distribution functions $P_{(\eta)}$ and $P_{(\theta)}$ for η and θ distributions respectively are

$$P_{(\theta)} = \int_0^{\pi/2} \frac{1}{\pi} \sin\eta \cos\eta \, d\eta = \frac{1}{2\pi}$$

$$P_{(\eta)} = \int_0^{2\pi} \frac{1}{\pi} \sin\eta \cos\eta \, d\theta = 2 \sin\eta \cos\eta$$

Therefore the corresponding random numbers are

$$U_\theta = \int_0^{\theta} \frac{1}{2\pi} d\theta = \frac{\theta}{2\pi}$$

$$U_\eta = \int_0^{\eta} 2 \sin\eta \cos\eta \, d\eta = \sin^2\eta$$

which means

$$\theta = 2\pi \cdot U_\theta \tag{4.7}$$

$$\eta = \sin^{-1}\sqrt{U_\eta} \tag{4.8}$$

Equations (4.7) and (4.8) are the relations between the random numbers U_θ and U_η drawn from the random number generator and the values of θ and η used to determine the trajectory.

4.4 EMITTING SURFACE GEOMETRY PACKAGE

The geometry package in the view factor calculation involves two parts. The first part is the geometry of the emitting surface which will be discussed here. The second part is the geometry of the target surfaces which is the same package used in heating rate computation and was discussed in the preceding section.

The emitting geometry package includes nine surfaces, i.e., half cylinder, half frustum, hemisphere, parallelogram, annular disk, cylinder, frustum and sphere. The input and output of these surfaces are all done in a subroutine VFEMIT. When the subroutine is called to output a trajectory, a point on the emitting surface is first chosen as follows:

1. Cylinder

$$HELV = H \cdot RN1$$

$$TH = (0.5 - RN2) \cdot \pi/2$$

where

HELV is the height above the base
H is the height of the cylinder
TH is the azimuthal angle, and
RN1 and RN2 are two random numbers.

2. Frustum

$$HELV = H \cdot (R2 - RL)/(R2 - R1)$$

$$TH = (0.5 - RN1) \cdot \pi/2$$

where

R1 and R2 are the radii of the base and the top of the frustum, respectively, and

$RL = R2 * \sqrt{RN2}$.

If $RL < R1$, another RN2 is drawn.

3. Sphere

A random direction is chosen. The point on the spherical surface is determined by a trajectory starting from the center of the sphere in the chosen direction to the point on the surface. A final check is made to ensure the point falls within the range of the hemisphere. If the point on the spherical surface is not within the given hemisphere, another random direction is generated and the process is repeated.

4. Parallelogram

$$D1 = RN1 \cdot H12$$

$$D2 = RN2 \cdot H23$$

$$\vec{X} = \vec{P1} + \overrightarrow{C12} \cdot D1 + \overrightarrow{C23} \cdot D2$$

where

$\vec{X}$ is the position vector of the random point on the plane

$\vec{P1}$ is the position vector of corner P1

H12, H23 are the distance P1 to P2 and P2 to P3, respectively, and

$\overrightarrow{C12}, \overrightarrow{C23}$ are the direction vectors of the lines P1 to P2 and P2 to P3, respectively.

5. Annular Disk

$$TH = RN2 \cdot 2\pi$$
$$RR = R2 \sqrt{RN1}$$

where

TH is the azimuthal angle subtended by the random point, and

RR is the random radius. If RR is less than the inner radius R1, then another RN1 is generated

Now that the random point on the emitting surface is chosen, the direction of the emission is the next to be determined which is described in the following paragraphs.

4.5 RAY TRACING

When a random point is chosen on the emitting surface, the direction cosines of the local normal at that point are known. The direction of the emitting trajectory is then generated by random numbers in such a way that the direction would fall into a cosine distribution about the local normal. A set of direction cosines (U1', U2', U3') with respect to the local coordinates are generated as follows.

$$\theta' = 2\pi \cdot RN1$$

$$\phi' = \sin^{-1} \sqrt{RN2}$$

$$U1' = \cos\phi'$$

$$U2' = \sin\phi' \cos\theta'$$

$$U3' = \sin\phi' \sin\theta'$$

The local coordinates which coincide with the local normal at the chosen surface point can be related back to the central coordinates. The direction

cosines (U1', U2', U3') are transformed into (U1, U2, U3) which are based on the central coordinates. Let the local normal be (N1, N2, N3). The transformation is:

$$\begin{vmatrix} U1 \\ U2 \\ U3 \end{vmatrix} = \begin{vmatrix} \cos\phi & o & \sin\phi \\ \sin\phi \sin\theta & \cos\theta & -\cos\phi \sin\theta \\ -\sin\phi \cos\theta & \sin\theta & \cos\phi \cos\theta \end{vmatrix} \begin{vmatrix} U1' \\ U2' \\ U3' \end{vmatrix}$$

where

$$\phi = \text{ACOS}(N1)$$
$$\theta = \pi/2 + \text{ATAN}(N3, N2)$$

Now that the location of the starting point and the direction of emission are known, this information can be fed into SORTNG subroutine to determine if and where the target surface is hit. The number of hits are recorded according to the sub-areas on each target surface.

When the specified number of trajectories are dispensed, the view factor and its reciprocal view factor of each sub-area are computed by dividing the number of hits by the total emissions. The results are grouped together by each target surface in the output.

5. EXAMPLES AND RESULTS

5.1 RESULTS CONCERNING PLUME CHARACTERISTICS

The two plumes from the two SRBs are assumed to be axisymmetric and identical to each other. The radiative power of the plumes varies with many parameters, e.g., trajectory point, particle size and density, afterburning, gas constituents, etc. The influence of these plume flowfield properties is reflected in the Monte Carlo solution to the radiation transport problem.

The energy bundles are traced within the plume until the energy bundles leave the plume boundary. Data tapes are generated recording the direction and the location of the line of sight of each energy bundle leaving the plume. These data tapes are used to define the line of sight of energy bundles leaving the plume in the radiation heating rate calculation. This circumvents the necessity of performing the Monte Carlo simulation for every computer run and provides a substantial saving in computer execution time with no sacrifice of sample size or accuracy.

Distributions of the energy bundles as they leave the boundary of a single plume are plotted on the following pages. Figure 5-1 shows the distribution in the X_1 direction which is along the axis of a single plume. Figure 5-2 shows the distribution of the bundles leaving a single plume relative to the angle η. The η angle is the angle between the trajectory of the energy bundle and the X_1 axis. Distribution of energy bundles in the ϕ direction is always uniform.

5.2 EXAMPLES OF HEATING RATE CALCULATIONS

The radiant heat flux to a disk at a distance -0.1 R_{ex} over a single plume for sea level and 72,000 ft trajectory points is plotted in Fig. 5-3. Figure 5-4

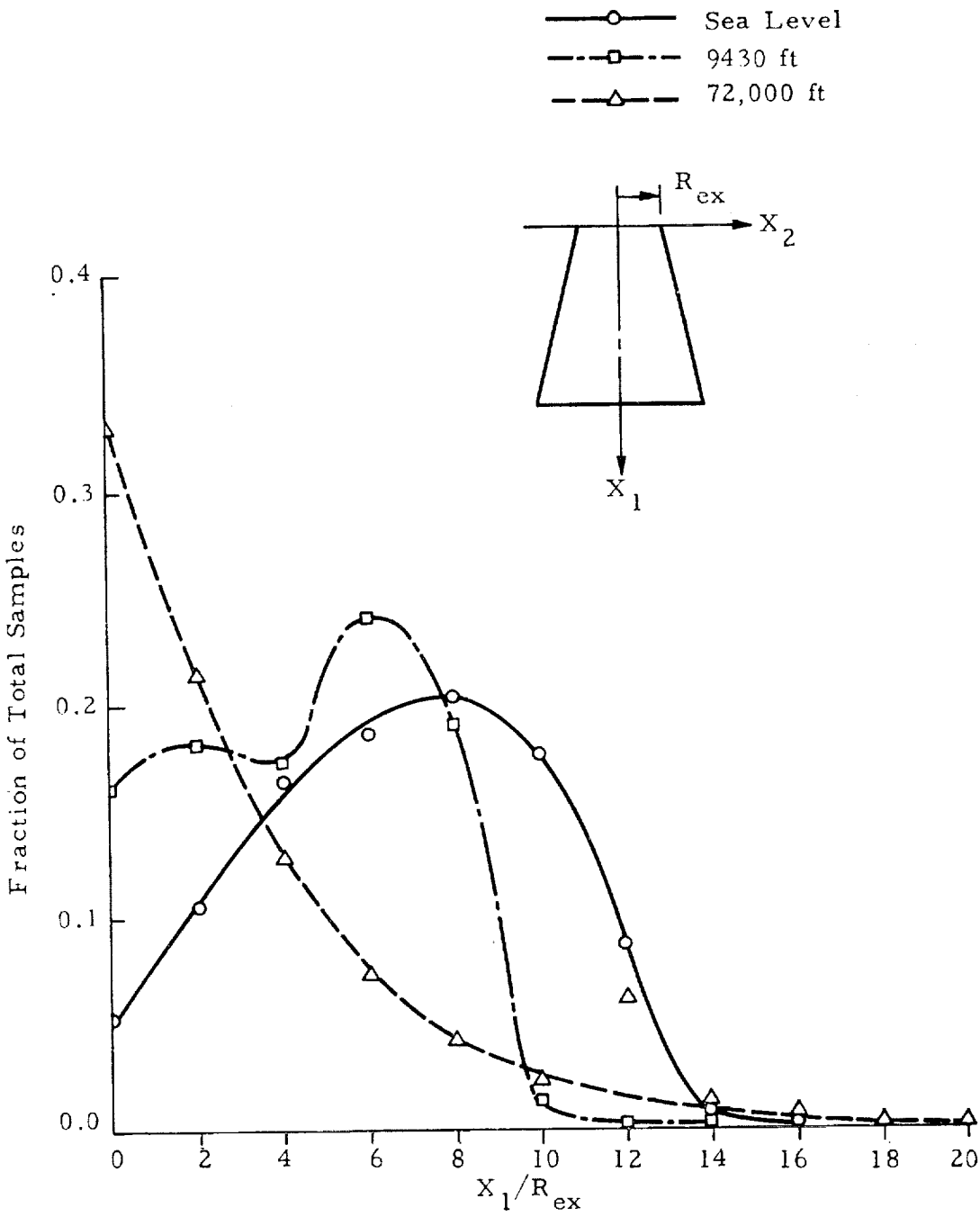

Fig. 5-1 - Distribution of Energy Bundles in X_1 Direction

η	0 - 90°	90 - 180°
Sea Level	0.5031	0.4979
9430 ft	0.5165	0.4835
72,000 ft	0.4106	0.5894

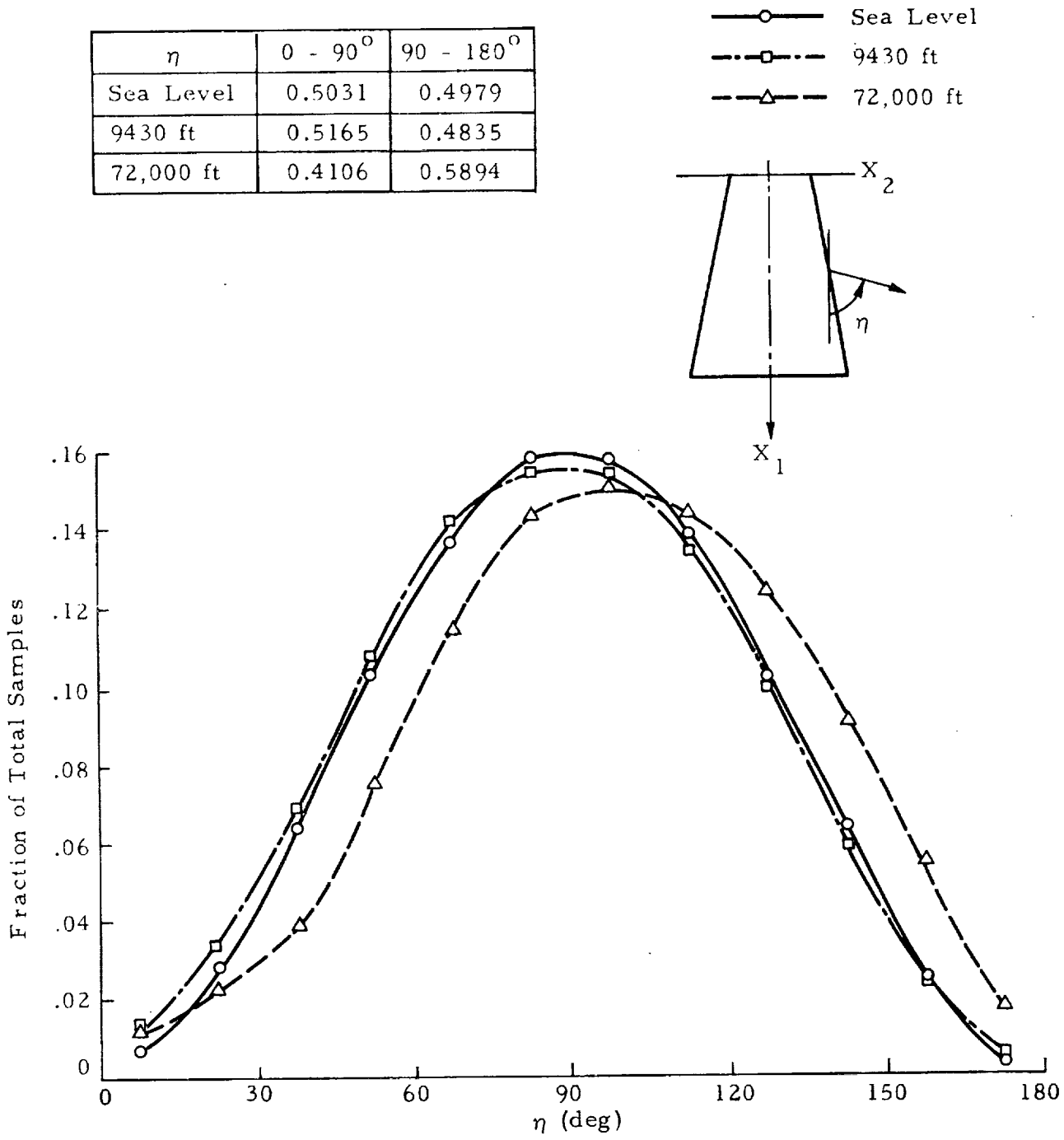

Fig. 5-2 - Distribution of Energy Bundle in η Direction

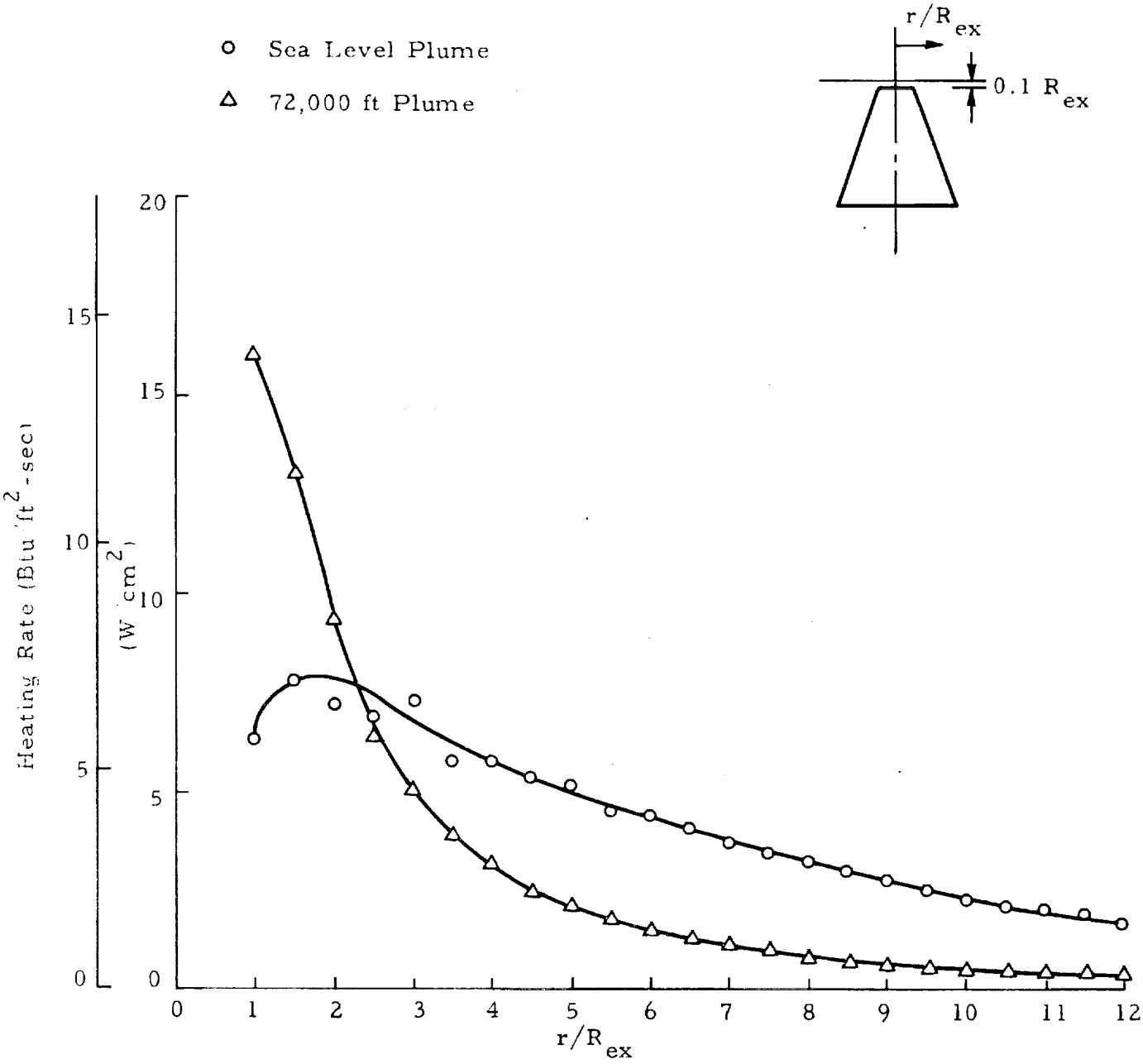

Fig. 5-3 - Heating Rate on a Disk Standing 0.1 R_{ex} Above the Exit Plane of a Plume (sample size = 100,000)

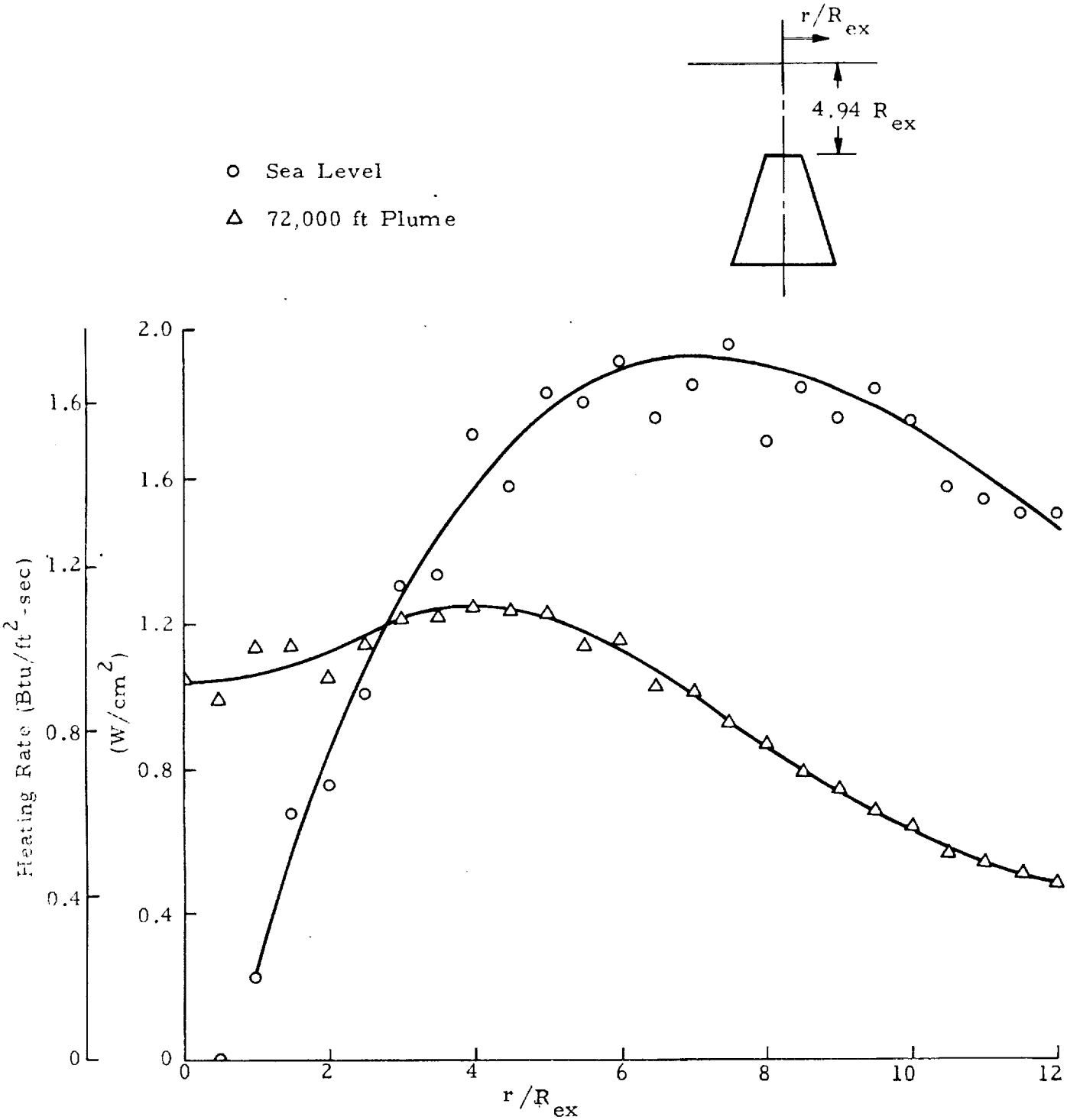

Fig. 5-4 - Heating Rate on a Disk at 4.94 R_{ex} over a Single Plume (sample size = 100,000)

shows similar data for a single plume except the disk is -4.94 R_{ex} above the exit plane, which is about the same elevation of the bottom of the ET.

The effects of gimbal angles and different altitudes on the radiant heat fluxes are shown in Figs. 5-5 through 5-10 for the dual SRB plumes. The heating rates are shown for a rectangular plane extending from X_2 = -6 to 6 and X_3 = -5 to 5 over the dual plume. Figure 5-5 shows the heating rates along the strips parallel to X_2 axis. The two obvious dips along the center strip are due to the shading of the nozzles. The distance between the rectangular plane and the nozzle exit plane is denoted by X_1. Figure 5-6 shows the similar case, except the plane is located at X_1 = -4.94 where the plane is tangent to the bottom of the external tank. The heat flux is more uniform at X_1 = 4.94 and the intensity is reduced by a factor of 2 to 3 as compared to the X_1 = 0 location.

Figures 5-7 and 5-8 show the effect of gimbal angle for the sea level plumes. Figure 5-7 shows the heat flux on strips of the rectangular plane when the plumes are tilting 30 deg toward the X_3 axis, i.e., σ = -30 deg, ψ = 0 deg. The heat flux on the side where $X_3 > 0$ is a marked increase over the side where $X_3 < 0$. The heat flux on the strip toward which the plumes are tilting is 3 to 10 times higher than that on the strip away from the plumes. Figure 5-8 shows the heat flux on strips of the rectangular plane when the plumes are tilting 25 deg toward the X_2 axis, i.e., σ = 25 deg, ψ = 90 deg. The heat fluxes are lopsided to the same direction the plumes are tilting.

The heat fluxes along one strip near the edge of the rectangular plane are plotted in Fig. 5-9 for the 9430 ft plumes. The four curves represent the following cases: (1) $\sigma = 0^\circ, \psi = 0^\circ, X_1 = 0$; (2) $\sigma = 0^\circ, \psi = 0^\circ, X_1 = -4.94$; (3) $\sigma = 25^\circ, \psi = 0^\circ, X_1 = 0$; and (4) $\sigma = -30^\circ, \psi = 0^\circ, X_1 = 0$. It is seen that the gimbaling of the σ angle would increase or decrease the heat flux at this particular location by a factor of 2.

The heat fluxes for no gimbal for the 72,000 ft plume are plotted in Fig. 5-10. The bottom curve is the heat flux at X_1 = -4.94. The heat flux

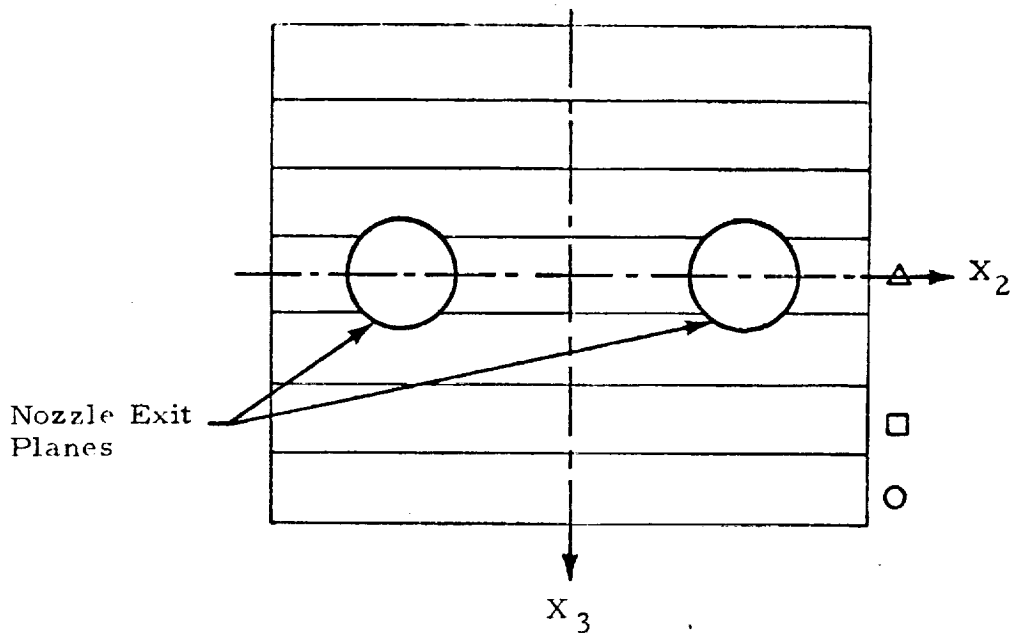

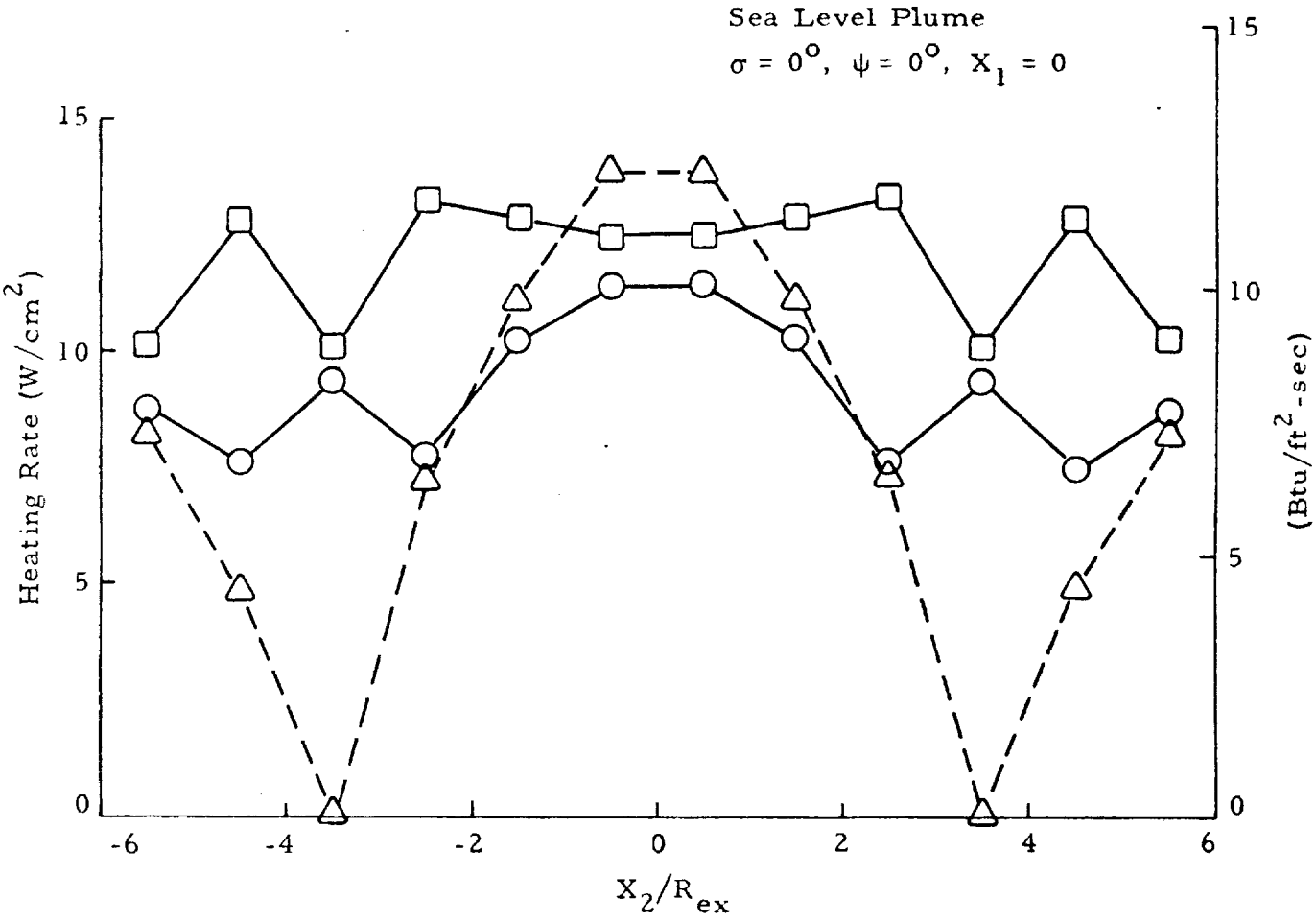

Fig. 5-5 - Heating Rate of a Rectangular Plane

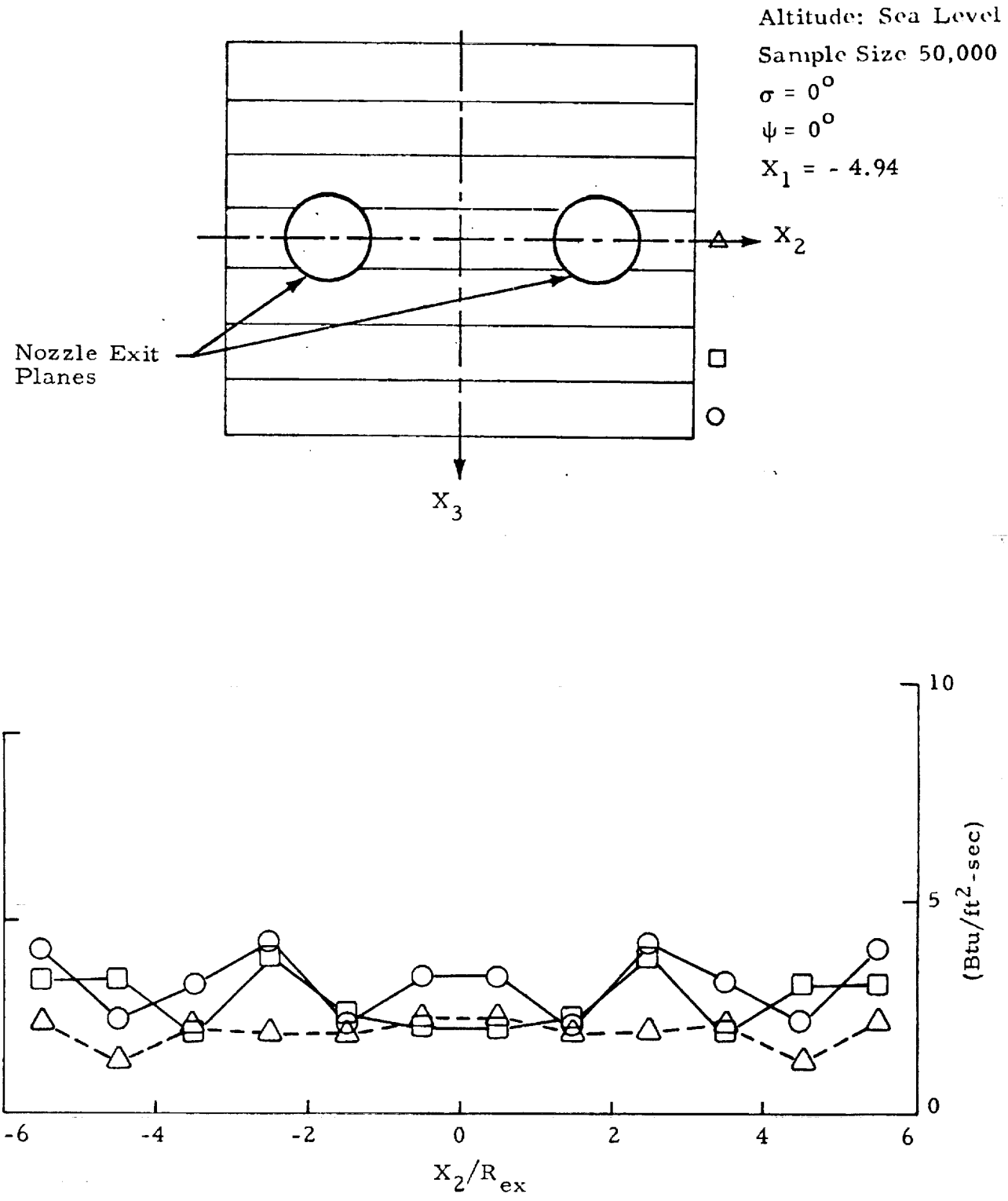

Fig. 5-6 - Heating Rate of a Rectangular Plane

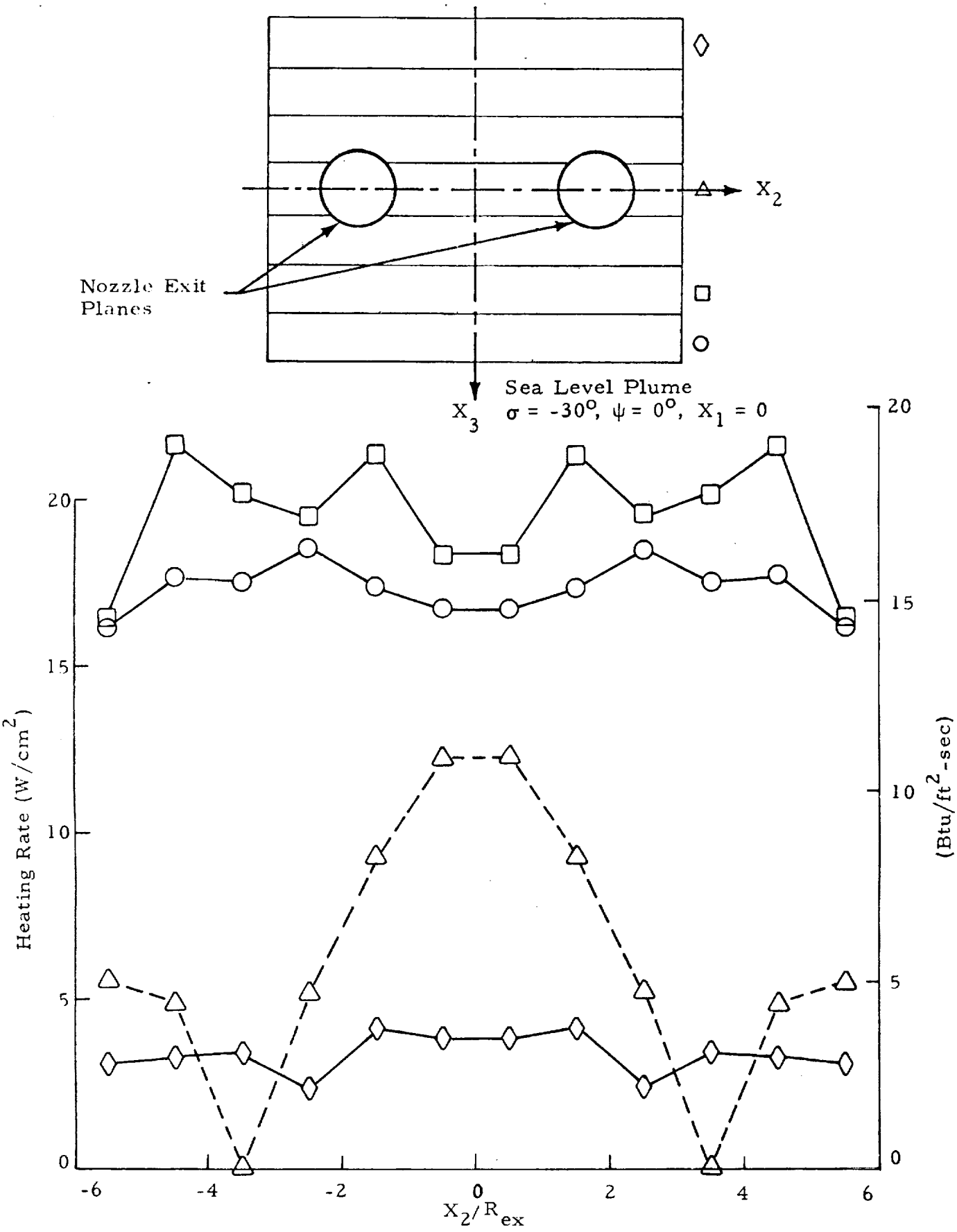

Fig. 5-7 - Heating Rate of a Rectangular Plane

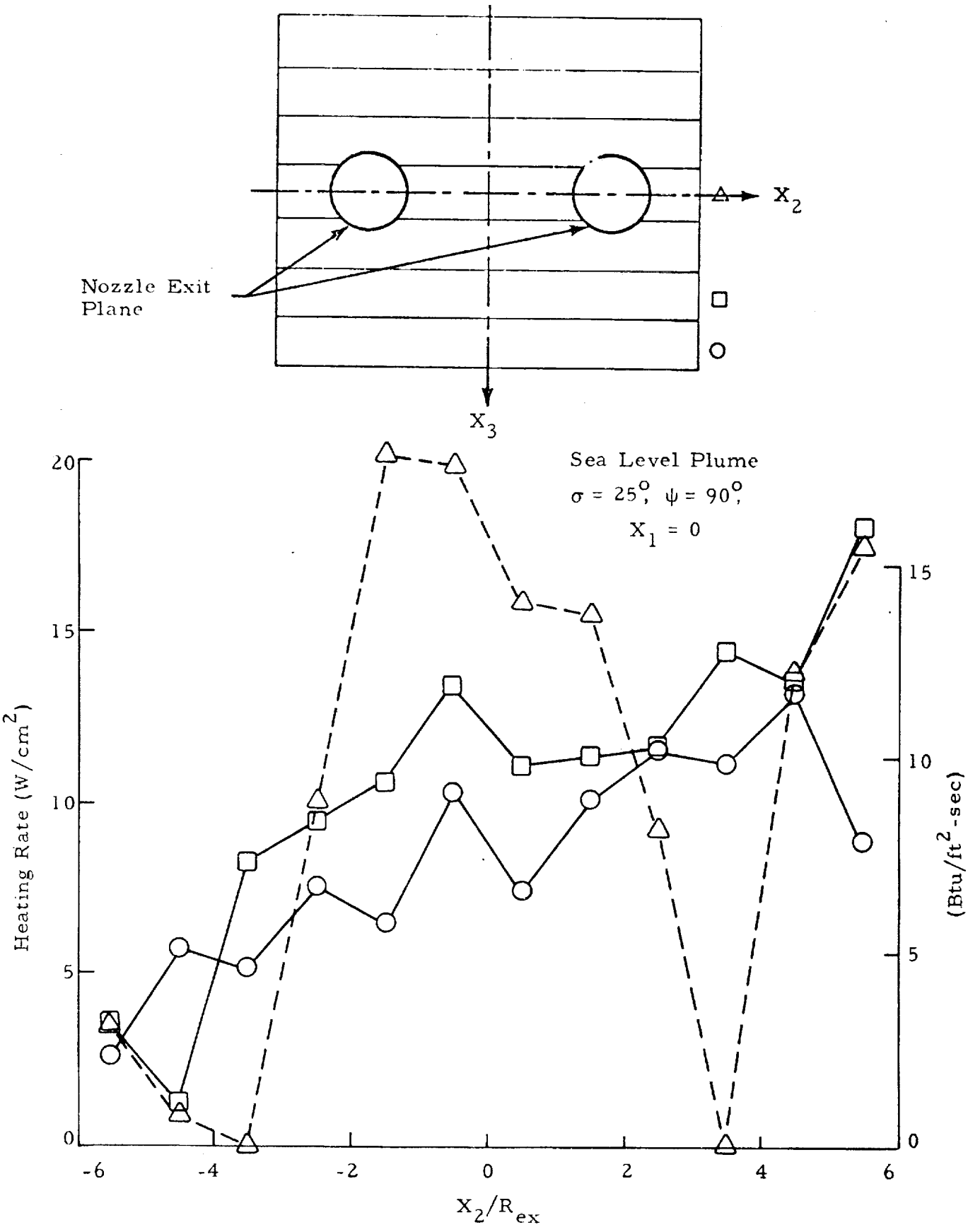

Fig. 5-8 - Heating Rate of a Rectangular Plane

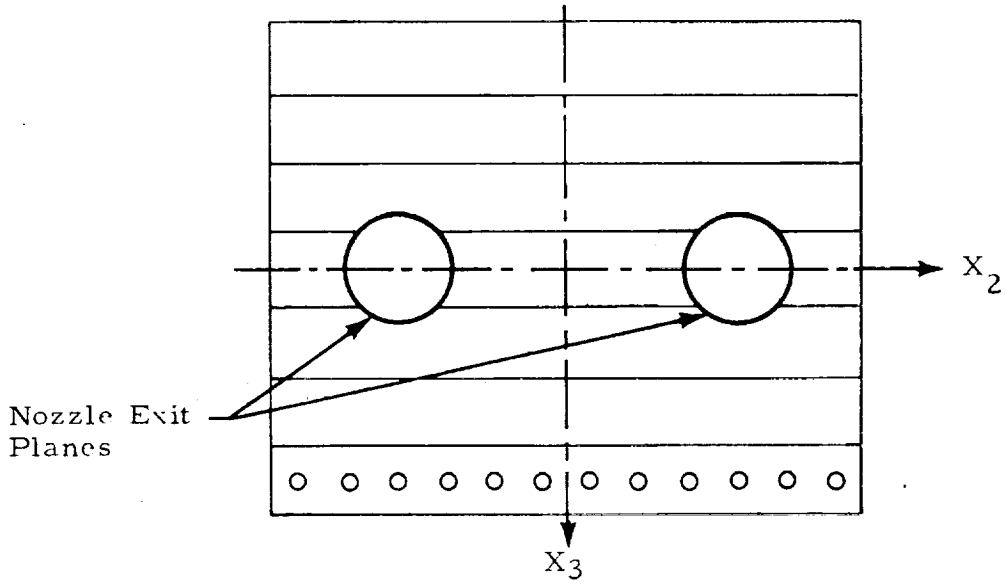

○ Nozzle Plane, $\sigma = 0^\circ$, $\psi = 0^\circ$ (50,000 Samples)

△ $X_1 = -4.94$, $\sigma = 0^\circ$, $\psi = 0^\circ$ (50,000 Samples)

◇ Nozzle Plane, $\sigma = 25^\circ$, $\psi = 0^\circ$ (20,000 Samples)

□ Nozzle Plane, $\sigma = -30^\circ$, $\psi = 0^\circ$ (20,000 Samples)

Altitude = 9430 ft

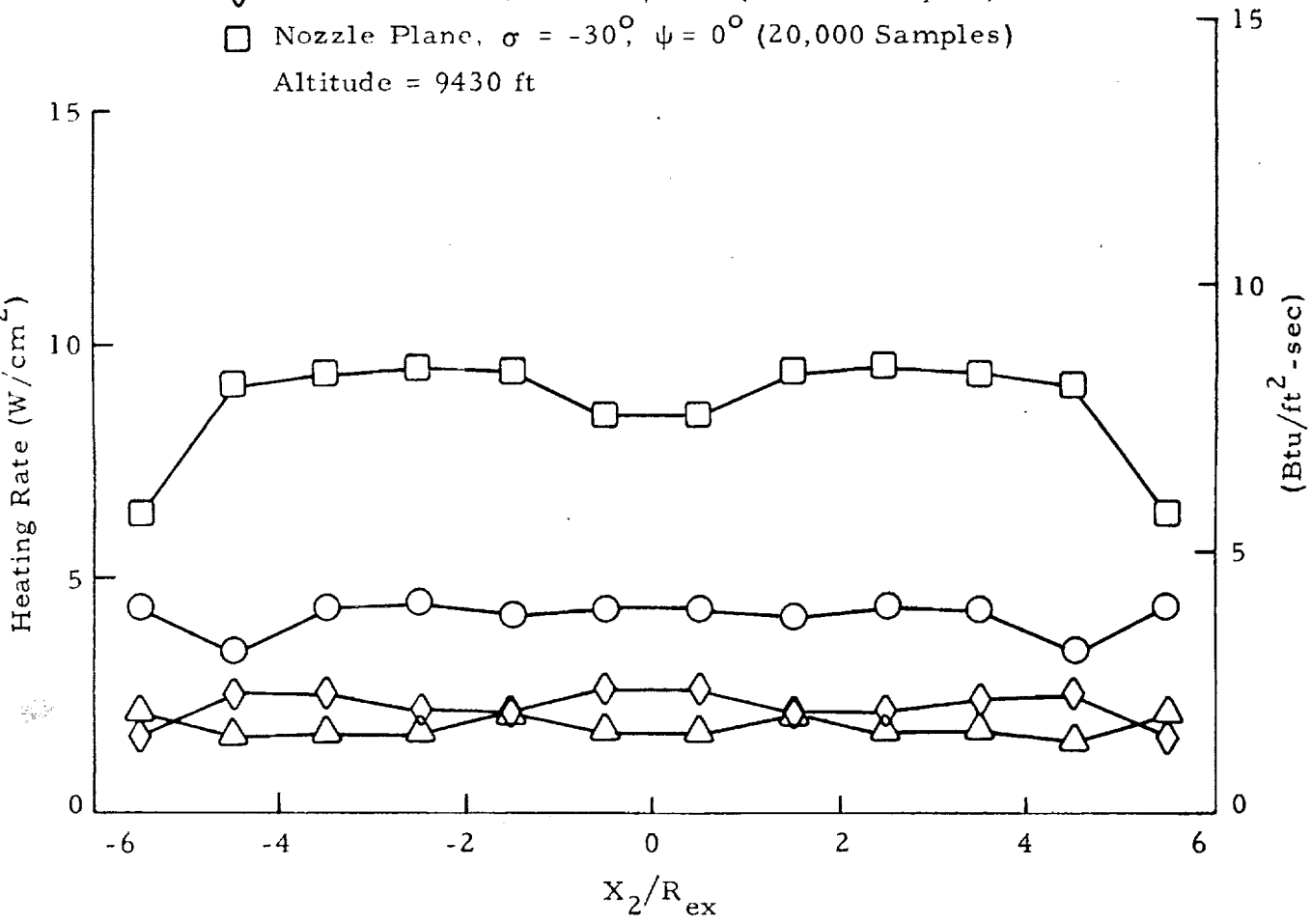

Fig. 5-9 - Heating Rate of a Rectangular Plane

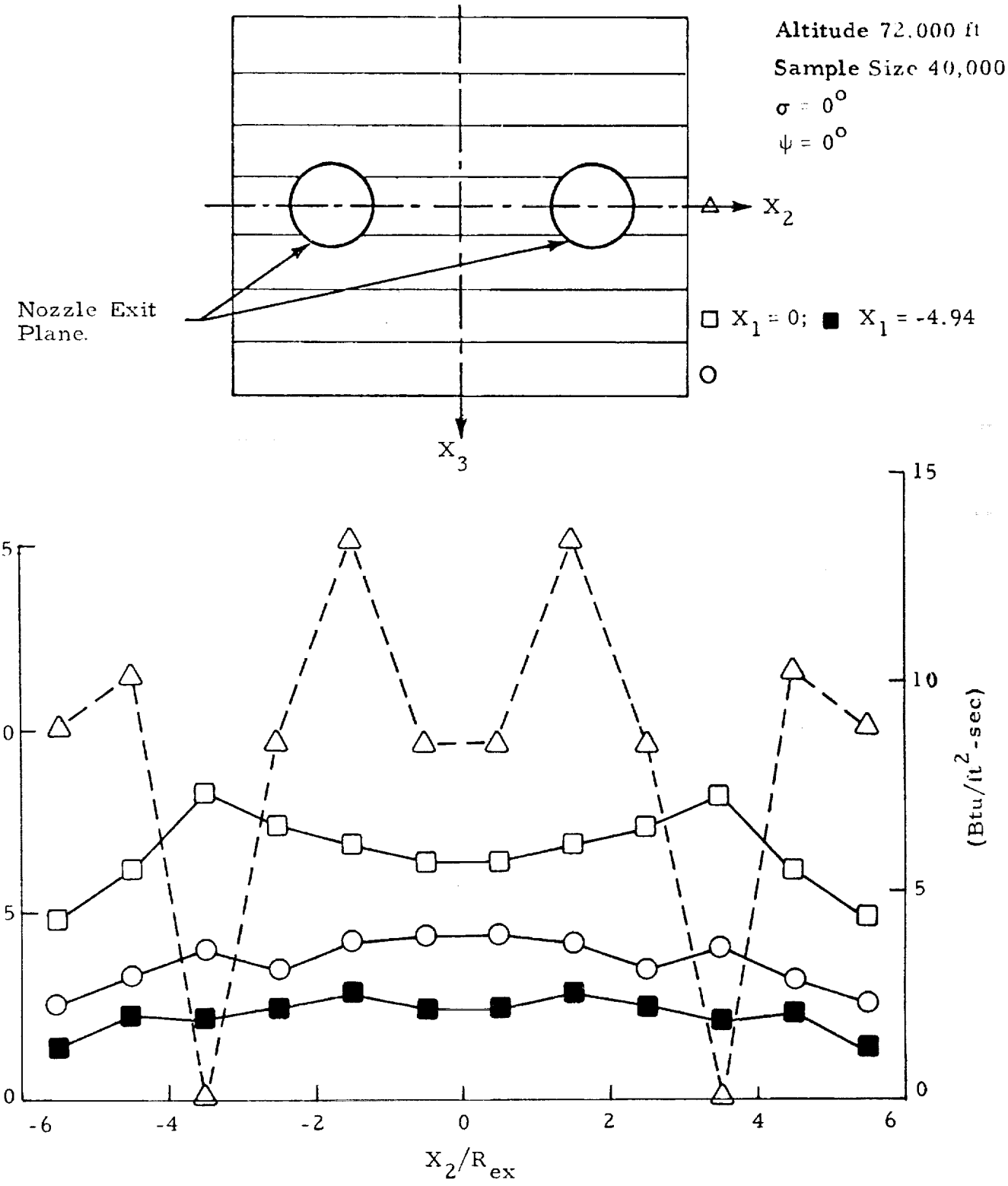

Fig. 5-10 - Heating Rate of a Rectangular Plane

at $X_1 = -4.94$ is seen to be only one third of that at $X_1 = 0$ for the same row of subtargets.

A simple geometry package (see Fig. 5-11) was put together to compute the heat flux at the end dome of the ET. The shading effects of the nozzle are simulated with a disk placed at the nozzle exit plane. The end of the ET is divided into three rings which are further divided into four parts. The heat flux on each division is summarized in Table 5-1. Table 5-2 shows the heat flux when the sea level plumes are gimbaled in pitch plane and in yaw plane. The effects of gimbaling are especially pronounced when the plumes have large pitch angles (σ large, $\psi = 0$). Table 5-3 shows the heat flux of gimbaled dual plumes at 72,000 ft altitude. It is observed that the gimbal angles in both the pitch plane or yaw plane increase the heat flux at the ET dome substantially.

Two models were made to facilitate the study of heat flux within the nozzle shroud enclosure. One model is shown in Fig. 5-12. Four target surfaces constitute the model. Surface 2 is the skirt of the nozzle plus the end constraint plane and a stiffener. Surface 4 is another stiffener at the mid-height of the skirt. The heat fluxes on these two surfaces are given in Table 5-4 for a single plume at three altitudes.

Another nozzle enclosure model is shown in Fig. 5-13. This model is in closer agreement in its dimensions to the actual shroud design on the SRB. The target surfaces are designated by numbers. The heat fluxes are given in Table 5-5 for a single plume at three altitudes.

The geometry model of the ET and SRB structure is shown in Fig. 5-14. The target surfaces are designated by numbers. The end dome of the ET is divided into four rings on its surface. The plumes at three altitudes are not gimbaled. The heat fluxes are summarized in Table 5-6.

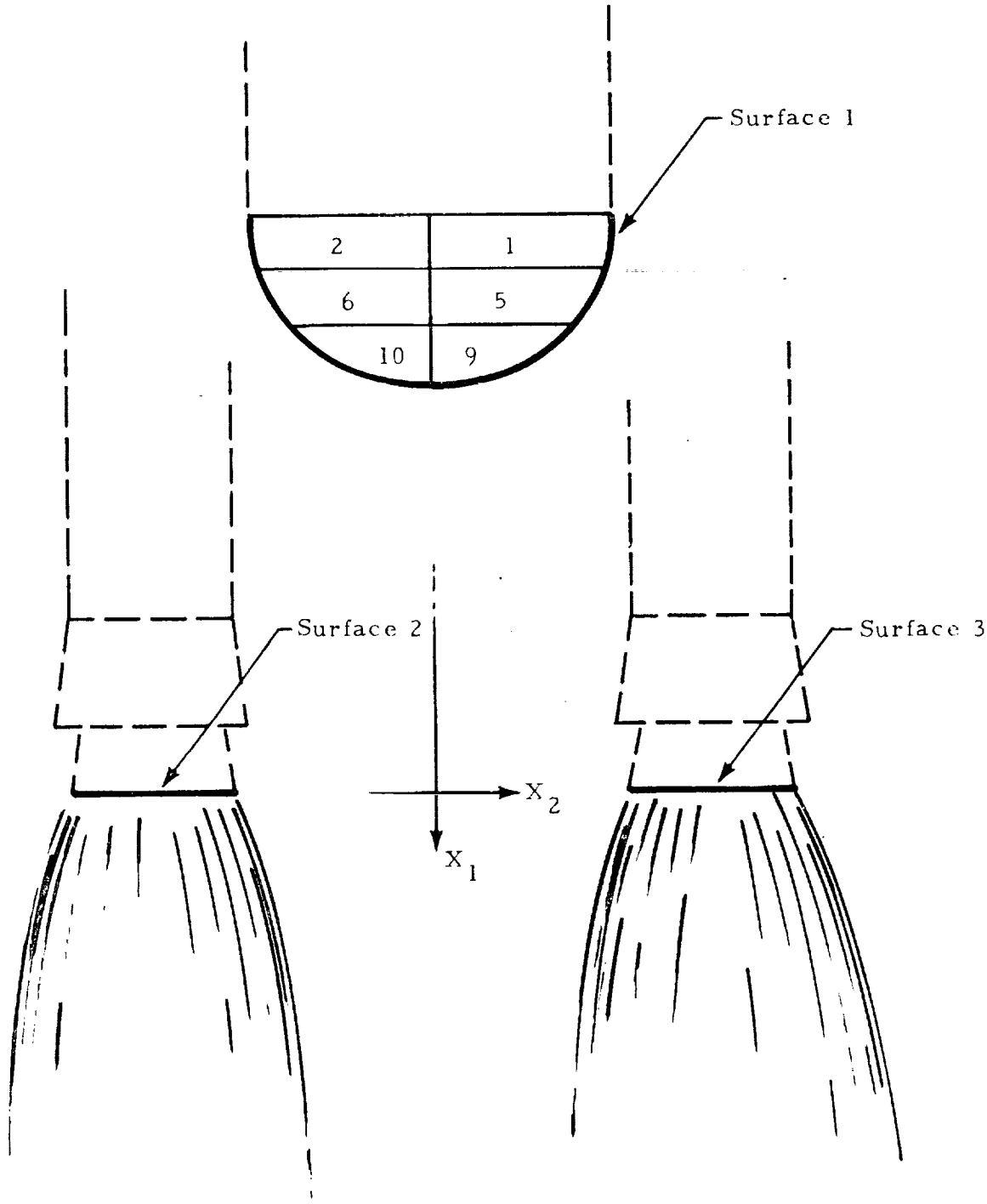

Fig. 5-11 - Schematic of ET End Dome

Table 5-1

HEAT FLUX ON THE ET DOME

Target	Sea Level		9430 ft		72,000 ft	
	W/cm^2	Btu/ft^2-sec	W/cm^2	Btu/ft^2-sec	W/cm^2	Btu/ft^2-sec
1	1.05	0.93	0.49	0.43	0.76	0.66
2	1.05	0.93	0.49	0.43	0.76	0.66
3	1.61	1.42	0.38	0.33	0.79	0.70
4	1.61	1.42	0.38	0.33	0.79	0.70
Avg.	1.33	1.17	0.43	0.38	0.77	0.68
5	0.93	0.82	0.90	0.79	1.03	0.91
6	0.93	0.82	0.90	0.79	1.03	0.91
7	2.32	2.05	0.67	0.59	1.17	1.03
8	2.32	2.05	0.67	0.59	1.17	1.03
Avg.	1.63	1.44	0.78	0.69	1.10	0.97
9	1.48	1.30	0.94	0.82	1.62	1.43
10	1.48	1.30	0.94	0.82	1.62	1.43
11	1.59	1.40	0.98	0.86	1.46	1.28
12	1.59	1.40	0.98	0.86	1.46	1.28
Avg.	1.54	1.35	0.96	0.84	1.54	1.35

Sample = 50,000, $\sigma = 0^{\circ}, \psi = 0^{\circ}$

Table 5-2

EFFECTS OF GIMBAL ANGLES ON HEAT FLUXES AT ET DOME FROM DUAL SEA LEVEL PLUMES

Target	ψ (deg)	0	90	0	90	0
	σ (deg)	0	8	8	35	35
1		1.14*	1.13	0.32	1.78	0.81
2		1.14	1.62	0.32	1.62	0.81
3		1.46	0.97	0.97	1.46	2.27
4		1.46	1.14	0.97	2.27	2.27
Avg.		1.30	1.22	0.65	1.78	1.54
5		0.93	1.12	1.31	1.68	1.31
6		0.93	1.87	1.31	2.24	1.31
7		2.43	1.12	1.31	2.06	2.62
8		2.43	0.75	1.31	2.62	2.62
Avg.		1.68	1.22	1.31	2.15	1.96
9		0.91	1.83	2.05	4.34	2.05
10		0.91	1.83	2.05	2.51	2.05
11		1.83	3.65	2.97	4.11	4.79
12		1.83	1.83	2.97	4.11	4.79
Avg.		1.37	2.28	2.51	3.77	3.42

*Heat flux in Btu/ft^2-sec

Table 5-3

HEAT FLUX ON THE ET DOME WITH GIMBALED PLUMES AT 72,000 FT

Target	σ (deg)	0	35	35
	ψ (deg)	0	90	0
1		0.67*	0.88	0.60
2		0.67	1.00	0.60
3		0.70	0.88	1.33
4		0.70	1.05	1.33
Avg.		0.68	0.96	0.97
5		0.91	1.57	1.01
6		0.91	1.54	1.01
7		1.03	1.42	1.80
8		1.03	1.36	1.80
Avg.		0.97	1.47	1.45
9		1.43	2.03	1.78
10		1.43	2.37	1.78
11		1.28	2.32	2.69
12		1.28	2.37	2.69
Avg.		1.36	2.27	2.24

*Heat flux in Btu/ft^2-sec.

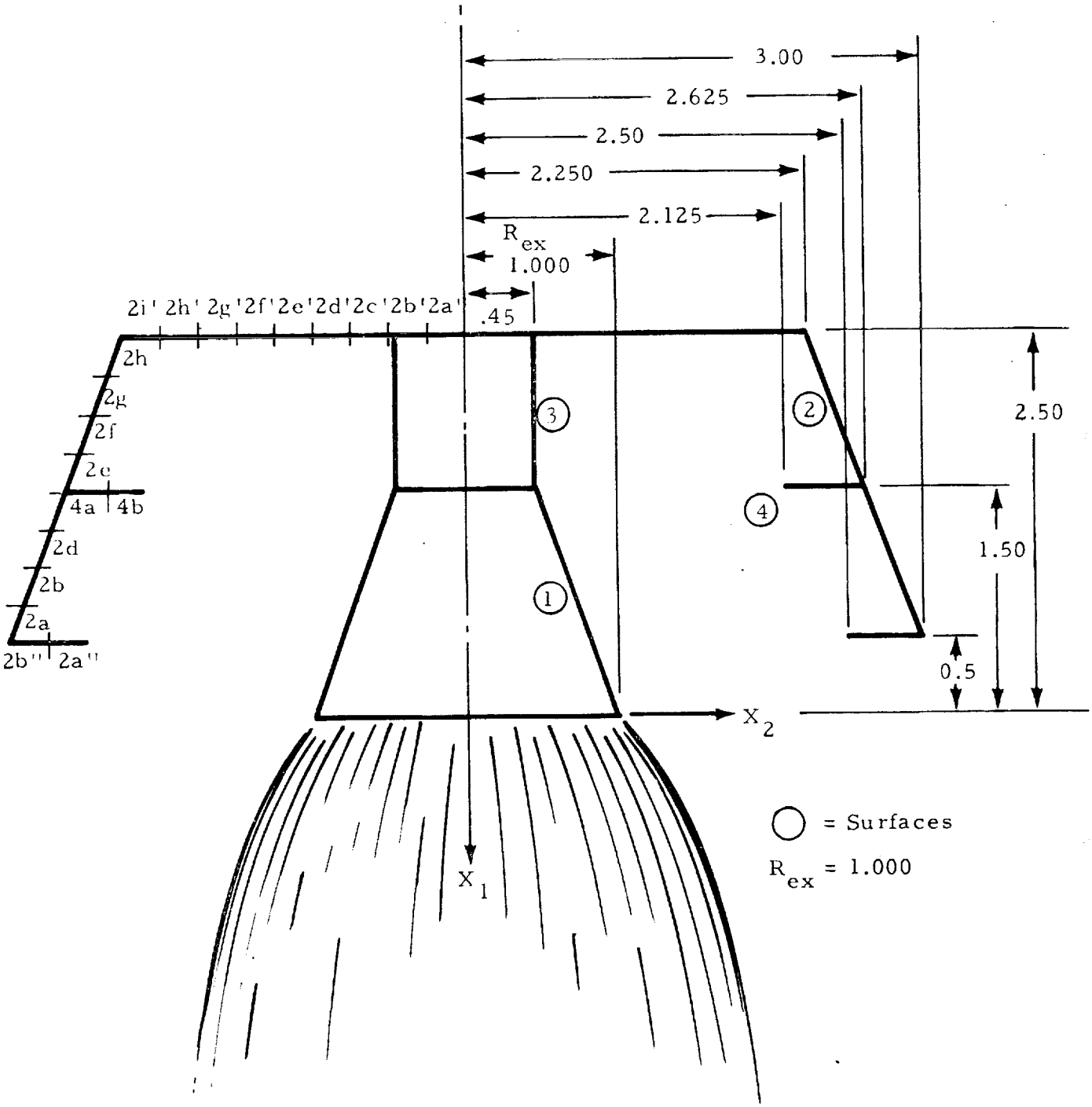

Fig. 5-12 - Model of Nozzle, Shroud and Stiffener

Table 5-4

HEAT FLUX ON NOZZLE SHROUD MODEL

Target	Sea Level		9430 ft		72,000 ft	
	W/cm^2	Btu/ft^2-sec	W/cm^2	Btu/ft^2-sec	W/cm^2	Btu/ft^2-sec
2a	0.10	0.09	0.13	0.12	0.38	0.34
2b	1.93	1.70	2.11	1.86	3.87	3.41
2c	2.96	2.61	2.71	2.39	5.45	4.80
2d	2.62	2.31	2.66	2.34	4.58	4.04
2e	0.23	0.21	2.04	1.80	1.50	1.32
2f	0.00	0.00	0.0	0.0	1.29	1.14
2g	0.50	0.44	0.77	0.68	1.24	1.09
2h	1.20	1.06	1.32	1.16	1.57	1.38
2a'	0.0	0.0	0.0	0.0	0.0	0.0
2b'	0.0	0.0	0.0	0.0	0.37	0.32
2c'	0.0	0.0	0.0	0.0	1.59	1.40
2d'	0.0	0.0	0.0	0.0	1.96	1.73
2e'	0.42	0.37	0.37	0.33	1.31	1.16
2f'	0.58	0.51	0.92	0.81	1.92	1.69
2g'	1.22	1.08	0.95	0.84	1.69	1.49
2h'	1.53	1.34	1.50	1.32	2.25	1.98
2i'	1.35	1.19	1.59	1.40	2.20	1.94
2a''	5.79	5.10	5.61	4.95	6.60	5.82
2b''	5.59	4.92	5.76	5.07	6.10	5.38
4a	3.11	2.74	2.87	2.53	4.18	3.68
4b	3.59	3.17	3.65	3.21	4.74	4.17

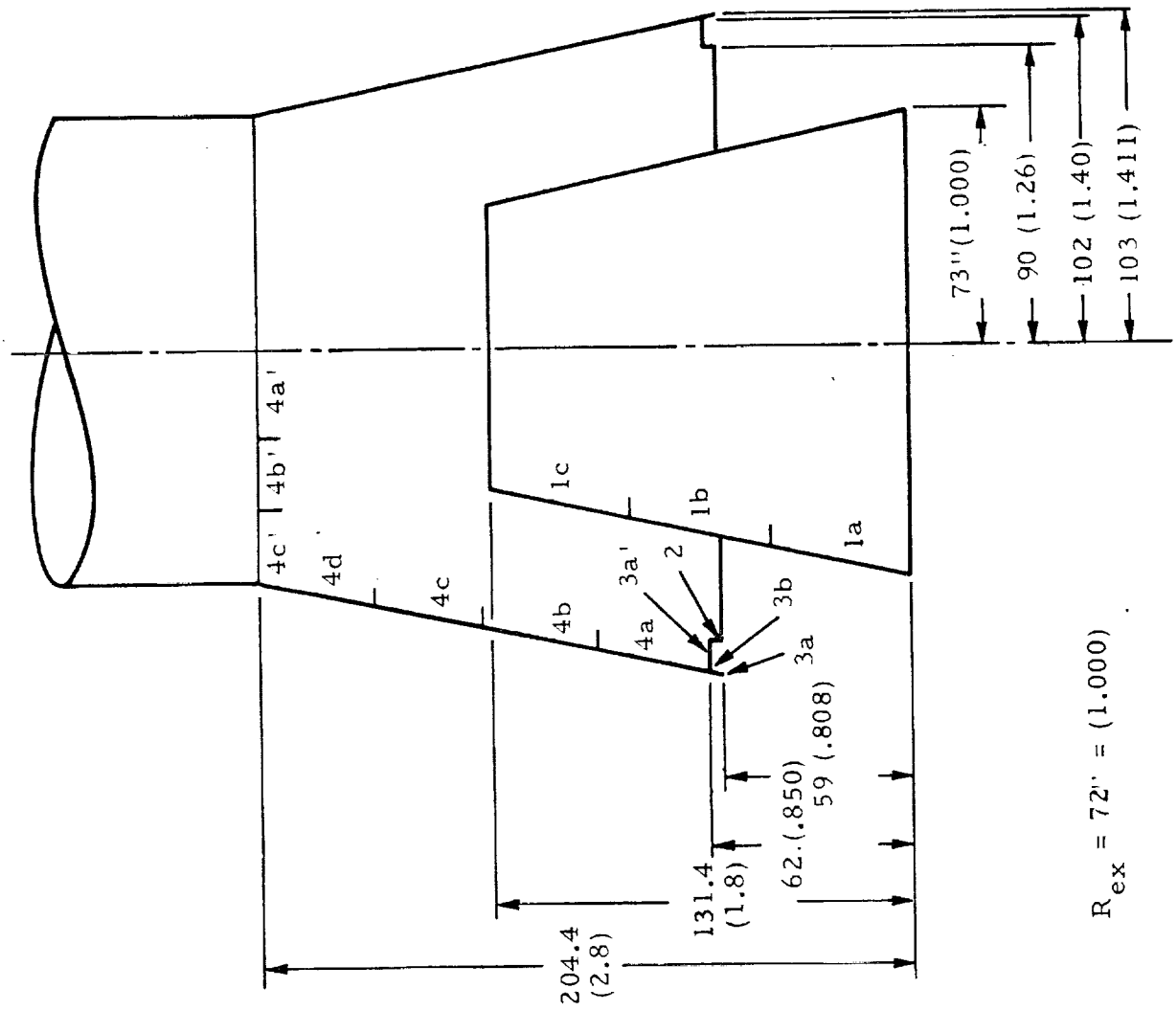

Fig. 5-13 - Model of Nozzle, Shroud and Stiffener

Table 5-5

HEAT FLUX ON A NOZZLE SHROUD MODEL

Altitude	Sea Level		9430 ft		72,000 ft	
Target	W/cm^2	Btu/ft^2-sec	W/cm^2	Btu/ft^2-sec	W/cm^2	Btu/ft^2-sec
1a	0.0	0.0	0.015	0.013	0.22	0.19
1b	0.0	0.0	0.0	0.0	0.07	0.06
1c	0.0	0.0	0.0	0.0	0.04	0.04
2	0.0	0.0	0.79	0.69	0.33	0.29
3a	0.0	0.0	0.27	0.24	1.51	1.33
3b	1.53	1.34	1.64	1.45	3.97	3.50
3a'	3.24	2.86	2.02	1.78	4.76	4.20
4a	0.10	0.09	0.15	1.13	0.22	0.20
4b	0.11	0.10	0.21	0.19	0.56	0.50
4c	0.12	0.01	0.13	0.12	0.32	0.28
4d	0.00	0.0	0.03	0.03	0.30	0.26
4a'	0.0	0.0	0.0	0.0	0.02	0.18
4b'	0.0	0.0	0.0	0.0	0.76	0.67
4c'	0.0	0.0	0.03	0.03	1.37	1.21

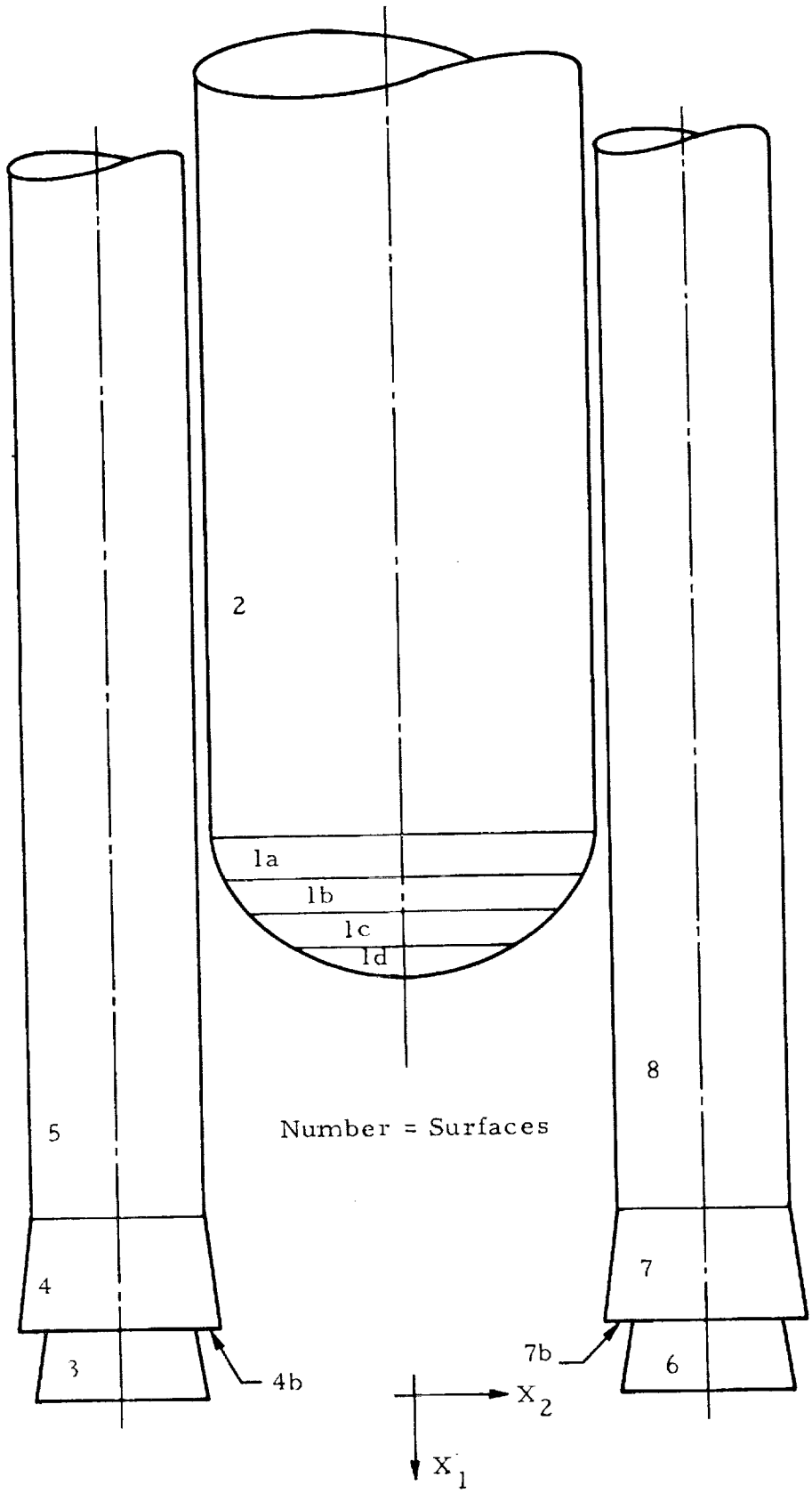

Fig. 5-14 - Model of the External Tank and Solid Rocket Boosters

Table 5-6

HEAT FLUX ON ET AND SRB DUE TO THE SRB PLUMES

Altitude	Sea Level		9430 ft		72,000 ft	
Target	W/cm^2	Btu/ft^2-sec	W/cm^2	Btu/ft^2-sec	W/cm^2	Btu/ft^2-sec
1a	1.33	1.17	0.19	0.17	0.50	0.44
1b	1.47	1.30	0.42	0.37	0.81	0.71
1c	1.91	1.69	1.15	1.01	1.30	1.15
1d	1.77	1.56	0.97	0.86	1.46	1.29
2 Max.	0.0	0.0	0.0	0.0	0.07	0.06
3 Avg.	0.91	0.80	0.61	0.54	0.78	0.69
3 Max.	3.45	3.04	1.95	1.72	2.19	1.93
4 Avg.	0.71	0.63	0.53	0.46	0.59	0.52
4 Max.	2.75	2.42	1.50	1.32	1.65	1.46
4b	2.73	2.40	1.76	1.55	3.53	3.11
4b Max.	6.64	5.85	4.03	3.55	6.02	5.31
5 Max.	1.03	0.91	0.56	0.49	0.98	0.86
6 Avg.	0.91	0.80	0.61	0.54	0.78	0.69
6 Max.	3.45	3.04	1.95	1.72	2.19	1.93
7 Avg.	0.71	0.63	0.53	0.46	0.59	0.52
7 Max.	2.75	2.42	1.50	1.32	1.65	1.46
7b	2.73	2.40	1.76	1.55	3.53	3.11
7b Max.	6.64	5.85	4.03	3.55	6.02	5.31
8 Max.	1.03	0.91	0.61	0.49	0.98	0.86

$\sigma = 0^o$, $\psi = 0^o$

5.3 EXAMPLES OF VIEW FACTOR CALCULATIONS

Several examples of view factor calculations are presented in this section. The first example involves the geometry of three disks, as shown in Fig. 5-15. The surface 1 is the emitting surface.

To compare the results with the exact solution and the results obtained with different sample sizes, the view factor of the entire surfaces is used although the view factors from the emitting surface to the sub-areas on the target surface are also available. The exact solution of view factor F_{1-2} is given as follows (Ref. 6):

$$R_1 = r_1/h, \quad R_2 = r_2/h$$

$$X = 1 + (1 + R_2^2)/R_1^2$$

$$F_{1-2} = (X - \sqrt{X^2 - 4\,(R_2/R_1)^2})/2$$

The results are summarized in Table 5-7.

A second example is given in Fig. 5-16, where a hemispherical emitting surface of unit radius is facing a dish-shaped target surface. The exact solution of the view factor calculation is available in the literature (Ref. 6) and is given as follows:

$$F_{1-2} = 1 - \frac{1}{\sqrt{1 - \left(\frac{r}{h}\right)^2}}$$

Comparisons of results are given in Table 5-8.

The third example demonstrates the heat flux calculation to a point in the base plane and a point on the base of the ET using the view factor method. A small disk with a radius of 0.001 is placed at either position 1 or position 2 at the end point of the ET (Fig. 5-17). The two SRB plumes for the 72,000 ft

$h = 3.0$

$d = 5.0$

$r_1 = 1.0$

$r_2 = 2.0$

$r_3 = 2.0$

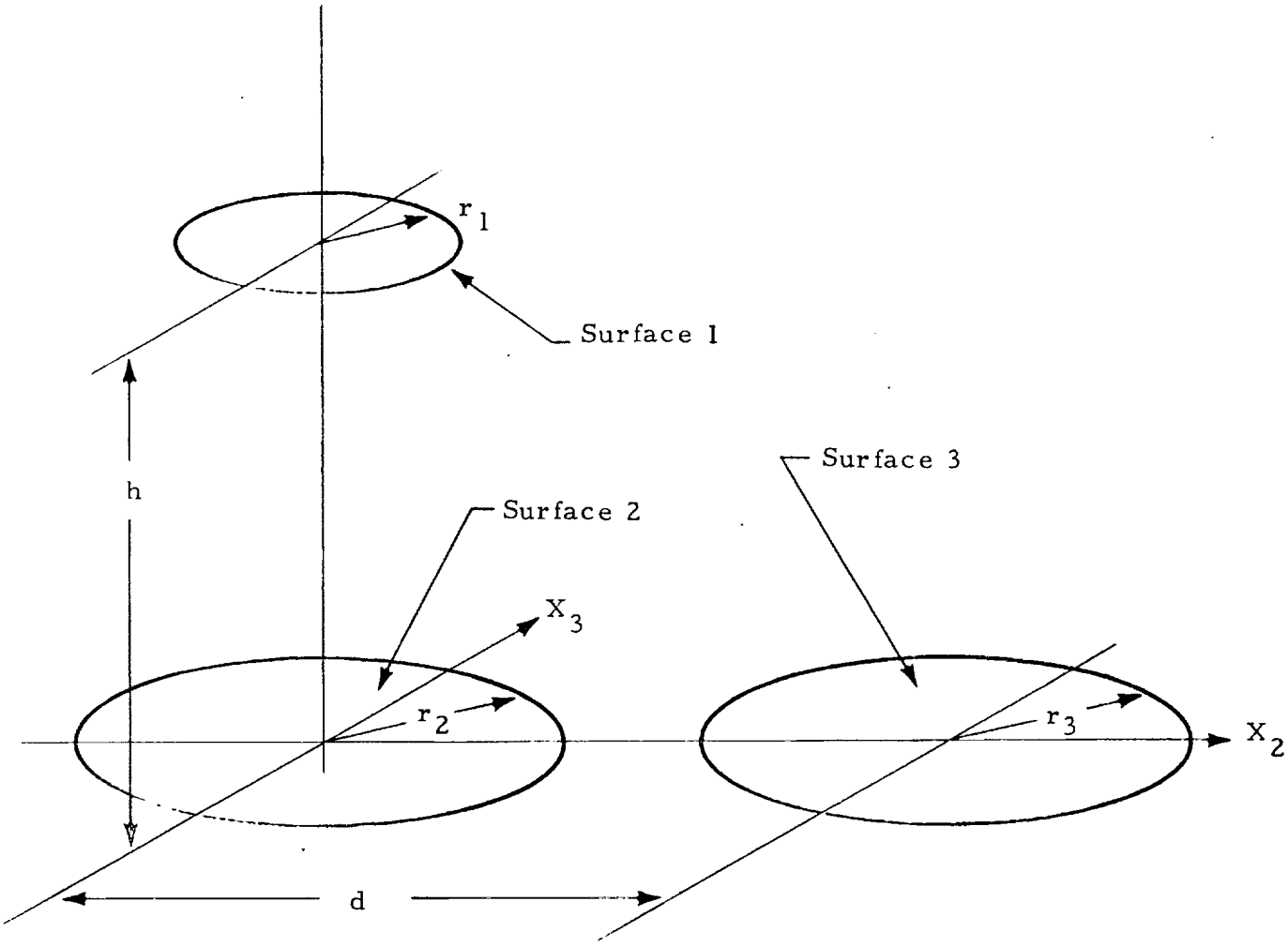

Fig. 5-15 - First Example of View Factor Calculation

Table 5-7

COMPARISON OF RESULTS FOR EXAMPLE 1

View Factor / Sample or Method	F_{1-2}	F_{2-1}	F_{1-3}	F_{3-1}
1000	0.2840	0.0710	0.0370	0.00925
2000	0.3020	0.0755	0.0345	0.00863
5000	0.2950	0.0738	0.0322	0.00805
10,000	0.2871	0.0718	0.0336	0.0084
20,000	0.2911	0.0728	0.0358	0.00894
Analytical	0.2918	0.07295	—	—

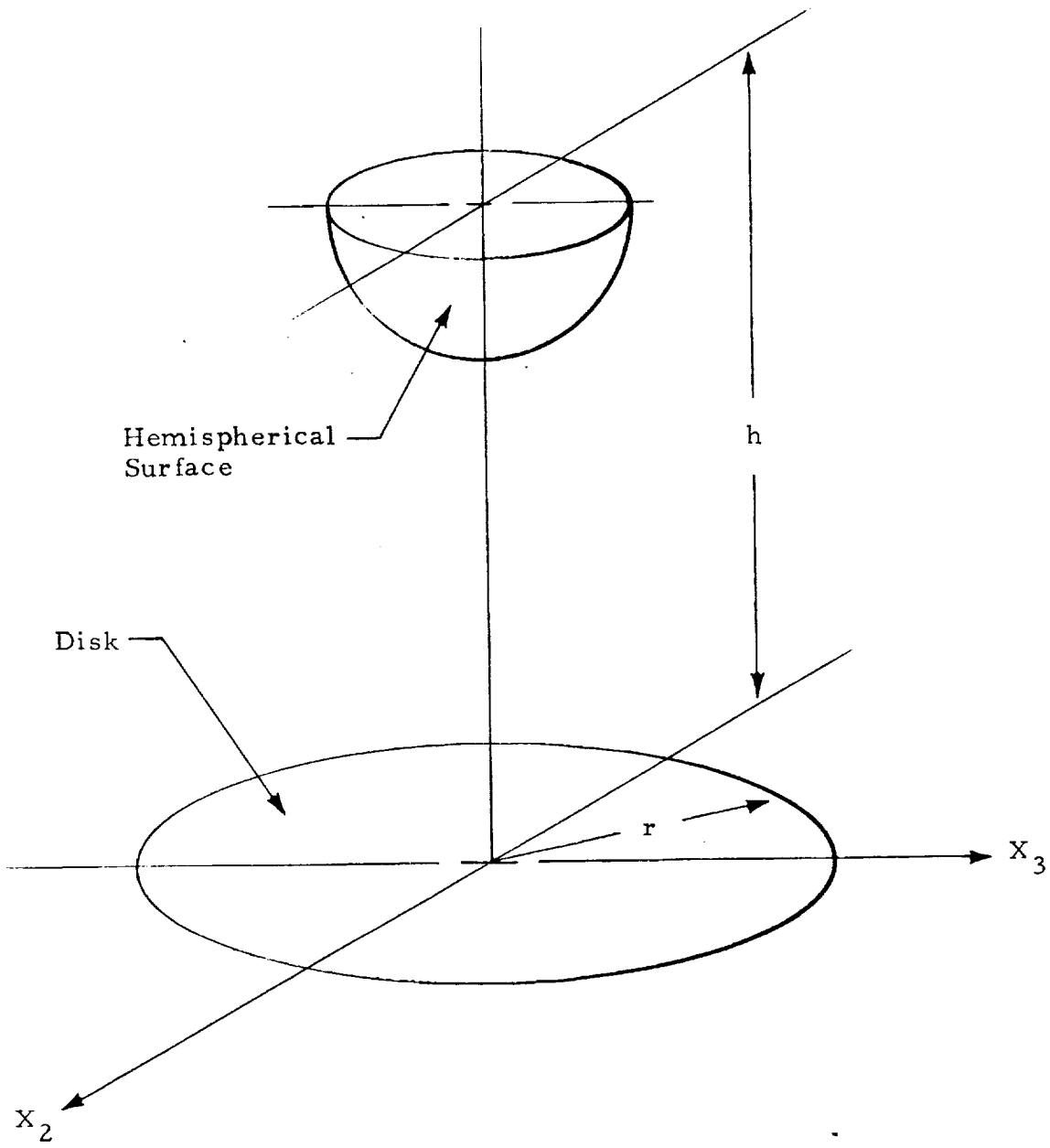

Fig. 5-16 - Second Example of View Factor Calculation

Table 5-8
COMPARISON OF RESULTS FOR EXAMPLE 2

View Factor / Sample or Method	r	h	F_{1-2}	F_{2-1}
Analytical	1	5	0.01942	0.03884
7500	1	5	0.01960	0.03920
Analytical	5	5	0.29289	0.02343
7500	5	5	0.2944	0.02355
5000*	5	5	0.2896	0.09267

*Radius of emitting hemisphere = 2.

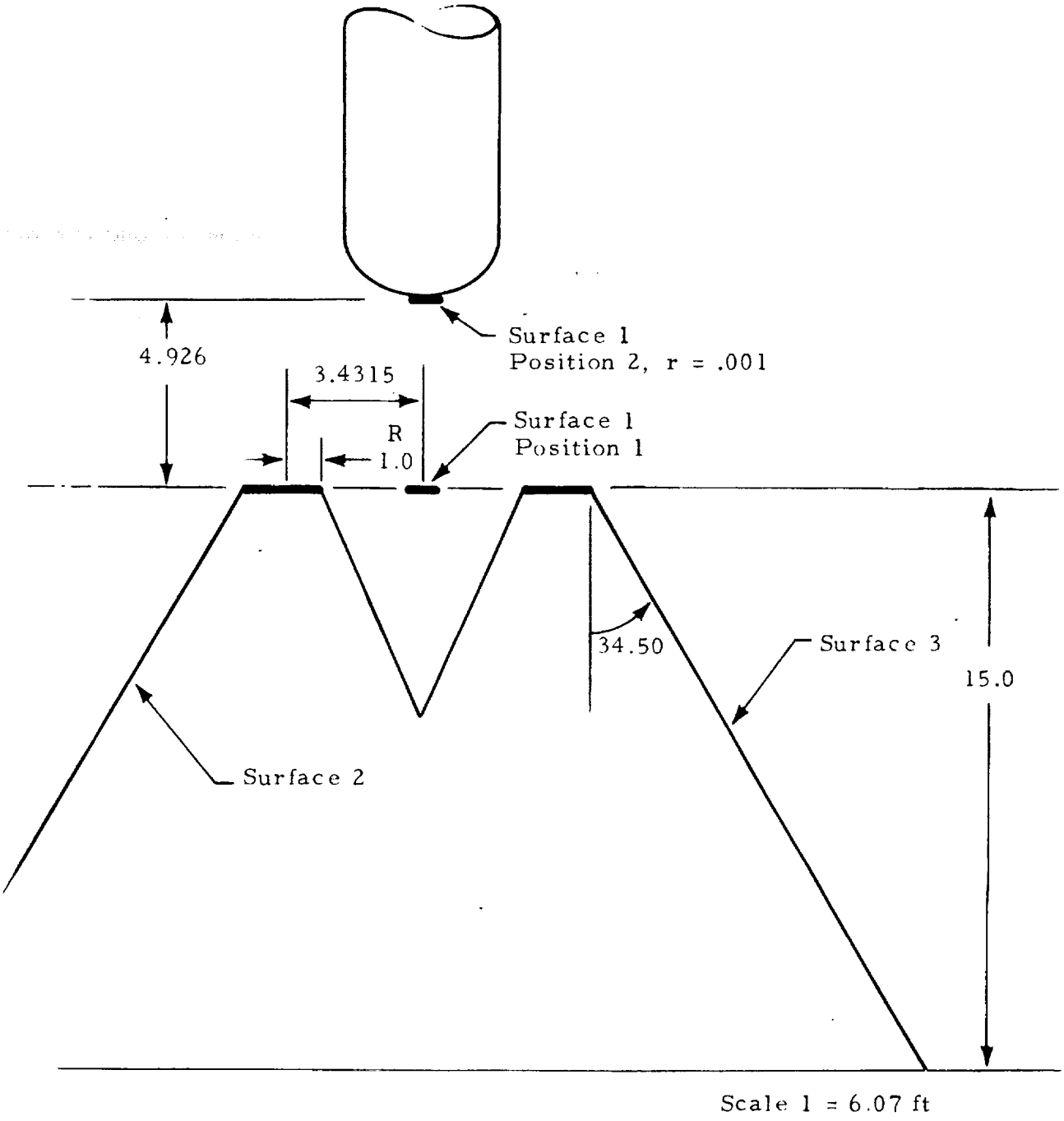

Fig. 5-17 - Calculation of Heating Rate by View Factors

trajectory point are represented by two frustum bodies. The average emissive power of the plume is assumed to be either 40 Btu/ft^2-sec or 25 Btu/ft^2-sec. The results are summarized in Table 5-9. The schematic of the SRB plumes and target points is shown in Fig. 5-17.

As a demonstration case, view factors from a sphere and a cylindrical rod (simulating a strut) to the surfaces within the nozzle shroud enclosure shown in Fig. 5-12 were computed. The orientations of the sphere and rod relative to the shroud are shown in Fig. 5-18. The surfaces are designated as target 1, target 2 and so on and their orientation is seen in Fig. 5-12. The emitting surfaces are the sphere and rod and are designated as number 1 and 2, respectively. The computer output is reproduced in Table 5-10. To limit the data printout to a reasonable number of pages, only data for target 1 (the nozzle) and target 2 (the conical shroud) are shown.

Table 5-9

HEATING RATES BY VIEW FACTORS FOR 72,000 FT PLUME

Location	1	2
View Factor F_{2-1}	1.9329-09	6.0481-10
View Factor F_{3-1}	1.8959-09	6.0736-10
Sum $F = F_{2-1} + F_{3-1}$	3.8288-09	1.2122-09
Heat Flux, Btu/ft^2-sec		
at 40 Btu/ft^2-sec	28.28	8.95
at 25 Btu/ft^2-sec	17.66	5.59

Emitting Surface: $r = 0.001^*$; $A_e = 3.14159^* \times 10^{-6} = 1.1575 \times 10^{-4}$ ft^2

Surface Area 2 or 3 = $580^* = 21370$ ft^2

Total Emission from 2 or 3 = $E_1 = 21370 \times 40 = 8.55 \times 10^5$ Btu/sec

$E_2 = 21370 \times 25 = 5.34 \times 10^5$ Btu/sec

Heat Flux at 40 Btu/ft^2-sec = $8.55 \times 10^5 \times F/A_e$

Heat Flux at 25 Btu/ft^2-sec = $5.34 \times 10^5 \times F/A_e$

*Non-dimensional.

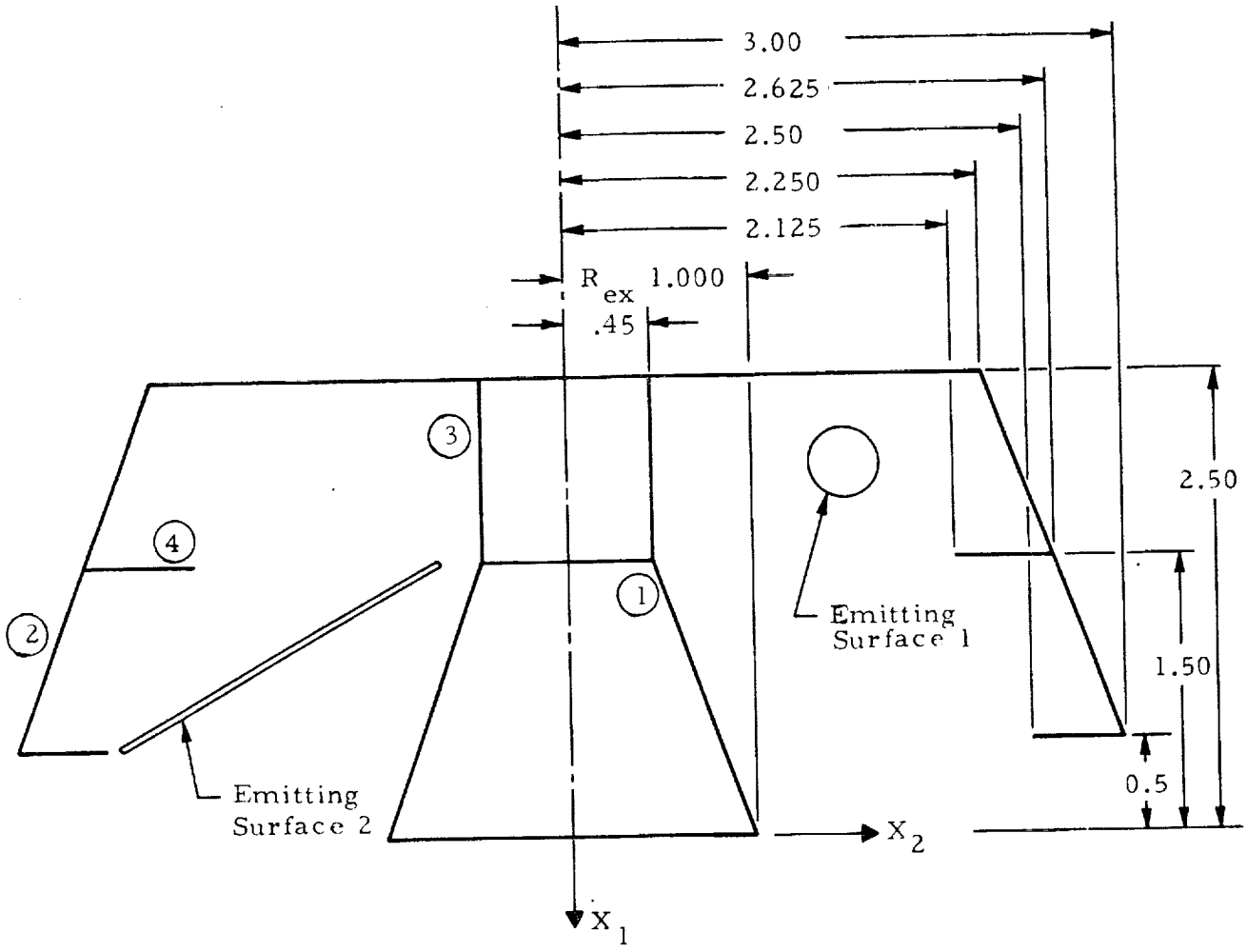

Fig. 5-18 - Geometry of View Factor Calculation in the Nozzle Shroud

Table 5-10

VIEW FACTORS FOR SHROUD GEOMETRY

INPUT DATA FOR TARGET NO. 1

2 12 3 1 1 1.0000 .0000 .0000 .4500

-1.5000 .0000 .0000 .0000 .0000 .0000 -1.5000 .0000 .4500

TRANSFORMATION MATRIX

.100000+01 .000000 .000000

.000000 .100000+01 .000000

.000000 .000000 .100000+01

COEFFICIENTS FOR A CONE

C1 = -.100000+01

C2 = .100000+01

C3 = .100000+01

C4 = .000000

C5 = .000000

C6 = .000000

C7 = -.750000+00

C8 = .000000

C9 = .000000

C9,1 = -.100000+01

RBOND(NDATA), RBONDU(NDATA) .100000+01 .450000+00

COEFFICIENTS FOR CONSTRAINT PLANES

C11 = .100000+01

C12 = .000000

C13 = .000000

C9,1 = -.150000+01

C9,2 = .000000

REFERENCE POINTS ON CONSTRAINT DISK T(.00000 .00000 1.00000) S(.00000 1.00000 .00000)

COMPONENTS FOR VIEW POINT VECTORS

1.	VP1= -.250000+00	VP2= .235894+00	VP3= .877383+00	AREA= .253283+00
2.	VP1= -.250000+00	VP2= .642289+00	VP3= .642289+00	AREA= .253283+00
3.	VP1= -.250000+00	VP2= .877383+00	VP3= .235894+00	AREA= .253283+00
4.	VP1= -.250000+00	VP2= .877383+00	VP3= -.235894+00	AREA= .253283+00
5.	VP1= -.250000+00	VP2= .642289+00	VP3= -.642289+00	AREA= .253283+00
6.	VP1= -.250000+00	VP2= .235894+00	VP3= -.877383+00	AREA= .253283+00
7.	VP1= -.250000+00	VP2= -.235894+00	VP3= -.877383+00	AREA= .253283+00
8.	VP1= -.250000+00	VP2= -.642289+00	VP3= -.642289+00	AREA= .253283+00
9.	VP1= -.250000+00	VP2= -.877383+00	VP3= -.235894+00	AREA= .253283+00
10.	VP1= -.250000+00	VP2= -.877383+00	VP3= .235894+00	AREA= .253283+00
11.	VP1= -.250000+00	VP2= -.642289+00	VP3= .642289+00	AREA= .253283+00
12.	VP1= -.250000+00	VP2= -.235894+00	VP3= .877383+00	AREA= .253283+00
13.	VP1= -.750000+00	VP2= .187644+00	VP3= .700296+00	AREA= .202161+00
14.	VP1= -.750000+00	VP2= .512652+00	VP3= .512652+00	AREA= .202161+00
15.	VP1= -.750000+00	VP2= .700296+00	VP3= .187644+00	AREA= .202161+00
16.	VP1= -.750000+00	VP2= .700296+00	VP3= -.187644+00	AREA= .202161+00
17.	VP1= -.750000+00	VP2= .512652+00	VP3= -.512652+00	AREA= .202161+00
18.	VP1= -.750000+00	VP2= .187644+00	VP3= -.700296+00	AREA= .202161+00
19.	VP1= -.750000+00	VP2= -.187644+00	VP3= -.700296+00	AREA= .202161+00
20.	VP1= -.750000+00	VP2= -.512652+00	VP3= -.512652+00	AREA= .202161+00
21.	VP1= -.750000+00	VP2= -.700296+00	VP3= -.187644+00	AREA= .202161+00
22.	VP1= -.750000+00	VP2= -.700296+00	VP3= .187644+00	AREA= .202161+00

23.	VP1= -.750000+00	VP2= -.512652+00	VP3= .512652+00	AREA= .202161+00
24.	VP1= -.750000+00	VP2= -.187644+00	VP3= .700296+00	AREA= .202161+00
25.	VP1= -.125000+01	VP2= .140194+00	VP3= .523210+00	AREA= .151040+00
26.	VP1= -.125000+01	VP2= .383016+00	VP3= .383016+00	AREA= .151040+00
27.	VP1= -.125000+01	VP2= .523210+00	VP3= .140194+00	AREA= .151040+00
28.	VP1= -.125000+01	VP2= .523210+00	VP3= -.140194+00	AREA= .151040+00
29.	VP1= -.125000+01	VP2= .383016+00	VP3= -.383016+00	AREA= .151040+00
30.	VP1= -.125000+01	VP2= .140194+00	VP3= -.523210+00	AREA= .151040+00
31.	VP1= -.125000+01	VP2= -.140194+00	VP3= -.523210+00	AREA= .151040+00
32.	VP1= -.125000+01	VP2= -.383016+00	VP3= -.383016+00	AREA= .151040+00
33.	VP1= -.125000+01	VP2= -.523210+00	VP3= -.140194+00	AREA= .151040+00
34.	VP1= -.125000+01	VP2= -.523210+00	VP3= .140194+00	AREA= .151040+00
35.	VP1= -.125000+01	VP2= -.383016+00	VP3= .383016+00	AREA= .151040+00
36.	VP1= -.125000+01	VP2= -.140194+00	VP3= .523210+00	AREA= .151040+00

OU CONSTRAINT DISK NO.1

	RMEAN	AREA
1	.229000+00	.533144-01

OU CONSTRAINT DISK NO.2

	RMEAN	AREA
1	.500000+00	.261799+00

INPUT DATA FOR TARGET NO. 2

2 12 8 9 2 3.0000 .0000 2.5000 2.2500
-2.5000 .0000 .0000 -.5000 .0000 .0000 -2.5000 .0000 2.2500

TRANSFORMATION MATRIX

.100000+01 .000000 .000000
.000000 .100000+01 .000000
.000000 .000000 .100000+01

COEFFICIENTS FOR A CONE

C1 = -.145625+01
C2 = .100000+01
C3 = .100000+01
C4 = .000000
C5 = .000000
C6 = .000000
C7 = -.234762+01
C8 = .000000
C9 = .000000
CONST = -.101602+02
RADIUS(NDATA), ROUNDU(NDATA) .375000+01 .225000+01

COEFFICIENTS FOR CONSTRAINT PLANES

C11 = .100000+01
C12 = .000000
C13 = .000000
CONST = -.250000+01
CHANGE = -.000000+00
REFERENCE POINTS ON CONSTRAINT DISK T(-.50000 .00000 3.00000) S(-.50000 3.00000 .00000)

COMPONENTS FOR VIEW POINT VECTORS

1.	VP1= -.625000+00	VP2= .764325+00	VP3= .285250+01	AREA= .412850+00
2.	VP1= -.625000+00	VP2= .208817+01	VP3= .208817+01	AREA= .412850+00
3.	VP1= -.625000+00	VP2= .285250+01	VP3= -.764325+00	AREA= .412850+00
4.	VP1= -.625000+00	VP2= .208817+01	VP3= -.208817+01	AREA= .412850+00
5.	VP1= -.625000+00	VP2= .764325+00	VP3= -.285250+01	AREA= .412850+00
6.	VP1= -.625000+00	VP2= -.764325+00	VP3= -.285250+01	AREA= .412850+00
7.	VP1= -.625000+00	VP2= -.208817+01	VP3= -.208817+01	AREA= .412850+00
8.	VP1= -.625000+00	VP2= -.285250+01	VP3= -.764325+00	AREA= .412850+00
9.	VP1= -.625000+00	VP2= -.285250+01	VP3= .764325+00	AREA= .412850+00
10.	VP1= -.625000+00	VP2= -.208817+01	VP3= .208817+01	AREA= .412850+00
11.	VP1= -.625000+00	VP2= -.764325+00	VP3= .285250+01	AREA= .412850+00
12.	VP1= -.625000+00	VP2= -.740261+00	VP3= .276194+01	AREA= .399743+00
13.	VP1= -.875000+00	VP2= .202188+01	VP3= .202188+01	AREA= .399743+00
14.	VP1= -.875000+00	VP2= .276194+01	VP3= .740261+00	AREA= .399743+00
15.	VP1= -.875000+00	VP2= .276194+01	VP3= -.740261+00	AREA= .399743+00
16.	VP1= -.875000+00	VP2= .202188+01	VP3= -.202188+01	AREA= .399743+00
17.	VP1= -.875000+00	VP2= .740261+00	VP3= -.276194+01	AREA= .399743+00
18.	VP1= -.875000+00	VP2= -.740261+00	VP3= -.276194+01	AREA= .399743+00
19.	VP1= -.875000+00	VP2= -.202188+01	VP3= -.202188+01	AREA= .399743+00
20.	VP1= -.875000+00	VP2= -.276194+01	VP3= -.740261+00	AREA= .399743+00
21.	VP1= -.875000+00	VP2= -.276194+01	VP3= .740261+00	AREA= .399743+00
22.	VP1= -.875000+00	VP2= -.202188+01	VP3= .202188+01	AREA= .399743+00

23.	VP1= -.875000+00	VP2= -.202188+01	VP3= .202188+01	AREA= .399743+00
24.	VP1= -.875000+00	VP2= -.743061+00	VP3= .276194+01	AREA= .399743+00
25.	VP1= -.112500+01	VP2= .715796+00	VP3= .267139+01	AREA= .386637+00
26.	VP1= -.112500+01	VP2= .195559+01	VP3= .195559+01	AREA= .386637+00
27.	VP1= -.112500+01	VP2= .267139+01	VP3= .715796+00	AREA= .386637+00
28.	VP1= -.112500+01	VP2= .267139+01	VP3= -.715796+00	AREA= .386637+00
29.	VP1= -.112500+01	VP2= .195559+01	VP3= -.195559+01	AREA= .386637+00
30.	VP1= -.112500+01	VP2= .715797+00	VP3= -.267139+01	AREA= .386637+00
31.	VP1= -.112500+01	VP2= -.715796+00	VP3= -.267139+01	AREA= .386637+00
32.	VP1= -.112500+01	VP2= -.195559+01	VP3= -.195559+01	AREA= .386637+00
33.	VP1= -.112500+01	VP2= -.267139+01	VP3= -.715797+00	AREA= .386637+00
34.	VP1= -.112500+01	VP2= -.267139+01	VP3= .715796+00	AREA= .386637+00
35.	VP1= -.112500+01	VP2= -.195559+01	VP3= .195559+01	AREA= .386637+00
36.	VP1= -.112500+01	VP2= -.715797+00	VP3= .267139+01	AREA= .386637+00
37.	VP1= -.137500+01	VP2= .691532+00	VP3= .258083+01	AREA= .373531+00
38.	VP1= -.137500+01	VP2= .188930+01	VP3= .188930+01	AREA= .373531+00
39.	VP1= -.137500+01	VP2= .258083+01	VP3= .691532+00	AREA= .373531+00
40.	VP1= -.137500+01	VP2= .258083+01	VP3= -.691532+00	AREA= .373531+00
41.	VP1= -.137500+01	VP2= .188930+01	VP3= -.188930+01	AREA= .373531+00
42.	VP1= -.137500+01	VP2= .691532+00	VP3= -.258083+01	AREA= .373531+00
43.	VP1= -.137500+01	VP2= -.691532+00	VP3= -.258083+01	AREA= .373531+00
44.	VP1= -.137500+01	VP2= -.188930+01	VP3= -.188930+01	AREA= .373531+00
45.	VP1= -.137500+01	VP2= -.258083+01	VP3= -.691532+00	AREA= .373531+00
46.	VP1= -.137500+01	VP2= -.258083+01	VP3= .691532+00	AREA= .373531+00
47.	VP1= -.137500+01	VP2= -.188930+01	VP3= .188930+01	AREA= .373531+00
48.	VP1= -.137500+01	VP2= -.691532+00	VP3= .258083+01	AREA= .373531+00
49.	VP1= -.162500+01	VP2= .667268+00	VP3= .249028+01	AREA= .360424+00
50.	VP1= -.162500+01	VP2= .182301+01	VP3= .182301+01	AREA= .360424+00
51.	VP1= -.162500+01	VP2= .249028+01	VP3= .667268+00	AREA= .360424+00
52.	VP1= -.162500+01	VP2= .249028+01	VP3= -.667268+00	AREA= .360424+00
53.	VP1= -.162500+01	VP2= .182301+01	VP3= -.182301+01	AREA= .360424+00
54.	VP1= -.162500+01	VP2= .667268+00	VP3= -.249028+01	AREA= .360424+00
55.	VP1= -.162500+01	VP2= -.667268+00	VP3= -.249028+01	AREA= .360424+00
56.	VP1= -.162500+01	VP2= -.182301+01	VP3= -.182301+01	AREA= .360424+00
57.	VP1= -.162500+01	VP2= -.249028+01	VP3= -.667268+00	AREA= .360424+00
58.	VP1= -.162500+01	VP2= -.249028+01	VP3= .667268+00	AREA= .360424+00
59.	VP1= -.162500+01	VP2= -.182301+01	VP3= .182301+01	AREA= .360424+00
60.	VP1= -.162500+01	VP2= -.667268+00	VP3= .249028+01	AREA= .360424+00
61.	VP1= -.187500+01	VP2= .643004+00	VP3= .239972+01	AREA= .347318+00
62.	VP1= -.187500+01	VP2= .175672+01	VP3= .175672+01	AREA= .347318+00
63.	VP1= -.187500+01	VP2= .239972+01	VP3= .643004+00	AREA= .347318+00
64.	VP1= -.187500+01	VP2= .239972+01	VP3= -.643003+00	AREA= .347318+00
65.	VP1= -.187500+01	VP2= .175672+01	VP3= -.175672+01	AREA= .347318+00
66.	VP1= -.187500+01	VP2= .643004+00	VP3= -.239972+01	AREA= .347318+00
67.	VP1= -.187500+01	VP2= -.643004+00	VP3= -.239972+01	AREA= .347318+00
68.	VP1= -.187500+01	VP2= -.175672+01	VP3= -.175672+01	AREA= .347318+00
69.	VP1= -.187500+01	VP2= -.239972+01	VP3= -.643004+00	AREA= .347318+00
70.	VP1= -.187500+01	VP2= -.239972+01	VP3= .643003+00	AREA= .347318+00
71.	VP1= -.187500+01	VP2= -.175672+01	VP3= .175672+01	AREA= .347318+00
72.	VP1= -.187500+01	VP2= -.643004+00	VP3= .239972+01	AREA= .347318+00
73.	VP1= -.212500+01	VP2= .618739+00	VP3= .230917+01	AREA= .334212+00
74.	VP1= -.212500+01	VP2= .169043+01	VP3= .169043+01	AREA= .334212+00
75.	VP1= -.212500+01	VP2= .230917+01	VP3= .618739+00	AREA= .334212+00
76.	VP1= -.212500+01	VP2= .230917+01	VP3= -.618739+00	AREA= .334212+00
77.	VP1= -.212500+01	VP2= .169043+01	VP3= -.169043+01	AREA= .334212+00
78.	VP1= -.212500+01	VP2= .618739+00	VP3= -.230917+01	AREA= .334212+00

79.	VP1= -.212500+01	VP2= -.618739+00	VP3= -.230917+01	AREA= .334212+00
80.	VP1= -.212500+01	VP2= -.169043+01	VP3= -.169043+01	AREA= .334212+00
81.	VP1= -.212500+01	VP2= -.230917+01	VP3= -.618739+00	AREA= .334212+00
82.	VP1= -.212500+01	VP2= -.230917+01	VP3= .618739+00	AREA= .334212+00
83.	VP1= -.212500+01	VP2= -.169043+01	VP3= .169043+01	AREA= .334212+00
84.	VP1= -.212500+01	VP2= -.618739+00	VP3= .230917+01	AREA= .334212+00
85.	VP1= -.237500+01	VP2= .594475+00	VP3= .221861+01	AREA= .321105+00
86.	VP1= -.237500+01	VP2= .162414+01	VP3= .162414+01	AREA= .321105+00
87.	VP1= -.237500+01	VP2= .221861+01	VP3= .594475+00	AREA= .321105+00
88.	VP1= -.237500+01	VP2= .221861+01	VP3= -.594475+00	AREA= .321105+00
89.	VP1= -.237500+01	VP2= .162414+01	VP3= -.162414+01	AREA= .321105+00
90.	VP1= -.237500+01	VP2= .594475+00	VP3= -.221861+01	AREA= .321105+00
91.	VP1= -.237500+01	VP2= -.594475+00	VP3= -.221861+01	AREA= .321105+00
92.	VP1= -.237500+01	VP2= -.162414+01	VP3= -.162414+01	AREA= .321105+00
93.	VP1= -.237500+01	VP2= -.221861+01	VP3= -.594475+00	AREA= .321105+00
94.	VP1= -.237500+01	VP2= -.221861+01	VP3= .594475+00	AREA= .321105+00
95.	VP1= -.237500+01	VP2= -.162414+01	VP3= .162414+01	AREA= .321105+00
96.	VP1= -.237500+01	VP2= -.594475+00	VP3= .221861+01	AREA= .321105+00

ON CONSTRAINT DISK NO.1

	RMEAN	AREA
1	.125000+00	.163425-01
2	.375000+00	.490274-01
3	.625000+00	.818123-01
4	.875000+00	.114537+00
5	.112500+01	.147262+00
6	.137500+01	.179987+00
7	.162500+01	.212712+00
8	.187500+01	.245437+00
9	.212500+01	.278162+00

ON CONSTRAINT DISK NO.2

	RMEAN	AREA
1	.262500+01	.343612+00
2	.287500+01	.376337+00

VIEW FACTOR OUTPUT

TOTAL SAMPLE = 30000 NSTART = 123456 MHITP = 0 MMISS = 7467 MHITG = 22533

EAREA = 5.026544-01

TARGET NO. 1

TARGET MAIN SURFACE, L = 1

AREA NUMBER	NO. OF HITS	AREA NUMBER	VIEW FACTOR	HITAREA	AREA NUMBER	VIEW FACTOR BY RECIPROCITY
1	13.	1	4.3333-04	2.5328-01	1	8.5998-04
2	44.	2	1.4667-03	2.5328-01	2	2.9107-03
3	104.	3	3.4667-03	2.5328-01	3	6.8798-03
4	152.	4	5.0667-03	2.5328-01	4	6.7475-03
5	49.	5	1.6333-03	2.5328-01	5	3.2414-03
6	8.	6	2.6667-04	2.5328-01	6	5.2922-04
7	0.	7	0.0000	2.5328-01	7	0.0000
8	0.	8	0.0000	2.5328-01	8	0.0000
9	0.	9	0.0000	2.5328-01	9	0.0000
10	0.	10	0.0000	2.5328-01	10	0.0000
11	0.	11	0.0000	2.5328-01	11	0.0000
12	0.	12	0.0000	2.5328-01	12	0.0000
13	13.	13	4.3333-04	2.0216-01	13	1.0774-03
14	77.	14	2.5667-03	2.0216-01	14	6.3818-03
15	155.	15	5.1667-03	2.0216-01	15	1.2846-02
16	176.	16	5.8667-03	2.0216-01	16	1.4587-02
17	70.	17	2.3333-03	2.0216-01	17	5.8016-03
18	9.	18	3.0000-04	2.0216-01	18	7.4592-04
19	0.	19	0.0000	2.0216-01	19	0.0000
20	0.	20	0.0000	2.0216-01	20	0.0000
21	0.	21	0.0000	2.0216-01	21	0.0000
22	0.	22	0.0000	2.0216-01	22	0.0000
23	0.	23	0.0000	2.0216-01	23	0.0000
24	0.	24	0.0000	2.0216-01	24	0.0000
25	9.	25	3.0000-04	1.5104-01	25	9.9839-04
26	108.	26	3.6000-03	1.5104-01	26	1.1981-02
27	194.	27	6.4667-03	1.5104-01	27	2.1521-02
28	213.	28	7.1000-03	1.5104-01	28	2.3628-02
29	106.	29	3.5333-03	1.5104-01	29	1.1759-02
30	16.	30	5.3333-04	1.5104-01	30	1.7749-03
31	0.	31	0.0000	1.5104-01	31	0.0000
32	0.	32	0.0000	1.5104-01	32	0.0000

33	0.	33	0.0000	1.5104-01	33	0.0000
34	0.	34	0.0000	1.5104-01	34	0.0000
35	0.	35	0.0000	1.5104-01	35	0.0000
36	0.	36	0.0000	1.5104-01	36	0.0000

TOTAL HIT = 1466. VIEW FACTOR = 4.8867-02 RECIPR VF = 3.3751-03

TARGET NO. 1

ON CONSTRAINT DISK PASSING THRU P1, L = 2

AREA NUMBER	NO. OF HITS	AREA NUMBER	VIEW FACTOR	HITAREA	AREA NUMBER	VIEW FACTOR BY RECIPROCITY
1	0.	1	0.0000	5.3014-02	1	0.0000
2	0.	2	0.0000	5.3014-02	2	0.0000
3	0.	3	0.0000	5.3014-02	3	0.0000
4	0.	4	0.0000	5.3014-02	4	0.0000
5	0.	5	0.0000	5.3014-02	5	0.0000
6	0.	6	0.0000	5.3014-02	6	0.0000
7	0.	7	0.0000	5.3014-02	7	0.0000
8	0.	8	0.0000	5.3014-02	8	0.0000
9	0.	9	0.0000	5.3014-02	9	0.0000
10	0.	10	0.0000	5.3014-02	10	0.0000
11	0.	11	0.0000	5.3014-02	11	0.0000
12	0.	12	0.0000	5.3014-02	12	0.0000

TOTAL HIT = 0. VIEW FACTOR = 0.0000 RECIPR VF = 0.0000

TARGET NO. 1

ON CONSTRAINT DISK PASSING THRU P2, L = 3

AREA NUMBER	NO. OF HITS	AREA NUMBER	VIEW FACTOR	HITAREA	AREA NUMBER	VIEW FACTOR BY RECIPROCITY
1	0.	1	0.0000	2.6180-01	1	0.0000
2	0.	2	0.0000	2.6180-01	2	0.0000
3	0.	3	0.0000	2.6180-01	3	0.0000
4	0.	4	0.0000	2.6180-01	4	0.0000
5	0.	5	0.0000	2.6180-01	5	0.0000
6	0.	6	0.0000	2.6180-01	6	0.0000
7	0.	7	0.0000	2.6180-01	7	0.0000
8	0.	8	0.0000	2.6180-01	8	0.0000

9	0.	9	0.0000	2.6180-01	9	0.0000
10	0.	10	0.0000	2.6180-01	10	0.0000
11	0.	11	0.0000	2.6180-01	11	0.0000
12	0.	12	0.0000	2.6180-01	12	0.0000

TOTAL HIT = 0. VIEW FACTOR = 0.0000 RECIPR VF = 0.0000

TARGET NO. 2

TARGET MAIN SURFACE, L = 1

AREA NUMBER	NO. OF HITS	AREA NUMBER	VIEW FACTOR	HITAREA	AREA NUMBER	VIEW FACTOR BY RECIPROCITY
1	93.	1	1.4333-03	4.1285-01	1	1.7451-03
2	56.	2	1.8667-03	4.1285-01	2	2.2727-03
3	81.	3	2.7[illegible]-03	4.1285-01	3	3.2873-03
4	101.	4	3.3667-03	4.1285-01	4	4.0990-03
5	68.	5	2.2667-03	4.1285-01	5	2.7597-03
6	29.	6	9.6667-04	4.1285-01	6	1.1769-03
7	13.	7	4.3333-04	4.1285-01	7	5.2759-04
8	1.	8	3.3333-05	4.1285-01	8	4.0584-05
9	0.	9	[illegible]	4.1285-01	9	0.0000
10	0.	10	[illegible]	4.1285-01	10	0.0000
11	1.	11	3.3333-05	4.1285-01	11	4.0584-05
12	17.	12	5.6667-04	4.1285-01	12	6.8993-04
13	42.	13	1.4[illegible]-03	3.9974-01	13	1.7604-03
14	81.	14	2.7[illegible]-03	3.9974-01	14	3.3951-03
15	105.	15	3.5[illegible]-03	3.9974-01	15	4.4011-03
16	101.	16	3.3667-03	3.9974-01	16	4.2334-03
17	86.	17	2.8667-03	3.9974-01	17	3.6047-03
18	33.	18	1.1[illegible]-03	3.9974-01	18	1.3832-03
19	5.	19	1.6667-04	3.9974-01	19	2.0957-04
20	0.	20	[illegible]	3.9974-01	20	0.0000
21	0.	21	[illegible]	3.9974-01	21	0.0000
22	0.	22	[illegible]	3.9974-01	22	0.0000
23	0.	23	[illegible]	3.9974-01	23	0.0000
24	4.	24	1.3333-04	3.9974-01	24	1.6766-04
25	26.	25	8.6667-04	3.8664-01	25	1.1267-03
26	68.	26	2.2667-03	3.8664-01	26	2.9468-03
27	42.	27	1.4[illegible]-03	3.8664-01	27	1.8201-03
28	54.	28	1.8[illegible]-03	3.8664-01	28	2.3401-03
29	71.	29	2.3667-03	3.8664-01	29	3.0769-03
30	34.	30	1.1333-03	3.8664-01	30	1.4734-03
31	2.	31	6.6667-05	3.8664-01	31	8.6671-05
32	0.	32	[illegible]	3.8664-01	32	0.0000
33	0.	33	[illegible]	3.8664-01	33	0.0000
34	0.	34	[illegible]	3.8664-01	34	0.0000
35	0.	35	[illegible]	3.8664-01	35	0.0000
36	2.	36	6.6667-05	3.8664-01	36	8.6671-05
37	1.	37	3.3333-05	3.7353-01	37	4.4856-05
38	3.	38	1.[illegible]-04	3.7353-01	38	1.3457-04
39	1.	39	3.3333-05	3.7353-01	39	4.4856-05

40	2.	40	6.6667-05	3.7353-01	40	8.9712-05
41	6.	41	2.0000-04	3.7353-01	41	2.6914-04
42	2.	42	6.6667-05	3.7353-01	42	8.9712-05
43	0.	43	0.0000	3.7353-01	43	0.0000
44	0.	44	0.0000	3.7353-01	44	0.0000
45	0.	45	0.0000	3.7353-01	45	0.0000
46	0.	46	0.0000	3.7353-01	46	0.0000
47	0.	47	0.0000	3.7353-01	47	0.0000
48	0.	48	0.0000	3.7353-01	48	0.0000
49	2.	49	6.6667-05	3.6042-01	49	9.2975-05
50	146.	50	4.8667-03	3.6042-01	50	6.7871-03
51	435.	51	1.4500-02	3.6042-01	51	2.0222-02
52	370.	52	1.2333-02	3.6042-01	52	1.7200-02
53	156.	53	5.2000-03	3.6042-01	53	7.2520-03
54	1.	54	3.3333-05	3.6042-01	54	4.6487-05
55	0.	55	0.0000	3.6042-01	55	0.0000
56	0.	56	0.0000	3.6042-01	56	0.0000
57	0.	57	0.0000	3.6042-01	57	0.0000
58	0.	58	0.0000	3.6042-01	58	0.0000
59	0.	59	0.0000	3.6042-01	59	0.0000
60	0.	60	0.0000	3.6042-01	60	0.0000
61	0.	61	0.0000	3.4732-01	61	0.0000
62	174.	62	5.8000-03	3.4732-01	62	8.3940-03
63	547.	63	1.8233-02	3.4732-01	63	2.6388-02
64	521.	64	1.7367-02	3.4732-01	64	2.5134-02
65	182.	65	6.0667-03	3.4732-01	65	8.7800-03
66	0.	66	0.0000	3.4732-01	66	0.0000
67	0.	67	0.0000	3.4732-01	67	0.0000
68	0.	68	0.0000	3.4732-01	68	0.0000
69	0.	69	0.0000	3.4732-01	69	0.0000
70	0.	70	0.0000	3.4732-01	70	0.0000
71	0.	71	0.0000	3.4732-01	71	0.0000
72	0.	72	0.0000	3.4732-01	72	0.0000
73	6.	73	2.0000-04	3.3421-01	73	3.0080-04
74	218.	74	7.2667-03	3.3421-01	74	1.0929-02
75	684.	75	2.2800-02	3.3421-01	75	3.4291-02
76	703.	76	2.3433-02	3.3421-01	76	3.5244-02
77	203.	77	6.7667-03	3.3421-01	77	1.0177-02
78	6.	78	2.0000-04	3.3421-01	78	3.0080-04
79	0.	79	0.0000	3.3421-01	79	0.0000
80	0.	80	0.0000	3.3421-01	80	0.0000
81	0.	81	0.0000	3.3421-01	81	0.0000
82	0.	82	0.0000	3.3421-01	82	0.0000
83	0.	83	0.0000	3.3421-01	83	0.0000
84	0.	84	0.0000	3.3421-01	84	0.0000
85	14.	85	4.6667-04	3.2111-01	85	7.3051-04
86	209.	86	6.9667-03	3.2111-01	86	1.0906-02
87	722.	87	2.4067-02	3.2111-01	87	3.8039-02

88	737.	88	2.4567-02	3.2111-01	88	3.8456-02
89	235.	89	7.8333-03	3.2111-01	89	1.2262-02
90	9.	90	3.0000-04	3.2111-01	90	4.6962-04
91	0.	91	0.0000	3.2111-01	91	0.0000
92	0.	92	0.0000	3.2111-01	92	0.0000
93	0.	93	0.0000	3.2111-01	93	0.0000
94	0.	94	0.0000	3.2111-01	94	0.0000
95	0.	95	0.0000	3.2111-01	95	0.0000
96	0.	96	0.0000	3.2111-01	96	0.0000

TOTAL HIT = 7468. VIEW FACTOR = 2.4893-01 RECIPR VF = 3.5517-03

TARGET NO. 2

ON CONSTRAINT DISK PASSING THRU PT. L = 2

AREA NUMBER	NO. OF HITS	AREA NUMBER	VIEW FACTOR	HITAREA	AREA NUMBER	VIEW FACTOR BY RECIPROCITY
1	0.	1	0.0000	1.6362-02	1	0.0000
2	0.	2	0.0000	1.6362-02	2	0.0000
3	0.	3	0.0000	1.6362-02	3	0.0000
4	0.	4	0.0000	1.6362-02	4	0.0000
5	0.	5	0.0000	1.6362-02	5	0.0000
6	0.	6	0.0000	1.6362-02	6	0.0000
7	0.	7	0.0000	1.6362-02	7	0.0000
8	0.	8	0.0000	1.6362-02	8	0.0000
9	0.	9	0.0000	1.6362-02	9	0.0000
10	0.	10	0.0000	1.6362-02	10	0.0000
11	0.	11	0.0000	1.6362-02	11	0.0000
12	0.	12	0.0000	1.6362-02	12	0.0000
13	5.	13	1.6667-04	4.9087-02	13	1.7067-03
14	7.	14	2.3333-04	4.9087-02	14	2.3893-03
15	11.	15	3.6667-04	4.9087-02	15	3.7547-03
16	7.	16	2.3333-04	4.9087-02	16	2.3893-03
17	7.	17	2.3333-04	4.9087-02	17	2.3893-03
18	4.	18	1.3333-04	4.9087-02	18	1.3653-03
19	0.	19	0.0000	4.9087-02	19	0.0000
20	0.	20	0.0000	4.9087-02	20	0.0000
21	0.	21	0.0000	4.9087-02	21	0.0000
22	0.	22	0.0000	4.9087-02	22	0.0000
23	0.	23	0.0000	4.9087-02	23	0.0000
24	0.	24	0.0000	4.9087-02	24	0.0000
25	35.	25	1.1667-03	8.1812-02	25	6.1440-03
26	48.	26	1.6000-03	8.1812-02	26	9.8304-03
27	91.	27	3.0333-03	8.1812-02	27	1.8637-02

28	98.	28	3.2667-03	8.1812-02	28	2.0070-02
29	56.	29	1.8667-03	8.1812-02	29	1.1469-02
30	19.	30	6.3333-04	8.1812-02	30	3.8912-03
31	13.	31	4.3333-04	8.1812-02	31	2.6624-03
32	1.	32	3.3333-05	8.1812-02	32	2.0480-04
33	0.	33	0.0000	8.1812-02	33	0.0000
34	0.	34	0.0000	8.1812-02	34	0.0000
35	1.	35	3.3333-05	8.1812-02	35	2.0480-04
36	14.	36	4.6667-04	8.1812-02	36	2.8672-03
37	26.	37	8.6667-04	1.1454-01	37	3.8034-03
38	100.	38	3.3333-03	1.1454-01	38	1.4629-02
39	195.	39	6.5000-03	1.1454-01	39	2.8526-02
40	237.	40	7.9000-03	1.1454-01	40	3.4670-02
41	88.	41	2.9333-03	1.1454-01	41	1.2873-02
42	36.	42	1.2000-03	1.1454-01	42	5.2663-03
43	21.	43	7.0000-04	1.1454-01	43	3.0720-03
44	5.	44	1.6667-04	1.1454-01	44	7.3143-04
45	0.	45	0.0000	1.1454-01	45	0.0000
46	0.	46	0.0000	1.1454-01	46	0.0000
47	1.	47	3.3333-05	1.1454-01	47	1.4629-04
48	17.	48	5.6667-04	1.1454-01	48	2.4869-03
49	42.	49	1.4000-03	1.4726-01	49	4.7787-03
50	143.	50	4.7667-03	1.4726-01	50	1.6270-02
51	460.	51	1.5333-02	1.4726-01	51	5.2338-02
52	438.	52	1.4600-02	1.4726-01	52	4.9835-02
53	139.	53	4.6333-03	1.4726-01	53	1.5815-02
54	31.	54	1.0333-03	1.4726-01	54	3.5271-03
55	18.	55	6.0000-04	1.4726-01	55	2.0480-03
56	4.	56	1.3333-04	1.4726-01	56	4.5511-04
57	0.	57	0.0000	1.4726-01	57	0.0000
58	0.	58	0.0000	1.4726-01	58	0.0000
59	4.	59	1.3333-04	1.4726-01	59	4.5511-04
60	12.	60	4.0000-04	1.4726-01	60	1.3653-03
61	31.	61	1.0333-03	1.7999-01	61	2.8858-03
62	119.	62	3.9667-03	1.7999-01	62	1.1078-02
63	866.	63	2.8867-02	1.7999-01	63	8.0617-02
64	865.	64	2.8833-02	1.7999-01	64	8.0524-02
65	136.	65	4.5333-03	1.7999-01	65	1.2660-02
66	35.	66	1.1667-03	1.7999-01	66	3.2582-03
67	16.	67	5.3333-04	1.7999-01	67	1.4895-03
68	8.	68	2.6667-04	1.7999-01	68	7.4473-04
69	0.	69	0.0000	1.7999-01	69	0.0000
70	0.	70	0.0000	1.7999-01	70	0.0000
71	9.	71	3.0000-04	1.7999-01	71	8.3782-04
72	12.	72	4.0000-04	1.7999-01	72	1.1171-03
73	37.	73	1.2333-03	2.1271-01	73	2.9145-03
74	128.	74	4.2667-03	2.1271-01	74	1.0082-02
75	991.	75	3.3033-02	2.1271-01	75	7.8060-02

76	879.	76	2.9300E-02	2.1271E-01	76	6.9238E-02
77	120.	77	4.3000E-03	2.1271E-01	77	1.0161E-02
78	37.	78	1.2333E-03	2.1271E-01	78	2.9145E-03
79	16.	79	5.3333E-04	2.1271E-01	79	1.2603E-03
80	8.	80	2.6667E-04	2.1271E-01	80	6.3015E-04
81	0.	81	0.0000	2.1271E-01	81	0.0000
82	0.	82	0.0000	2.1271E-01	82	0.0000
83	6.	83	2.0000E-04	2.1271E-01	83	4.7261E-04
84	26.	84	8.6667E-04	2.1271E-01	84	2.0486E-03
85	28.	85	9.3333E-04	2.4544E-01	85	1.9115E-03
86	108.	86	3.6000E-03	2.4544E-01	86	7.3728E-03
87	661.	87	2.2033E-02	2.4544E-01	87	4.5124E-02
88	712.	88	2.3733E-02	2.4544E-01	88	4.8606E-02
89	94.	89	3.1333E-03	2.4544E-01	89	6.4171E-03
90	27.	90	9.0000E-04	2.4544E-01	90	1.8432E-03
91	17.	91	5.6667E-04	2.4544E-01	91	1.1605E-03
92	4.	92	1.3333E-04	2.4544E-01	92	2.7307E-04
93	0.	93	0.0000	2.4544E-01	93	0.0000
94	0.	94	0.0000	2.4544E-01	94	0.0000
95	9.	95	3.0000E-04	2.4544E-01	95	6.1440E-04
96	14.	96	4.6667E-04	2.4544E-01	96	9.5573E-04
97	26.	97	8.6667E-04	2.7816E-01	97	1.5661E-03
98	89.	98	2.9667E-03	2.7816E-01	98	5.3609E-03
99	453.	99	1.5100E-02	2.7816E-01	99	2.7287E-02
100	395.	100	1.3167E-02	2.7816E-01	100	2.3793E-02
101	88.	101	2.9333E-03	2.7816E-01	101	5.3007E-03
102	30.	102	1.0000E-03	2.7816E-01	102	1.8071E-03
103	16.	103	5.3333E-04	2.7816E-01	103	9.6376E-04
104	8.	104	2.6667E-04	2.7816E-01	104	4.8188E-04
105	0.	105	0.0000	2.7816E-01	105	0.0000
106	0.	106	0.0000	2.7816E-01	106	0.0000
107	10.	107	3.3333E-04	2.7816E-01	107	6.0235E-04
108	21.	108	7.0000E-04	2.7816E-01	108	1.2649E-03

TOTAL HIT = 9593. VIEW FACTOR = 3.1977E-01 RECIPR VF = 1.0106E-02

TARGET NO. 2

ON CONSTRAINT DISK PASSING THRU P2. L = 3

AREA NUMBER	NO. OF HITS	AREA NUMBER	VIEW FACTOR	HITAREA	AREA NUMBER	VIEW FACTOR BY RECIPROCITY
1	43.	1	1.4333E-03	3.4361E-01	1	2.0968E-03
2	96.	2	3.2000E-03	3.4361E-01	2	4.6911E-03
3	163.	3	5.4333E-03	3.4361E-01	3	7.9482E-03

4	154.	4	5.1333-03	3.4361-01	4	7.5093-03
5	93.	5	3.1000-03	3.4361-01	5	4.5349-03
6	41.	6	1.3667-03	3.4361-01	6	1.9992-03
7	18.	7	6.0000-04	3.4361-01	7	8.7771-04
8	18.	8	6.0000-04	3.4361-01	8	8.7771-04
9	2.	9	6.6667-05	3.4361-01	9	9.7524-05
10	3.	10	1.0000-04	3.4361-01	10	1.4629-04
11	11.	11	3.6667-04	3.4361-01	11	5.3638-04
12	19.	12	6.3333-04	3.4361-01	12	9.2648-04
13	48.	13	1.6000-03	3.7634-01	13	2.1370-03
14	76.	14	2.5333-03	3.7634-01	14	3.3836-03
15	136.	15	4.5333-03	3.7634-01	15	6.0550-03
16	122.	16	4.0667-03	3.7634-01	16	5.4316-03
17	81.	17	2.7000-03	3.7634-01	17	3.6063-03
18	42.	18	1.4000-03	3.7634-01	18	1.8699-03
19	35.	19	1.1667-03	3.7634-01	19	1.3357-03
20	21.	20	7.0000-04	3.7634-01	20	9.3496-04
21	0.	21	0.0000	3.7634-01	21	0.0000
22	1.	22	3.3333-05	3.7634-01	22	4.4522-05
23	23.	23	7.6667-04	3.7634-01	23	1.0240-03
24	28.	24	9.3333-04	3.7634-01	24	1.2466-03

TOTAL HIT = 1269. VIEW FACTOR = 4.2300-02 RECIPR VF = 2.4611-03

EMITTING SURFACE IEMIT = 7 R1,R2 = .050 .050 NORMAL D.C. = .0000 .0000 1.0000

P1 = -1.5000 -.6000 .0000 P2 = -.5000 -2.4000 .0000 P3 = .0000 .0000 .0000

VIEW FACTOR OUTPUT

TOTAL SAMPLE = 40000 NSTART = 123456 MHITP = 0 MMISS = 14683 MHITG = 25317

EAREA = 6.468933-01

TARGET NO. 1

TARGET MAIN SURFACE, L = 1

AREA NUMBER	NO. OF HITS	AREA NUMBER	VIEW FACTOR	HITAREA	AREA NUMBER	VIEW FACTOR BY RECIPROCITY
1	0.	1	0.0000	2.5328-01	1	0.0000
2	0.	2	0.0000	2.5328-01	2	0.0000
3	0.	3	0.0000	2.5328-01	3	0.0000
4	0.	4	0.0000	2.5328-01	4	0.0000
5	0.	5	0.0000	2.5328-01	5	0.0000
6	0.	6	0.0000	2.5328-01	6	0.0000
7	1.	7	2.5000-05	2.5328-01	7	6.3851-05
8	116.	8	2.9000-03	2.5328-01	8	7.4067-03
9	426.	9	1.0650-02	2.5328-01	9	2.7200-02
10	419.	10	1.0475-02	2.5328-01	10	2.6754-02
11	118.	11	2.9500-03	2.5328-01	11	7.5344-03
12	3.	12	7.5000-05	2.5328-01	12	1.9155-04
13	0.	13	0.0000	2.0216-01	13	0.0000
14	0.	14	0.0000	2.0216-01	14	0.0000
15	0.	15	0.0000	2.0216-01	15	0.0000
16	0.	16	0.0000	2.0216-01	16	0.0000
17	0.	17	0.0000	2.0216-01	17	0.0000
18	0.	18	0.0000	2.0216-01	18	0.0000
19	2.	19	5.0000-05	2.0216-01	19	1.5999-04
20	145.	20	3.6250-03	2.0216-01	20	1.1600-02
21	564.	21	1.4100-02	2.0216-01	21	4.5118-02
22	572.	22	1.4300-02	2.0216-01	22	4.5758-02
23	130.	23	3.2500-03	2.0216-01	23	1.0400-02
24	5.	24	1.2500-04	2.0216-01	24	3.9999-04
25	0.	25	0.0000	1.5104-01	25	0.0000
26	0.	26	0.0000	1.5104-01	26	0.0000
27	0.	27	0.0000	1.5104-01	27	0.0000
28	0.	28	0.0000	1.5104-01	28	0.0000
29	0.	29	0.0000	1.5104-01	29	0.0000
30	0.	30	0.0000	1.5104-01	30	0.0000
31	1.	31	2.5000-05	1.5104-01	31	1.0707-04
32	96.	32	2.4000-03	1.5104-01	32	1.0279-02

33	701.	33	1.7525-02	1.5104-01	33	7.5058-02
34	695.	34	1.7375-02	1.5104-01	34	7.4416-02
35	87.	35	2.1750-03	1.5104-01	35	9.3154-03
36	1.	36	2.5000-05	1.5104-01	36	1.0707-04

TOTAL HIT = 4082. VIEW FACTOR = 1.0205-01 RECIPR VF = 9.0708-03

TARGET NO. 1

ON CONSTRAINT DISK PASSING THRU P1, L = 2

AREA NUMBER	NO. OF HITS	AREA NUMBER	VIEW FACTOR	HITAREA	AREA NUMBER	VIEW FACTOR BY RECIPROCITY
1	0.	1	0.0000	5.3014-02	1	0.0000
2	0.	2	0.0000	5.3014-02	2	0.0000
3	0.	3	0.0000	5.3014-02	3	0.0000
4	0.	4	0.0000	5.3014-02	4	0.0000
5	0.	5	0.0000	5.3014-02	5	0.0000
6	0.	6	0.0000	5.3014-02	6	0.0000
7	0.	7	0.0000	5.3014-02	7	0.0000
8	0.	8	0.0000	5.3014-02	8	0.0000
9	0.	9	0.0000	5.3014-02	9	0.0000
10	0.	10	0.0000	5.3014-02	10	0.0000
11	0.	11	0.0000	5.3014-02	11	0.0000
12	0.	12	0.0000	5.3014-02	12	0.0000

TOTAL HIT = 0. VIEW FACTOR = 0.0000 RECIPR VF = 0.0000

TARGET NO. 1

ON CONSTRAINT DISK PASSING THRU P2, L = 3

AREA NUMBER	NO. OF HITS	AREA NUMBER	VIEW FACTOR	HITAREA	AREA NUMBER	VIEW FACTOR BY RECIPROCITY
1	0.	1	0.0000	2.6180-01	1	0.0000
2	0.	2	0.0000	2.6180-01	2	0.0000
3	0.	3	0.0000	2.6180-01	3	0.0000
4	0.	4	0.0000	2.6180-01	4	0.0000
5	0.	5	0.0000	2.6180-01	5	0.0000
6	0.	6	0.0000	2.6180-01	6	0.0000
7	0.	7	0.0000	2.6180-01	7	0.0000
8	0.	8	0.0000	2.6180-01	8	0.0000

9	0.	9	0.0000	2.618C-01	9	0.0000
10	0.	10	0.0000	2.618C-01	10	0.0000
11	0.	11	0.0000	2.618C-01	11	0.0000
12	0.	12	0.0000	2.618C-01	12	0.0000

TOTAL HIT = 0. VIEW FACTOR = 0.0000 RECIPR VF = 0.0000

TARGET NO. 2

TARGET MAIN SURFACE, L = 1

AREA NUMBER	NO. OF HITS	AREA NUMBER	VIEW FACTOR	HITAREA	AREA NUMBER	VIEW FACTOR BY RECIPROCITY
1	1.	1	2.5000-05	4.1285-01	1	3.9172-05
2	2.	2	5.0000-05	4.1285-01	2	7.8345-05
3	0.	3	0.0000	4.1285-01	3	0.0000
4	0.	4	0.0000	4.1285-01	4	0.0000
5	1.	5	2.5000-05	4.1285-01	5	3.9172-05
6	3.	6	7.5000-05	4.1285-01	6	1.1752-04
7	6.	7	1.5000-04	4.1285-01	7	2.3503-04
8	189.	8	4.7250-03	4.1285-01	8	7.4036-03
9	420.	9	1.0500-02	4.1285-01	9	1.6452-02
10	396.	10	9.9000-03	4.1285-01	10	1.5512-02
11	183.	11	4.5750-03	4.1285-01	11	7.1686-03
12	1.	12	2.5000-05	4.1285-01	12	3.9172-05
13	8.	13	2.0000-04	3.9974-01	13	3.2365-04
14	0.	14	0.0000	3.9974-01	14	0.0000
15	0.	15	0.0000	3.9974-01	15	0.0000
16	0.	16	0.0000	3.9974-01	16	0.0000
17	1.	17	2.5000-05	3.9974-01	17	4.0457-05
18	6.	18	1.5000-04	3.9974-01	18	2.4274-04
19	20.	19	5.0000-04	3.9974-01	19	8.0914-04
20	252.	20	6.3000-03	3.9974-01	20	1.0195-02
21	557.	21	1.3925-02	3.9974-01	21	2.2534-02
22	577.	22	1.4425-02	3.9974-01	22	2.3344-02
23	211.	23	5.2750-03	3.9974-01	23	8.5364-03
24	26.	24	6.5000-04	3.9974-01	24	1.0519-03
25	13.	25	3.2500-04	3.8664-01	25	5.4377-04
26	4.	26	1.0000-04	3.8664-01	26	1.6731-04
27	0.	27	0.0000	3.8664-01	27	0.0000
28	0.	28	0.0000	3.8664-01	28	0.0000
29	1.	29	2.5000-05	3.8664-01	29	4.1828-05
30	9.	30	2.2500-04	3.8664-01	30	3.7645-04
31	44.	31	1.1000-03	3.8664-01	31	1.8404-03
32	265.	32	6.6250-03	3.8664-01	32	1.1084-02
33	672.	33	1.6800-02	3.8664-01	33	2.8109-02
34	617.	34	1.5425-02	3.8664-01	34	2.5808-02
35	296.	35	7.4000-03	3.8664-01	35	1.2381-02
36	51.	36	1.2750-03	3.8664-01	36	2.1332-03
37	12.	37	3.0000-04	3.7353-01	37	5.1955-04
38	6.	38	1.5000-04	3.7353-01	38	2.5978-04
39	0.	39	0.0000	3.7353-01	39	0.0000

40	0.	40	0.0000	3.7353-01	40	0.0000
41	8.	41	1.5000-04	3.7353-01	41	2.5978-04
42	14.	42	3.5000-04	3.7353-01	42	6.0614-04
43	82.	43	2.0500-03	3.7353-01	43	3.5503-03
44	292.	44	7.3000-03	3.7353-01	44	1.2642-02
45	591.	45	1.4775-02	3.7353-01	45	2.5588-02
46	593.	46	1.4750-02	3.7353-01	46	2.5545-02
47	279.	47	6.9750-03	3.7353-01	47	1.2080-02
48	86.	48	2.1500-03	3.7353-01	48	3.7234-03
49	11.	49	2.7500-04	3.6042-01	49	4.9357-04
50	5.	50	1.2500-04	3.6042-01	50	2.2435-04
51	0.	51	0.0000	3.6042-01	51	0.0000
52	1.	52	2.5000-05	3.6042-01	52	4.4870-05
53	4.	53	1.0000-04	3.6042-01	53	1.7948-04
54	10.	54	2.5000-04	3.6042-01	54	4.4870-04
55	47.	55	1.1750-03	3.6042-01	55	2.1089-03
56	112.	56	2.8000-03	3.6042-01	56	5.0255-03
57	105.	57	2.6250-03	3.6042-01	57	4.7114-03
58	146.	58	3.6500-03	3.6042-01	58	6.5511-03
59	89.	59	2.2250-03	3.6042-01	59	3.9935-03
60	72.	60	1.8000-03	3.6042-01	60	3.2307-03
61	29.	61	7.2500-04	3.4732-01	61	1.3503-03
62	14.	62	3.5000-04	3.4732-01	62	6.5189-04
63	0.	63	0.0000	3.4732-01	63	0.0000
64	0.	64	0.0000	3.4732-01	64	0.0000
65	11.	65	2.7500-04	3.4732-01	65	5.1220-04
66	31.	66	7.7500-04	3.4732-01	66	1.4435-03
67	102.	67	2.5500-03	3.4732-01	67	4.7495-03
68	208.	68	5.2000-03	3.4732-01	68	9.6852-03
69	235.	69	5.8750-03	3.4732-01	69	1.0942-02
70	264.	70	6.6000-03	3.4732-01	70	1.2293-02
71	204.	71	5.1000-03	3.4732-01	71	9.4989-03
72	138.	72	3.4500-03	3.4732-01	72	6.4258-03
73	46.	73	1.1500-03	3.3421-01	73	2.2259-03
74	14.	74	3.5000-04	3.3421-01	74	6.7745-04
75	1.	75	2.5000-05	3.3421-01	75	4.8389-05
76	2.	76	5.0000-05	3.3421-01	76	9.6779-05
77	12.	77	3.0000-04	3.3421-01	77	5.8067-04
78	60.	78	1.5000-03	3.3421-01	78	2.9034-03
79	137.	79	3.4250-03	3.3421-01	79	6.6294-03
80	243.	80	6.0750-03	3.3421-01	80	1.1759-02
81	318.	81	7.9500-03	3.3421-01	81	1.5388-02
82	315.	82	7.8750-03	3.3421-01	82	1.5243-02
83	219.	83	5.4750-03	3.3421-01	83	1.0597-02
84	153.	84	3.8250-03	3.3421-01	84	7.4036-03
85	73.	85	1.8250-03	3.2111-01	85	3.6766-03
86	23.	86	5.7500-04	3.2111-01	86	1.1584-03
87	1.	87	2.5000-05	3.2111-01	87	5.0365-05

88	0.	88	0.0000	3.2111-01	88	0.0000
89	2.	89	5.5000-04	3.2111-01	89	1.1080-03
90	74.	90	1.8500-03	3.2111-01	90	3.7270-03
91	122.	91	3.0500-03	3.2111-01	91	6.1445-03
92	190.	92	4.7500-03	3.2111-01	92	9.5693-03
93	242.	93	6.0500-03	3.2111-01	93	1.2188-02
94	264.	94	6.6000-03	3.2111-01	94	1.3296-02
95	223.	95	5.5750-03	3.2111-01	95	1.1231-02
96	126.	96	3.1500-03	3.2111-01	96	6.3459-03

TOTAL HIT = 11508. VIEW FACTOR = 2.8770-01 RECIPR VF = 5.2828-03

TARGET NO. 2

ON CONSTRAINT DISK PASSING THRU PT. L = 2

AREA NUMBER	NO. OF HITS	AREA NUMBER	VIEW FACTOR	HITAREA	AREA NUMBER	VIEW FACTOR BY RECIPROCITY
1	0.	1	0.0000	1.6362-02	1	0.0000
2	0.	2	0.0000	1.6362-02	2	0.0000
3	0.	3	0.0000	1.6362-02	3	0.0000
4	0.	4	0.0000	1.6362-02	4	0.0000
5	0.	5	0.0000	1.6362-02	5	0.0000
6	0.	6	0.0000	1.6362-02	6	0.0000
7	0.	7	0.0000	1.6362-02	7	0.0000
8	0.	8	0.0000	1.6362-02	8	0.0000
9	0.	9	0.0000	1.6362-02	9	0.0000
10	0.	10	0.0000	1.6362-02	10	0.0000
11	0.	11	0.0000	1.6362-02	11	0.0000
12	0.	12	0.0000	1.6362-02	12	0.0000
13	0.	13	0.0000	4.9087-02	13	0.0000
14	0.	14	0.0000	4.9087-02	14	0.0000
15	0.	15	0.0000	4.9087-02	15	0.0000
16	0.	16	0.0000	4.9087-02	16	0.0000
17	0.	17	0.0000	4.9087-02	17	0.0000
18	0.	18	0.0000	4.9087-02	18	0.0000
19	2.	19	5.0000-05	4.9087-02	19	6.5892-04
20	4.	20	1.0000-04	4.9087-02	20	1.3178-03
21	11.	21	2.7500-04	4.9087-02	21	3.6241-03
22	12.	22	3.0000-04	4.9087-02	22	3.9535-03
23	9.	23	2.2500-04	4.9087-02	23	2.9651-03
24	5.	24	1.2500-04	4.9087-02	24	1.6473-03
25	8.	25	2.0000-04	8.1812-02	25	1.5814-03
26	0.	26	0.0000	8.1812-02	26	0.0000
27	0.	27	0.0000	8.1812-02	27	0.0000

28	0.	28	0.0000	8.1812-02	28	0.0000
29	0.	29	0.0000	8.1812-02	29	0.0000
30	10.	30	2.5000-04	8.1812-02	30	1.9768-03
31	26.	31	6.5000-04	8.1812-02	31	5.1396-03
32	48.	32	1.2000-03	8.1812-02	32	9.4884-03
33	80.	33	2.0000-03	8.1812-02	33	1.5814-02
34	79.	34	1.9750-03	8.1812-02	34	1.5616-02
35	61.	35	1.5250-03	8.1812-02	35	1.2058-02
36	41.	36	1.0250-03	8.1812-02	36	8.1047-03
37	26.	37	6.5000-04	1.1454-01	37	3.6711-03
38	5.	38	1.2500-04	1.1454-01	38	7.0599-04
39	0.	39	0.0000	1.1454-01	39	0.0000
40	0.	40	0.0000	1.1454-01	40	0.0000
41	0.	41	0.0000	1.1454-01	41	0.0000
42	18.	42	4.5000-04	1.1454-01	42	2.5415-03
43	34.	43	8.5000-04	1.1454-01	43	4.8007-03
44	80.	44	2.0000-03	1.1454-01	44	1.1296-02
45	143.	45	3.5750-03	1.1454-01	45	2.0191-02
46	122.	46	3.0500-03	1.1454-01	46	1.7226-02
47	90.	47	2.2500-03	1.1454-01	47	1.2709-02
48	50.	48	1.2500-03	1.1454-01	48	7.0599-03
49	37.	49	9.2500-04	1.4726-01	49	4.0633-03
50	7.	50	1.7500-04	1.4726-01	50	7.6874-04
51	0.	51	0.0000	1.4726-01	51	0.0000
52	0.	52	0.0000	1.4726-01	52	0.0000
53	10.	53	2.5000-04	1.4726-01	53	1.0982-03
54	31.	54	7.7500-04	1.4726-01	54	3.4044-03
55	55.	55	1.3750-03	1.4726-01	55	6.0401-03
56	107.	56	2.6750-03	1.4726-01	56	1.1751-02
57	190.	57	4.7500-03	1.4726-01	57	2.0866-02
58	188.	58	4.7000-03	1.4726-01	58	2.0646-02
59	134.	59	3.3500-03	1.4726-01	59	1.1421-02
60	58.	60	1.4500-03	1.4726-01	60	6.3696-03
61	35.	61	8.7500-04	1.7999-01	61	3.1448-03
62	8.	62	2.0000-04	1.7999-01	62	7.1882-04
63	0.	63	0.0000	1.7999-01	63	0.0000
64	0.	64	0.0000	1.7999-01	64	0.0000
65	9.	65	2.2500-04	1.7999-01	65	8.0867-04
66	26.	66	6.5000-04	1.7999-01	66	2.3362-03
67	69.	67	1.7250-03	1.7999-01	67	6.1998-03
68	143.	68	3.5750-03	1.7999-01	68	1.2849-02
69	233.	69	5.8250-03	1.7999-01	69	2.0936-02
70	245.	70	6.1250-03	1.7999-01	70	2.2014-02
71	127.	71	3.1750-03	1.7999-01	71	1.1411-02
72	65.	72	1.6250-03	1.7999-01	72	5.8404-03
73	21.	73	5.2500-04	2.1271-01	73	1.5966-03
74	9.	74	2.2500-04	2.1271-01	74	6.8426-04
75	0.	75	0.0000	2.1271-01	75	0.0000

76	0.	76	0.0000	2.1271-01	76	0.0000
77	12.	77	3.0000-04	2.1271-01	77	9.1235-04
78	32.	78	8.0000-04	2.1271-01	78	2.4329-03
79	76.	79	1.9000-03	2.1271-01	79	5.7782-03
80	181.	80	4.5250-03	2.1271-01	80	1.3761-02
81	269.	81	6.7250-03	2.1271-01	81	2.0452-02
82	289.	82	7.2250-03	2.1271-01	82	2.1972-02
83	140.	83	3.5000-03	2.1271-01	83	1.0644-02
84	71.	84	1.7750-03	2.1271-01	84	5.3981-03
85	35.	85	8.7500-04	2.4544-01	85	2.3062-03
86	13.	86	3.2500-04	2.4544-01	86	8.5660-04
87	0.	87	0.0000	2.4544-01	87	0.0000
88	1.	88	2.5000-05	2.4544-01	88	6.5892-05
89	19.	89	4.7500-04	2.4544-01	89	1.2519-03
90	33.	90	8.2500-04	2.4544-01	90	2.1744-03
91	66.	91	1.6500-03	2.4544-01	91	4.3489-03
92	171.	92	4.2750-03	2.4544-01	92	1.1268-02
93	287.	93	7.1750-03	2.4544-01	93	1.8911-02
94	252.	94	6.3000-03	2.4544-01	94	1.6605-02
95	191.	95	4.7750-03	2.4544-01	95	1.2585-02
96	83.	96	2.0750-03	2.4544-01	96	5.4690-03
97	39.	97	9.7500-04	2.7816-01	97	2.2675-03
98	15.	98	3.7500-04	2.7816-01	98	8.7210-04
99	0.	99	0.0000	2.7816-01	99	0.0000
100	0.	100	0.0000	2.7816-01	100	0.0000
101	12.	101	3.0000-04	2.7816-01	101	6.9768-04
102	29.	102	7.2500-04	2.7816-01	102	1.6861-03
103	82.	103	2.0500-03	2.7816-01	103	4.7675-03
104	141.	104	3.5250-03	2.7816-01	104	8.1977-03
105	257.	105	6.4250-03	2.7816-01	105	1.4942-02
106	257.	106	6.4250-03	2.7816-01	106	1.4942-02
107	153.	107	3.8250-03	2.7816-01	107	8.8954-03
108	61.	108	1.5250-03	2.7816-01	108	3.5465-03

TOTAL HIT = 6008. VIEW FACTOR = 1.5020-01 RECIPR VF = 6.1092-03

TARGET NO. 2

ON CONSTRAINT DISK PASSING THRU P2, L = 3

AREA NUMBER	NO. OF HITS	AREA NUMBER	VIEW FACTOR	HITAREA	AREA NUMBER	VIEW FACTOR BY RECIPROCITY
1	16.	1	4.0000-04	3.4361-01	1	7.5305-04
2	6.	2	1.5000-04	3.4361-01	2	2.8239-04
3	0.	3	0.0000	3.4361-01	3	0.0000

4	0.	4	0.0000	3.4361-01	4	0.0000
5	1.	5	5.0000-05	3.4361-01	5	9.4131-05
6	23.	6	5.7500-04	3.4361-01	6	1.0825-03
7	46.	7	1.1500-03	3.4361-01	7	2.1650-03
8	69.	8	1.7250-03	3.4361-01	8	3.2475-03
9	171.	9	4.2750-03	3.4361-01	9	8.0482-03
10	165.	10	4.1250-03	3.4361-01	10	7.7658-03
11	85.	11	2.1250-03	3.4361-01	11	4.0006-03
12	28.	12	7.0000-04	3.4361-01	12	1.3178-03
13	14.	13	3.5000-04	3.7634-01	13	6.0162-04
14	6.	14	1.5000-04	3.7634-01	14	2.5784-04
15	0.	15	0.0000	3.7634-01	15	0.0000
16	0.	16	0.0000	3.7634-01	16	0.0000
17	5.	17	1.2500-04	3.7634-01	17	2.1487-04
18	12.	18	3.0000-04	3.7634-01	18	5.1568-04
19	11.	19	2.7500-04	3.7634-01	19	1.4611-03
20	50.	20	1.2500-03	3.7634-01	20	2.1487-03
21	91.	21	2.2750-03	3.7634-01	21	3.9105-03
22	80.	22	2.0000-03	3.7634-01	22	3.4378-03
23	59.	23	1.4750-03	3.7634-01	23	2.5354-03
24	35.	24	8.7500-04	3.7634-01	24	1.5041-03

TOTAL HIT = 997. VIEW FACTOR = 2.4925-02 RECIPR VF = 1.8663-03

6. CONCLUSIONS AND RECOMMENDATIONS

The SRB plume thermal radiation code is capable of defining the influence of plume flowfield structure on the magnitude and distribution of thermal radiation leaving the plume. Radiant heating rates may be calculated for a single SRB plume or for the dual SRB plumes astride the Space Shuttle. The plumes may be gimbaled in the yaw and pitch planes. Space Shuttle surface geometries are simulated with combinations of quadric surfaces. Surface shading effects are accounted for. The code also has the capability to calculate view factors between the SRB plumes and Space Shuttle surfaces as well as surface-to-surface view factors.

The capability of the SRB plume thermal radiation code can easily be extended to more accurately model the physics of the radiation transport phenomenon. The following extensions in the codes capability are suggested:

- Model the wavelength dependence of radiative properties on the magnitude and distribution of spectral thermal radiation leaving the plume.
- Provide the capability to calculate radiative interchange factors between surfaces. This will include the ability to model absorption and reflection at the surface. Reflection can be modeled as specular, diffuse and real surface reflection.
- Provide the capability to perform a complete calculation of radiative interchange factors between all surfaces of a Space Shuttle enclosure such as the volume contained within the SRB shroud.

7. REFERENCES

1. Penny, M.M., S.D. Smith, P.G. Anderson, P.R. Sulyma and M.L. Pearson, "Supersonic Flow of Chemically Reacting Gas-Particle Mixtures," LMSC-HREC TR D496555, Lockheed Missiles & Space Company, Inc., Huntsville, Ala., January 1976.
2. Abu-Romia, M.M., and C.L. Tien, "Appropriate Mean Absorption Coefficients for Infrared Radiation of Gases," Trans. ASME, J. Heat Trans., November 1967.
3. Watson, G.H., N.A. Logan and J.V. McAnally, "Prediction of Radiation Heat Transfer Characteristics from Solid Rocket Plumes Using the Monte Carlo Technique," LMSC-HREC TM D306995, Lockheed Missiles & Space Company, Huntsville, Ala., January 1974.
4. Howell, J.R., "Calculation of Radiant Heat Exchange by the Monte Carlo Method," Paper 65 WA/HT-54, Winter Annual Meeting of the ASME, 7-11 November 1965.
5. Univac 1108 Math-Pack, UP-7542, Sperry Rand Corporation, 1967.
6. Siegel, R., and J.R. Howell, "Thermal Radiation Heat Transfer," McGraw-Hill, New York, 1972.
7. Stockham, L.W., and T.J. Love, "Radiative Heat Transfer from a Cylindrical Cloud of Particles," AIAA J., Vol. 6, No. 10, October 1968.
8. Tien, C.L., and M.M. Abu-Romia, "Radiative Energy Transfer to Outer Base Regions of Cylindrical and Conical Gas Bodies," Report AS-63-4, Institute of Engineering Research, University of California, Berkeley, 1963.
9. Pond, J.E. et al., "Determination of Quadric Equation Coefficients Describing Three-Dimensional Surfaces," TSP 69-10435, NASA Technical Support Package, September 1969.